Analysis and control of light-induced processes in molecules: Electron and nuclear quantum dynamics for aspects of stereoisomerism and spectroscopy

Habilitationsschrift

zur Erlangung des akademischen Grades
doctor rerum naturalium habilitatus
in Theoretischer Chemie

Mathematisch-Naturwissenschaftliche Fakultät
der Universität Potsdam

vorgelegt von
Dr. Dominik Kröner
aus Göttingen

März 2013

Gutachter:	Prof. Dr. Peter Saalfrank Prof. Dr. Robert Berger Prof. Dr. Regina de Vivie-Riedle
Kolloquium:	25. Februar 2014
Probevorlesung:	9. April 2014
Titel:	*Solvatationsmodelle in der Theoretischen Chemie*

Published online at the
Institutional Repository of the University of Potsdam:
URL http://opus.kobv.de/ubp/volltexte/2014/7047/
URN urn:nbn:de:kobv:517-opus-70477
http://nbn-resolving.de/urn:nbn:de:kobv:517-opus-70477

Abstract

The habilitation thesis covers theoretical investigations on light-induced processes in molecules. The study is focussed on changes of the molecular electronic structure and geometry, caused either by photoexcitation in the event of a spectroscopic analysis, or by a selective control with shaped laser pulses. The applied and developed methods are predominantly based on quantum chemistry as well as on electron and nuclear quantum dynamics, and in parts on molecular dynamics. The studied scientific problems deal with stereoisomerism and the question of how to either switch or distinguish chiral molecules using laser pulses, and with the essentials for the simulation of the spectroscopic response of biochromophores, in order to unravel their photophysics. The accomplished findings not only explain experimental results and extend existing approaches, but also contribute significantly to the basic understanding of the investigated light-driven molecular processes. The main achievements can be divided in three parts:

First, a quantum theory for an enantio- and diastereoselective or, in general, stereoselective laser pulse control was developed and successfully applied to influence the chirality of molecular switches. The proposed axially chiral molecules possess different numbers of "switchable" stable chiral conformations, with one particular switch featuring even a true achiral "off"-state which allows to enantioselectively "turn on" its chirality. Furthermore, surface mounted chiral molecular switches with several well-defined orientations were treated, where a newly devised highly flexible stochastic pulse optimization technique provides high stereoselectivity and efficiency at the same time, even for coupled chirality-changing degrees of freedom. Despite the model character of these studies, the proposed types of chiral molecular switches and, all the more, the developed basic concepts are generally applicable to design laser pulse controlled catalysts for asymmetric synthesis, or to achieve selective changes in the chirality of liquid crystals or in chiroptical nanodevices, implementable in information processing or as data storage.

Second, laser-driven electron wavepacket dynamics based on ab initio calculations, namely time-dependent configuration interaction, was extended by the explicit inclusion of magnetic field-magnetic dipole interactions for the simulation of the qualitative and quantitative distinction of enantiomers in mass spectrometry by means of circularly polarized ultrashort laser pulses. The developed approach not only allows to explain the origin of the experimentally observed influence of the pulse duration on the detected circular dichroism in the ion yield, but also to predict laser pulse parameters for an optimal distinction of enantiomers by ultrashort shaped laser pulses. Moreover, these investigations in combination with the previous ones provide a fundamental understanding of the relevance of electric and magnetic interactions between linearly or non-linearly polarized laser pulses and (pro-)chiral molecules for either control by enantioselective excitation or distinction by enantiospecific excitation.

Third, for selected light-sensitive biological systems of central importance, like e.g. antenna complexes of photosynthesis, simulations of processes which take place during and after photoexcitation of their chromophores were performed, in order to explain experimental (spectroscopic) findings as well as to understand the underlying photophysical and photochemical principles. In particular, aspects of normal mode mixing due to geometrical changes upon photoexcitation and their impact on (time-dependent) vibronic and resonance Raman spectra, as well as on intramolecular energy redistribution were addressed. In order to explain unresolved experimental findings, a simulation program for the calculation of vibronic and resonance Raman spectra, accounting for changes in both vibrational frequencies and normal modes, was created based on a time-dependent formalism. In addition, the influence of the biochemical environment on the electronic structure of the chromophores was studied by electrostatic interactions and mechanical embedding using hybrid quantum-classical methods. Environmental effects were found to be of importance, in particular, for the excitonic coupling of chromophores in light-harvesting complex II. Although the simulations for such highly complex systems are still restricted by various approximations, the improved approaches and obtained results have proven to be important contributions for a better understanding of light-induced processes in biosystems which also adds to efforts of their artificial reproduction.

Zusammenfassung

Die Habilitationsschrift behandelt theoretische Untersuchungen von durch Licht ausgelösten Prozessen in Molekülen. Der Schwerpunkt liegt dabei auf Veränderungen in der Elektronenstruktur und der Geometrie der Moleküle, die durch Bestrahlung mit Licht entweder bei einer spektroskopischen Untersuchung oder bei gezielter Kontrolle durch geformte Laserpulse herbeigeführt werden. Um die dabei auftretende Elektronen- und Kerndynamik zu simulieren, wurden vornehmlich quantentheoretische Methoden eingesetzt und weiterentwickelt. Die wissenschaftlichen Fragestellungen beschäftigen sich mit dem gezielten Verändern und dem Erkennen der räumlichen Struktur von Molekülen ohne Drehspiegelachse, der sog. molekularen Chiralität, sowie mit durch Licht eingeleiteten Prozessen in biologisch relevanten Pigmenten auf sehr kurzen Zeitskalen. Die entwickelten Ansätze und gewonnenen Erkenntnisse lassen sich in drei Haupterfolge unterteilen:

Erstens gelang die Entwicklung einer generellen Kontrolltheorie für das Ein- und Umschalten von molekularer Chiralität mit geformten Laserpulsen. Dabei wird die räumliche Struktur der vorgeschlagenen molekularen Schalter zwischen ihren stabilen sog. stereoisomeren Formen selektiv geändert, was sich auf ihre optischen und chemischen Eigenschaften auswirkt. Für komplexere Bedingungen, wie z.B. auf einer Oberfläche verankerten molekularen Schaltern verschiedener Orientierung, wurde eine neue Pulsoptimierungsmethode basierend auf Wahrscheinlichkeiten und Statistik entwickelt. Solche laserpulskontrollierten chiralen molekularen Schalter hofft man u.a. in der Nanotechnologie zum Einsatz zu bringen, wo sie z.B. als Informationsspeicher dienen könnten.

Zweitens konnte geklärt werden, welche die wesentlichen Einflüsse sind, die das Erkennen von sog. Enantiomeren, das sind spiegelbildliche Moleküle von entgegengesetzter Chiralität, nach Ionisierung durch ultrakurze zirkular polarisierte Laserpulse ermöglichen. Diese Form des sog. Zirkulardichroismus in der Ionenausbeute erlaubt die quantitative und qualitative Unterscheidung von Enantiomeren in der Massenspektrometrie. Durch Simulation der Elektronendynamik während der Laseranregung konnte u.a. erstmals gezeigt werden, dass neben der Zirkularpolarisation der Laserpulse vor allem die schwachen magnetischen Wechselwirkungen für die Unterscheidung entscheidend sind.

Drittens wurden die Spektren von in der Natur vorkommenden Pigmenten simuliert, welche u.a. an wichtigen biologischen Funktionen, wie dem Sammeln von Sonnenenergie für die Photosynthese, beteiligt sind. Die Lichtanregung führt dabei zu einer Veränderung der Elektronenstruktur und Geometrie der Pigmente, wobei letzteres wichtige Konsequenzen für die Verteilung der Energie auf die spektroskopisch beobachteten Molekülschwingungen mit sich bringen. Auch der wichtige Einfluss der biochemischen Umgebung auf die Elektronenstruktur der Pigmente bzw. den Energietransfer zwischen solchen wurde untersucht. Neben der Klärung experimenteller Ergebnisse ermöglichen die Untersuchungen neue

Einblicke in die fundamentalen Prozesse kurz nach der Lichtanregung – Erkenntnisse, die auch für die technische Nachahmung der biologischen Funktionen von Bedeutung sein können.

Contents

1 Light-induced processes in molecules

Sunlight serves as energy source for (almost)[1] all life on Earth, either directly or indirectly via the food chain and cellular respiration, because it drives the photosynthesis, i.e. the production of carbohydrates and oxygen[2] from carbon dioxide and water. For photosynthesis various steps take place in the cells of plants, algae or bacteria, including absorption and transfer of the light energy, storage in form of chemical bonds and electron transfer. Ever since the early works of Willstätter[3] [1] and Calvin[4] [2] the detailed understanding of these processes was source of many studies and is, indeed, highly desirable, in particular, in view of the development of artificial photosynthesis or the processes it consists of, for instance, for solar energy conversion into electrical energy by bio-photovoltaic cells. For the initial, light-induced steps of the photosynthesis mechanism the interaction of light with matter on a quantum molecular level and its impact on subsequent physical and chemical processes are the key aspects. Aside from the knowledge of the electronic structure of the participating molecules, the study of the electron-nuclear quantum dynamics is essential, not only to follow the elementary steps of the chemical reactions, but also to unravel accompanying phenomena such as intramolecular (vibrational) energy redistribution (IVR), internal conversion (IC) (via non-adiabatic transitions), intersystem crossings (ISC), excited state lifetimes or electronic energy transfer (EET). Here theory can play an important role, because it is not only able to confirm experimental (spectroscopic) results, but also allows to simulate processes which are beyond the experimental setup and to make valuable predictions.

Remarkably, the glucose produced in photosynthesis is exclusively of D-form,[5] while the naturally occurring amino acids which constitute the proteins that deal with the sugar in living organisms, are of L-form. Although various reasonable theories exists, the origin of this homochirality in nature remains unclear [3], but it is of utterly importance for the synthesis of physiologically active chemicals, as the relative spatial arrangement of the atoms of the receptors in our organism determine their effect. Not only since the fundamental research of Cornforth and Prelog[6], stereochemistry has, hence, played a central role in chemistry for asymmetric synthesis as well as for the analysis and separation of stereoisomers.

Aside from photosynthesis, light-induced processes are, in general, central to a variety of prominent natural phenomena and applied (modern) technologies, such

[1] The exception are the chemotrophs, e.g. bacteria at deep sea vents.

[2] The exception is the anoxygenic photosynthesis.

[3] Nobel Prize in Chemistry 1915 for his research on *plant pigments, especially chlorophyll.*

[4] Nobel Prize in Chemistry 1961 for his research on the *carbon dioxide assimilation in plants.*

[5] Latin: D: dexter - right, L: leavus - left

[6] Nobel Prize in Chemistry 1975 for their *work on the stereochemistry of organic molecules and (enzymes catalyzed) reactions.*

as vision, heliotropism[7], or (digital) photography, (dye-sensitized) solar cells [4], and photolithography for microfabrication of integrated circuits. In addition, light does not necessarily have to trigger a chemical reaction, but may be used in spectroscopy for the analysis of electronic and nuclear structures of molecules. The range of spectroscopic methods is as wide as the spectrum of the employed (electromagnetic) radiation and covers various types of interactions, including absorption, emission and (elastic or inelastic) scattering. Typical important spectroscopies in Chemistry are, inter alia, X-ray crystallography, mass spectrometry, UV/vis absorption or emission (fluorescence, phosphorescence), nuclear magnetic resonance, (resonance) Raman[8] scattering and circular dichroism. The latter allows to distinguish optically active chiral molecules using circularly polarized light, and may even be used to investigate the stereochemistry of proteins, i.e. their secondary structure. For large biomolecules with embedded chromophores also resonance Raman spectroscopy is of particular interest, because it allows to detect only few vibrational modes of specific molecular groups or chromophores with high sensitivity. Either way, a spectrum offers not only a snapshot of the nuclei and electrons of the probed molecule (or rather their response to the radiation), but also allows the observation of their dynamics if employed time-resolved.

A detailed understanding of light-induced molecular processes is naturally the prerequisite for the manipulation or even selective control of molecular changes or of chemical reactions using well-defined light sources. In the last years, light sources became more efficient in terms of monochromaticity, coherence as well as intensity, and advances in pulse shaping allowed for ultrashort laser pulses of even complex polarization [5]. As such the observation of the elementary steps of chemical processes became possible on a timescale of femtoseconds, allowing to actually monitor nuclear motion as quantum wavepackets, see for instance the pioneering work by Zewail[9] [6]. And even timescales below femtoseconds are possible nowadays, making the observation of electron dynamics possible, not only in theory [7, 8], but also experimentally with attosecond laser pulses generated by higher harmonic generation [9]. In fact, shaped laser pulses may be used to initiate and steer chemical reactions, as demonstrated theoretically by control of the delay [10, 11] or phase between pulses [12, 13], and experimentally through adaptive close-loop optimization of the electric field [14]. An exciting experimental application is, for instance, the optimal femtosecond pump-dump control of the retinal isomerization in bacteriorhodopsin [15], which acts as a light-driven proton pump to create a proton gradient for subsequent conversion into chemical energy. In this way, light might even become the source which eventually drives and controls molecular machines in nanoscale devices [16].

[7] Motion of plant parts towards the direction of the sun.

[8] Nobel Prize in Chemistry 1930 for his work on *the scattering of light and for the discovery of the effect named after him.*

[9] Nobel Prize in Chemistry 1999 for his research on the *transitions states of chemical reactions using femtosecond spectroscopy.*

In the work at hand some of the named aspects of light-molecule interactions, in particular with respect to stereoisomerism of organic molecules and spectroscopy of biologically relevant chromophores, will be addressed. The discussion will focus on a selection of our theoretical investigations over the past years, dealing with the analysis and control of the said topics, mainly by means of electron and nuclear quantum chemistry and dynamics. The review of the achieved scientific accomplishments, predominantly published in the ten peer-reviewed articles listed in the Appendix, is split up in three chapters:

The first chapter, Chapter 2: *Laser control of chiral molecular switches*, focusses on the manipulation of molecular switches with shaped laser pulses, in particular, to control the handedness of their conformation. Various scenarios of selective isomerization are presented based on laser-driven nuclear wavepacket dynamics. Highly effective laser pulse optimization techniques are developed to cope with the challenging cases of full stereoselective control for molecules of diverse orientations with coupled internal degrees of freedom. Most of the discussed results are found in the references listed in Appendix A.

In the second chapter, Chapter 3: *Chiral recognition by ultrashort laser pulses*, aspects of stereoisomerism and pulsed circular polarized light are considered for the distinction of enantiomers in mass spectrometry. Here light-induced electron wavepacket dynamics based on ab initio calculations helps to understand recent experimental observations and to identify the essentials of the enantiospecific interactions. Appendix B gives the corresponding references.

The third and last chapter on the results, Chapter 4: *Electronic structure and spectroscopy of biochromophores*, covers a variety of spectroscopic investigations on biologically relevant chromophores in order to gain insight into their photophysics and photochemistry. Aside from the computation of steady-state spectra, explicitly time-dependent non-adiabatic dynamics are computed to study the processes taking place after light exposure. The observed changes of the nuclear framework upon electronic excitation plays also a role in the simulation of vibronic spectra, which are obtained applying time-dependent formalisms. All presented publications are given in Appendix C.

The report concludes in the final chapter, Chapter 5: *Achievements and other light-induced processes*, with a short résumé of the presented work, and by giving a brief overview of our other investigations on light-induced molecular processes on metal, metal oxide and non-metal surfaces, a subject not covered by the three main chapters, avoiding to stretch the limits of the discussed results too far.

2 Laser control of chiral molecular switches

2.1 From the purification of a racemate by light to chiroptical switches

Traditional chemistry has successfully established a variety of methods to synthesize the desired enantiomer of a chemical compound, for instance, employing chiral catalysts [17–19] or starting off with natural enantiopure molecules (*ex chiral pool*). Yet, the possibility to produce enantiomeric excess by external fields, e.g. exploiting the difference in the absorption coefficient of enantiomers for circularly polarized light (circular dichroism) [20], has also been investigated extensively, as it might additionally offer an insight of the origin of homochirality in nature. However, the success of asymmetric synthesis via external fields has been rather limited so far [21, 22].

In addition, in the past a variety of efforts have been made by theoreticians to quantum mechanically describe the influence of external fields on molecular chirality, often with the objective of controlling it [23–29]. As circular dichroism has a rather small impact on most molecules,[10] a branch of this theoretical research focussed entirely on laser pulses and electric field-electric dipole interactions, aiming for a stronger influence on molecular chirality. A good portion of such simulations based on molecular model systems may be attributed to studies in the groups of Shapiro and Brumer as well as Manz and Fujimura, who presented a variety of schemes for the laser pulse controlled selective preparation of pure enantiomers from a racemate [31–41]. It is worth to take a closer look at the basic concepts of those approaches, since some of them will become helpful for what we wish to accomplish in this work.

In 1991 Shapiro and Brumer proposed a *coherent control* scheme for the photodissociation of prochiral molecules, in order to produce one preferred chiral fragment using linearly polarized laser pulses [42]. Some years later they applied their approach for the production of one enantiomer from a racemate based on a model of a double well ground and an assumed single well electronic excited state potential [31], see Fig. 1. In the process three linearly polarized laser pulses electronically excite either the left- (L) or right-handed (R) form, by coupling $|0\mathsf{L}\rangle$ and $|0\mathsf{R}\rangle$ each with $|0+\rangle$ and $|1-\rangle$ as well as $|0+\rangle$ with $|1-\rangle$ ($+$ and $-$ denote *gerade* and *ungerade* symmetry). Is the correct phase between those states prepared, only one chiral form will be excited to the electronic excited state, from where it will eventually return to the ground state by relaxation. If relaxation results in equal population of the two ground state wells, the initially excited chiral form is reduced at last. By repeating these steps the concentration of the preferred enantiomer may successively be increased in this kind of *laser distillation*. Later on,

[10] This manifests itself in rather small (Kuhn) anisotropy factors [30].

simulations on 1,3-dimethylallene showed that the approach is well applicable to axially chiral molecules [32]. Are the three laser fields perpendicularly polarized, enantiomeric excess may also be achieved in an ensemble of randomly oriented molecules [33], even if energy dissipation and dephasing is explicitly accounted for [34, 35].

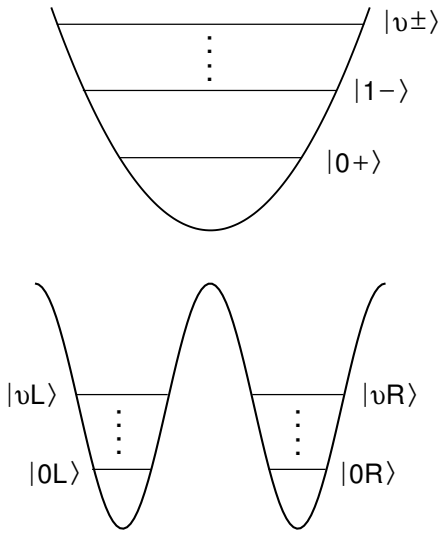

Figure 1: Potential energy curves of the ground and an electronic excited state for a quantum mechanical model of a chiral molecule. The two minima of the symmetric double well potential correspond to the two enantiomers, denoted L (for left-handed) and R (for right-handed). Barriers appear along degrees of freedom which allow the transformation between them. The symmetry of the electronic excited state is chosen such that it represents an achiral configuration of the molecule.

Already in 1999 Fujimura, Manz and coworkers applied elliptically polarized laser pulses to prepare a pure enantiomer of the axially chiral molecule H_2POSH [43]. The laser pulse controlled selective transformation of a racemate of oriented H_2POSH molecules to a pure enantiomer succeeded shortly after, due to the developed, so-called, *parking mechanism*, a sequence of five linearly polarized laser pulses [36, 44]. Later, a *pump-dump* control approach for the racemate purification of pre-oriented molecules was presented where the pump pulse transfers exclusively population, for instance, from $|0\mathsf{L}\rangle$ to $|0+\rangle$ and the dump pulse from $|0+\rangle$ to $|v\mathsf{R}\rangle$ [38,39], cf. Fig. 1. In the process, the electric field is linearly polarized such that its interaction with one enantiomer completely vanishes while it is to be maximized with its mirror image. Such linearly polarized *enantioselective laser pulses* may also be applied to only energetically separate the degenerate enantiomers in a racemate, e.g. by $|0\mathsf{L}\rangle \rightarrow |v\mathsf{L}\rangle$ ($|0\mathsf{R}\rangle \not\rightarrow |v\mathsf{R}\rangle$), as successfully demonstrated by us in quantum dynamical simulations for the double bond isomerisation of axially chiral (4-methyl-cyclohexylidene)fluoromethane [45, 46]. After the separation, a variety of possibilities exist for a transformation of the energetically excited enantiomer into its counterpart: The excited enantiomer may be transferred into an electronic excited state ($|v\mathsf{L}\rangle \rightarrow |v\pm\rangle$) of short lifetime, in order to create a cycle of enantioselective excitation and (at best) unselective relaxation analogous to the *laser distillation* approach. Alternatively, the excited state population is dumped into the minimum of the desired enantiomer by a second *enantioselective laser pulse* ($|v\pm\rangle \rightarrow |v\mathsf{R}\rangle$) to complete the purification. If the electronic excited

state is, however, dissociative, the undesired enantiomer may perish [40, 41]. Interestingly, *enantioselective laser excitation* even works if a degree of freedom is excited which does not directly support the transformation between the enantiomers, as shown by us for the pyramidalization of the terminal carbon atom at the double bond of (4-methyl-cyclohexylidene)fluoromethane [46, 47], indicating that the approach is not restricted to axially chiral molecules.

If a single linearly polarized *enantioselective laser pulse* is used, the orientation of the molecules with respect to the field becomes decisive. Thus, in an ensemble of randomly oriented molecules the enantioselectivity is lost. Possible extensions are circularly polarized laser pulses for axially chiral molecules freely rotating around their chiral axis [37], or two perpendicular propagating linearly polarized pulses for a random ensemble of unidirectionally oriented molecules [47].

Alternative approaches worth mentioning are based on *stimulated Raman adiabatic passage* (STIRAP) [48–51] or on multicomponent laser fields of non-coplanar polarization [52, 53]. Solá et al. and Ohta et al. developed STIRAP versions of the *parking mechanism* [48] and the *pump-dump* mechanism [49]. Král et al. combined an adiabatic passage type of two-photon transition with an one-photon transition to a phase-sensitive *cyclic population transfer* [50, 51]. These approaches have in common a high robustness with respect to the laser parameters and are, in particular, applicable to systems with fast decaying transition states. Zhdanov and Zadkov presented their version of laser driven racemate purification of randomly oriented molecules: They used multicomponent laser fields with non-coplanar polarization which coherently link states of the chiral doublets forming a chain of an odd number of electrodipole transitions [52, 53].

Although the purification of a racemate by laser pulses seems to be an attractive technique (if experimentally applicable), it can hardly compete with well-established techniques of asymmetric synthesis or even enantiomer separation via diastereomers[11]. The described laser pulses have, however, the advantage of not only being able to excite one enantiomer in the presence of the other, but also offering the possibility for a controlled transformation between (axially chiral) enantiomers. This fact may be used to design chiral molecular switches which change their handedness upon light irradiation, a task we want to address in this chapter.

In the last years the interest in molecular switches and motors jumped up due to their application as components of nanoscale devices [54]. Efforts to construct mechanical devices on molecular scale brought forth equivalences in form of, for instance, electrochemically driven pendula [55], temperature controlled turnstiles [56] or light induced switches [57]. In particular light-driven molecular functions, which often play a key role in natural processes, have been an inspiration for scientist to develop switches and rotors for molecular machines. Compared to

[11] That is, unless the laser control would allow to steer the reaction towards an enantiopure product making subsequent enantiomer separation unnecessary.

those driven by heat or chemical reactions, molecular machines driven by light have the advantage of being flexibly and efficiently addressable, even within a complex molecular environment, and show a fast response time, all due to the properties of light.

Among the first to synthesize molecular motors which perform a defined unidirectional rotation were Kelly et al. and Feringa et al. in 1999 [58, 59]. In both molecular motors chirality is actually a basic concept for the successful excitation of an unidirectional rotation. In the process, Feringa and coauthors managed to induce continuous rotation of a helically chiral alkene about its central C-C double bond by light and temperature, where all of the four chiral isomers are passed during a full rotation [59]. Based on a modified version of their light-driven rotor, Feringa and coworkers later presented a chiroptical molecular switch which changes its chirality upon monochromatic light-induced *cis-trans*-isomerisation. The process is fully reversible and allows for perfect stereoselectivity in both directions [60].

A variety of applications for chiroptical switches are possible in the field of nanotechnology, from liquid crystal displays to data storage and information processing [61]. Molecular switches may even trigger macroscopic movement, as shown e.g. for a liquid crystal film which may be bend along any direction due to azobenzene moieties in domains where they are aligned along the direction of the linearly polarized light [62]. When used as a dopant a chiral molecular switch may impart its (switchable) chirality to an achiral liquid crystal host and, thus, tune its physical [63] or optical properties, for instance, its reflection color [64], upon light irradiation. Eventually, a chiroptical switch may even be applicable as a light-controlled chiral catalyst.

In general, research on photo-switchable compounds has been focussed on *cis-trans* isomerisations, predominantly of azobenzene derivatives, and photocyclisation reactions [65, 66], as e.g. in simulations for the laser pulse controlled ring opening of 1,3-cyclohexadiene [67] or for the laser pulse driven double bond isomerisation of an axially chiral alkene derivative turning it into a molecular rotor [68]. Symptomatic for these isomerisations is the bond formation or breaking in the transition state, usually in an electronic excited state. But conformational changes which do not alter the bond grade may also serve as basis for photoswitchable systems. Umeda et al. performed quantum simulations for the optical isomerisation of helically chiral difluorobenzo[c]phenanthrene [69]. Moreover, Hoki et al. presented simulations for the change of chiral 1,1'-binaphthyl from its P- to M-form by torsion around a single bond employing optimal laser pulses [70]. Even nitrogen inversion may be induced by IR or UV laser pulses, as shown by us in quantum dynamical simulations for an azabicyclo[1.1.1]pentane derivative [71], which may also be turned into a chiral switch if substituted accordingly.

All above mentioned enantioselective laser control schemes (*laser distillation* [31], *parking mechanism* [36] and *enantioselective excitations* [38, 45]) require

certain properties of the chiral molecules and, therefore, are not equally well suited for the here investigated molecular switches. In the laser distillation via an electronic excited state [31], for instance, relaxation has to be waited for after every laser excitation step. The parking mechanism [36] depends on a series of state-to-state transition of specific symmetry putting a lot of restrictions to possible transitions. Therefore, following the success of the enantioselective laser pulse control for the selective preparation of a pure enantiomer from a racemate of (4-methyl-cyclohexylidene)fluoromethane [46], we sought for a more general approach to control the stereoisomerism of axially chiral molecules. A typical axially chiral molecule is a substituted biphenyl which supports up to four stereoisomers depending on the degree and symmetry of substitution. In particular, a 2,2'-fluorinated biphenyl supports four stereoisomers, namely two diastereomeric pairs of enantiomers, along the torsion about its central C-C single bond, see Fig. 2. Therefore, the developed pump-dump mechanism has to be *stereo*selective, i.e. *enantio*- and *diastereo*selective, in order to fully control the chirality of the molecule [72, A.1]. For a start, the goal of the control remains the purification of the racemate of the most stable stereoisomers, but now by a selective transformation of each enantiomer to the same chosen diastereomer. This approach allows for a full *stereoselective* laser pulse control, as described in the next section, Sec. 2.2.

In the subsequent sections these *stereoselective* laser pulses will be used to control the handedness of a new axially chiral molecular switch, Sec. 2.3, mounted on a surface, Sec. 2.5. As we will see later, laser control has to be further extended to account for different orientations of the switch on a surface, leading to the development of a new laser pulse optimization method, Sec. 2.4, and the consideration of coupled molecular degrees of freedom, Sec. 2.6. The chapter will be closed by discussing the restrictions of our laser pulse controlled chiral molecular switches and by looking at possible applications of them, Sec. 2.7.

2.2 Stereoselective laser control of axially chiral molecules [A.1]

Due to steric interactions of the 2,2'- and 6,6'-substituents, 2,2'-difluorobiphenyl is not planar but forms four stable chiral conformers, so-called atropisomers, distinguishable at very low temperature ($T < 30$ K). Fig. 2 depicts the two pairs of enantiomers, called aS_c/aR_c and aS_t/aR_t in the following, where the prefix a stands for axial [73]. The subindices c (= *cis*) and t (= *trans*) determine the relative positions of the two fluorine substituents pretending that the C-C single bond between the two phenyl rings was a double bond. Stereoisomers c and t are, therefore, diastereomers just like *cis*/*trans*-isomers.

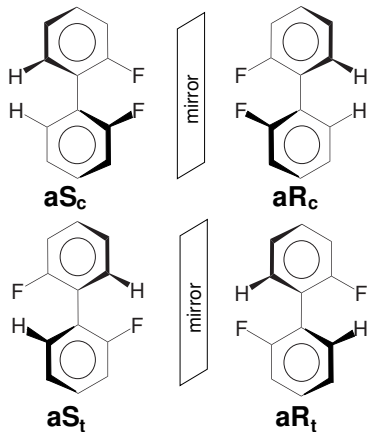

Figure 2: Four stereoisomers of 2,2'-difluorobiphenyl consisting of 2 diastereomeric (c = *cis* and t = *trans*) pairs of enantiomers (left and right of the mirror plane). Adapted from Ref. [72, A.1], with permission from Elsevier.

For the simulations the molecule is assumed to be oriented with its C_1-C'$_1$ bond along the z-axis, as shown in Fig. 3 (a). The degree of internal rotation is measured by the dihedral θ between C_2, C_1, C_1' and C_2', being 0° or 180° if the F-substituents become closest to or furthest away from each other, respectively. All other degrees of freedom are kept frozen in our rigid rotamer model. According to the four stereoisomers the potential energy curve exhibits four minima along θ, see Fig. 3 (a). The symmetry of the x- and y-components of the dipole moment $\vec{\mu}$ is either even or odd with respect to $\theta = 0/180°$, see Fig. 3 (b), which will be of importance for the desired stereoselective control with linearly polarized laser pulses [45].

Quantum mechanically the four stereoisomers are described by wavefunctions being localized in one of the four potential wells. These are obtained by either positive or negative superpositions of the respective *gerade* and *ungerade* eigenfunction of a doublet of eigenenergies [74]:

$$\Psi_{vS} = \frac{1}{\sqrt{2}} (\phi_{v+} + \phi_{v-}) \quad (1)$$

$$\Psi_{vR} = \frac{1}{\sqrt{2}} (\phi_{v+} - \phi_{v-}) \,. \quad (2)$$

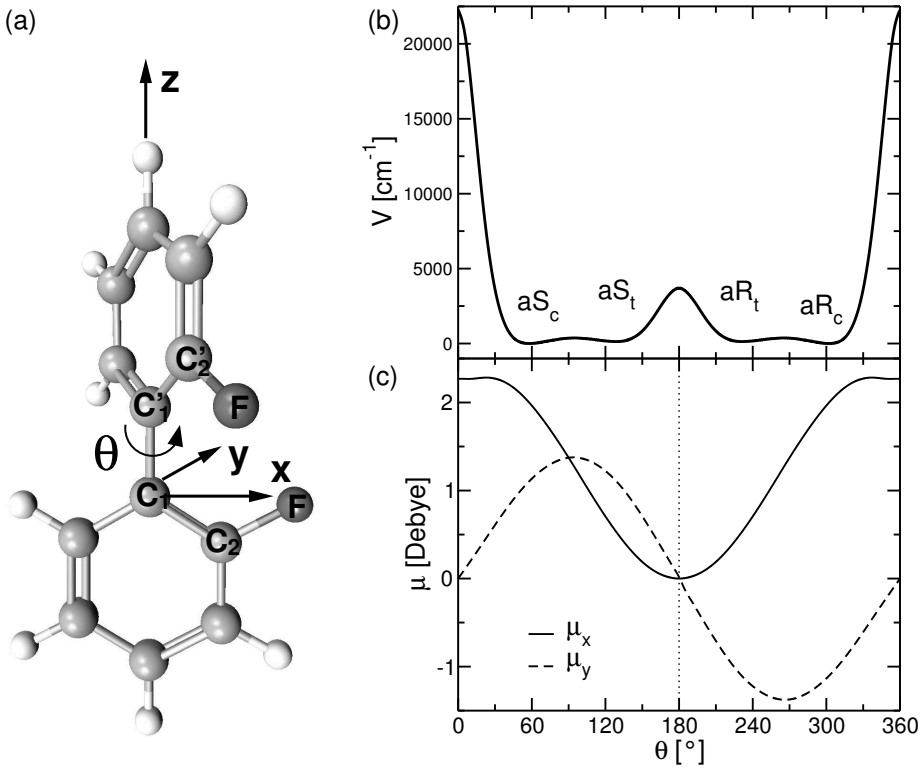

Figure 3: (a) Minimum energy conformer aR_c of 2,2'-difluorobiphenyl used as reference geometry for (b) the unrelaxed potential energy curve along θ, and (c) the x- and y-components of the dipole moment along θ (B3LYP/6-311+G(d)). Adapted from Ref. [72, A.1], with permission from Elsevier.

In analogy to a double well potential, the torsional eigenfunction $\phi_{v\pm}$ are denoted $+$ (*gerade*) if they are symmetric with respect to $\theta = 0/180°$ or $-$ (*ungerade*) if they are anti-symmetric, and cannot represent chirality because of this symmetry. Due to the two pairs of symmetric minima, doublets of almost degenerate eigenenergies $\varepsilon_{v\pm}$ appear below the *cis*/trans-barriers ($\theta = 90/270°$) whose corresponding eigenfunctions are entirely (or at least for the most part) localized in only one pair of the double wells. Therefore, it is possible to define localized wavefunctions $\Psi_{vS/R}$ for each diastereomer, where R and S refers to the corresponding enantiomer. These localized wavefunctions are no eigenfunctions of the system and their respective lifetime τ_v, i.e. the time to tunnel through the barriers ($\theta = 0/180°$) and become the mirror image, is anti-proportional to the energy splitting $\Delta\varepsilon_v = \varepsilon_{v-} - \varepsilon_{v+}$ of the doublet of eigenstates:

$$\Delta\varepsilon_v \; \tau_v = \frac{h}{2}. \tag{3}$$

Obviously, a (stable) chiral molecule is not represented by any of its quantum me-

chanical eigenstates,[12] a fact sometimes referred to as *Hund's paradox*. Without any claim to completeness, we just note here that, amongst other discussed effects, in particular environmental interactions, causing relaxation and dephasing, can prevent the localized wavefunctions from tunneling[13] or decaying into a pure eigenstate, making the experimental observation of stable enantiomers plausible, see for instance Ref. [75].

For 2,2'-difluorobiphenyl we found about ten doublets for each diastereomer whose lifetimes were sufficiently longer than the simulation time, allowing to spectroscopically monitor the success of the control or of subsequent chemical reactions, at least in principle. As initial state of the simulation the molecule is assumed to populate its lowest doublet of torsional eigenstates $\varepsilon_{0+/0-}$, i.e. at the low temperature limit ($T \to 0$ K), corresponding to a racemate of the aS_c- and aR_c-atropisomers, cf. Fig. 3 [36]:

$$\hat{\rho}(T \to 0\mathrm{K}) \approx \frac{1}{2}\hat{\rho}_{0+} + \frac{1}{2}\hat{\rho}_{0-} = \frac{1}{2}\hat{\rho}_{0S} + \frac{1}{2}\hat{\rho}_{0R} \equiv \hat{\rho}(t=0), \tag{4}$$

with $\hat{\rho}$ being the density operator $\hat{\rho} = |\Psi\rangle\langle\Psi|$. Note that, expression (4) becomes exact in the limit of $\Delta\varepsilon_0 \to 0$, i.e. for perfectly stable enantiomers. The goal is to simultaneously transform both energetically degenerate aS_c- and aR_c-enantiomers to only one of its diastereomers, for instance aS_t. Thus, not the direct purification of the racemate is desired here, but rather the preparation of a chosen stereoisomer with specific properties. This might be considered as switching the system from a "neutral" state, i.e. the optically inactive racemate, to an "activated" state of sought chirality and, hence, optical activity.

For now we account for the electric field-electric dipole interactions only and use the semi-classical dipole approximation, that is to say the interaction Hamiltonian $\hat{V}$ becomes:

$$\hat{V}(t) = -\vec{E}(t)\ \hat{\vec{\mu}}, \tag{5}$$

where the position dependence of the electric field $\vec{E}$ is neglected (as the wavelength is easily two orders of magnitude larger than the size of the molecule) and higher multipoles than the electric dipole $\vec{\mu}$ are ignored (which are typically at least two orders of magnitude smaller than the dipole).

In order to achieve the mentioned kind of chirality selective control, the laser pulses must be polarized such that the interaction of the electric field $\vec{E}$ with the transitions dipole moment vector which facilitate the *undesired* transition is suppressed. For an oriented molecule this may be achieved by choosing the polarization vector $\vec{e}_\alpha$ to be perpendicular to, for instance, $\langle\Psi_{vR}|\,\hat{\vec{\mu}}\,|\Psi_{v'R}\rangle$ rendering

[12] Parity violating weak interaction are not considered here.

[13] Note that in the limit of infinitely high tunnel barriers the eigenstates become pairwise degenerate and the tunneling times become infinite anyway.

the excitation of the R-enantiomer from v to v' impossible [38, 45]:

$$\vec{e}_\alpha \cdot \langle \Psi_{vR} | \hat{\vec{\mu}} | \Psi_{v'R} \rangle = 0 \quad (6)$$

$$\vec{e}_\alpha \cdot \langle \Psi_{vS} | \hat{\vec{\mu}} | \Psi_{v'S} \rangle \neq 0. \quad (7)$$

This implies that the desired transition, here $\langle \Psi_{vS} | \hat{\vec{\mu}} | \Psi_{v'S} \rangle$, is induced by the laser at the same time, i.e. the $\vec{e}_\alpha$ should not be perpendicular to all possible transitions. Here comes the symmetry of the components of the dipole moment into play: While one component remains the same (μ_x in Fig. 3 (b)), when comparing enantiomers, the other changes its sign (μ_y in Fig. 3 (b)). The results are non-parallel S- and R-transition dipole vectors allowing for the explained differentiation. Although condition (6) indicate that a successful control was only possible for oriented molecules, we will see later that this restriction may (partly) be resolved for surface-mounted molecules, see Sec. 2.5.

Conditions (6) and (7) (and their counterparts) enable us to independently excite (aS_c)- and (aR_c)-2,2'-difluorobiphenyl using linearly polarized pump pulses of the form:

$$\vec{E}(t) = \vec{e}_\alpha \; E_0 \; \cos(\omega \; (t - t_c) + \eta) \cdot s(t), \quad (8)$$

with ω being the transition frequency, η the phase, and E_0 the electric field amplitude. The shape-function $s(t)$ was chosen to be $\cos^2\left(\frac{\pi(t-t_c)}{2\mathsf{fwhm}}\right)$ for $|t - t_c| \leq \mathsf{fwhm}$ and zero otherwise, where fwhm is the full width at half maximum and t_c the center of the pulse. The polarization vector is given by $\vec{e}_\alpha = \vec{e}_x \cos\alpha + \vec{e}_y \sin\alpha$ ($\vec{e}_{x/y}$ are unit vectors). The polarization angle α is determined by equation (6) [46], for instance,

$$\tan\alpha = -\frac{\langle \Psi_{vR} | \mu_x | \Psi_{v'R} \rangle}{\langle \Psi_{vR} | \mu_y | \Psi_{v'R} \rangle}, \quad (9)$$

in order to exclusively induce the $vS \rightarrow v'S$-transition. A change of sign will change the enantioselectivity suppressing the $vS \rightarrow v'S$-transition completely.

In contrast to the various racemate purification schemes in the literature [31, 36, 45, 51], both enantiomers need to be excited in order to be transformed simultaneously to the selected diastereomer. This is accomplished by two simultaneous linearly polarized enantioselective pump pulses, followed by a dump pulse. The frequencies of both sub-pump pulses were chosen to be the same and match the excitation energy to the first excited torsional state, i.e. $\hbar\omega = \varepsilon_{1\pm} - \varepsilon_{0\pm}$. Although this implies a state-to-state transition, as promoted in previous investigations [31, 36, 45, 51], it actually causes a population ladder climbing resulting in a traveling wavepacket that corresponds to the torsion of the molecule. A direct state-to-state excitation to torsional states above the central barrier is inefficient anyway, because the overlap of the respective eigenfunctions is rather low requiring high field amplitudes for sufficient population transfer.

Two completely overlapping (same fwhm) linearly polarized laser pulses may result in a linearly or elliptically polarized laser pulse depending on whether their

frequency ω or phase η in Eq. (8) are equal or different. An overall linearly polarized pulse, however, results in synchronous torsion of both enantiomers making the preparation of the target state more challenging or even impossible due to the symmetry of the potential [72, A.1]. Hence, both linearly polarized pump subpulses were allowed to differ in η, fwhm and t_c, resulting in a non-linearly polarized pump pulse.

Fig. 4 shows the effect of the pump pulse in snapshots of the wavepacket dynamics, obtained from solving the time-dependent Schrödinger equation $i\hbar\frac{\partial\Psi}{\partial t} = (\hat{H}_0+\hat{V}(t))\Psi$ for the nuclear wavefunction $\Psi = \Psi(\theta;t)$, where $\hat{H}_0 = \hat{T}+V(\theta)$ is the molecular Hamiltonian for the transformation between the stereoisomers. Note that the laser induced torsion of the aS_c-enantiomer is not sufficient to overcome the central barrier ($\theta = 180°$); the conversion between the two S-diastereomers is, however, possible. The same pump pulse excites in turn the aR_t-enantiomer to a torsion which allows a conversion to any of the four stereoisomers.

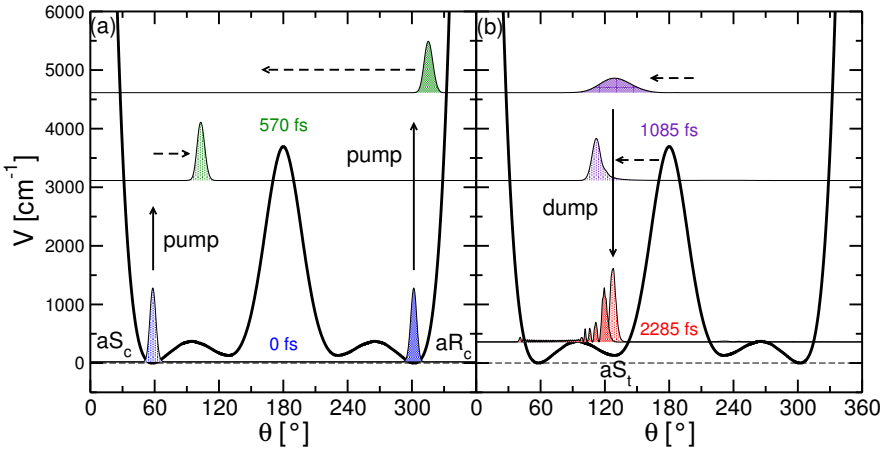

Figure 4: Snapshots of the wavepacket dynamics of the stereoselective conversion of a racemate into a pure diastereomer for specific times. Shown are the potential energy curve along θ as well as the density $|\Psi|^2$ of the wavepacket. The baseline of $|\Psi|^2$ corresponds to the total energy. Panel (a) shows the effect of the pump pulse on the wavefunction; the pump pulse ends at t = 570 fs. Panel (b) shows the result of the dump pulse which starts at t = 1085 fs and ends at t = 2285 fs. Adapted from Ref. [72, A.1], with permission from Elsevier.

The dump pulse is then timed such that it simultaneously de-excites the wavepacket of both enantiomers into the sought aS_t potential well. Its frequency is tuned to match the transition frequency between the two lowest doublets of the t-enantiomers causing a ladder descent to the lower doublets. The pulse is linearly polarized according to expression (9) to ensure that only the aS_t-enantiomer is affected, i.e. it can be considered diastereoselective. At the end of the dump pulse the wavepackets are localized in the aS_t minimum, see Fig. 4, where they remain

for the most part, because the population of the respective eigenstates, which are well below the barriers, add up to a total of about 75%. Its enantiomer, (aR_t)-2,2'-difluorobiphenyl, may be obtained by simply changing the sign of α of all three subpulses.

In summary, the concept of enantioselective laser pulses [38, 45] was generalized to selectively excite any stereoisomers of oriented axially chiral molecules, including diastereomers. Thus, the laser pulses are considered to be enantio- and diastereoselective or, more generally speaking, stereoselective. In addition, we showed that the laser pulses do not have to directly excite an eigenstate of specific symmetry above the torsion barriers or in an electronic excited potential [31, 36, 45, 51] in order to control molecular chirality. In a real molecule with energetically close lying (and possibly coupled) torsional and vibrational states of several degrees of freedom single transitions between eigenstates of specific symmetry will be difficult to achieve anyhow (for ultrashort pulses even more), even if selection rules are still valid for the most part. For the stereoselectivity, however, only the polarization of the laser is crucial. Here we realized that a non-linearly polarized pump pulse was used to selectively control two enantiomers simultaneously, although the molecules were assumed to be oriented. This is already a hint that the requirement of perfect orientation may be overcome.

The chosen model might be considered a simplification of common experimental examples for axially chiral molecules, for instance 1,1'-bi-2-naphthol (BINOL), a ligand for transition-metal catalysed asymmetric synthesis and a precursor for another axially chiral ligand 2,2'-bis(diphenylphosphino)-1,1'-binaphthyl (BINAP). Although the structure of 2,2'-difluorobiphenyl may safely be considered rather rigid, including for instance bending modes into our model would most certainly change the height of the barriers. However, as long as four stereoisomers are distinguishable, the proposed approach will still work and is not restricted to molecules with axial chirality. Yet, degrees of freedom coupled to the investigated torsion, as e.g. the overall rotation of the molecule, see e.g. Ref. [37] and Sec. 2.6, will make the control more challenging and possibly decrease its efficiency. Intramolecular vibrational redistribution (IVR) of the energy could, in contrast, even help to localize the wavepackets in the desired minimum.

Being able to selectively address chiral stereoisomers with laser pulses allows to induce conversion between them. For a molecule with a chiral axis this means its chirality may be *switched* by light, changing its optical activity and its reactivity in the presence of other chiral molecules. A molecule might also have an *achiral* stereoisomer due to a n-fold improper rotation axis ($n = 1$: mirror plane, $n = 2$: centre of inversion, $n > 2$: n-fold rotation-reflexion axis). Is this symmetry element lost by an isomerisation, the chirality of the molecule may be "switched on" using stereoselective laser pulses. This will be focus of the next section, Sec. 2.3.

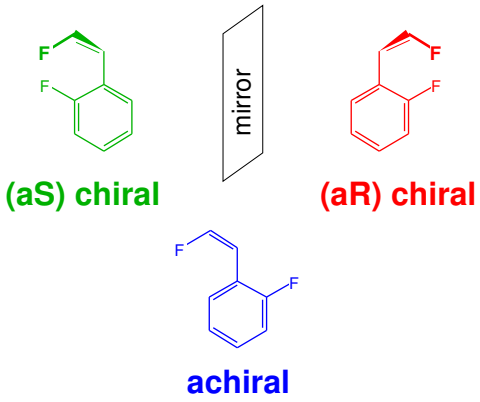

Figure 5: Three stereoisomers (atropisomers) of 1-(2-*cis*-fluoroethenyl)-2-fluorobenzene, two of them being chiral (green and read enantiomers) and one being achiral (blue).

2.3 Laser-operated chiral molecular switches [A.2]

By removing, formally stated, four carbon atoms of one of the benzene rings of 2,2'-difluorobiphenyl one can construct the di-fluorinated styrene derivative 1-(2-*cis*-fluoroethenyl)-2-fluorobenzene. In its most stable conformation all atoms are in plane resulting in C_s-symmetry. Thus, this conformation is achiral. Furthermore, a torsion around the central C-C single bond, connecting ethenyl and phenyl group, destroys the reflection symmetry and brings forth two more atropisomers which are axially chiral. Just as in case of the biphenyl derivative, the stability of these conformers results from the balance of steric interactions between the fluorine substituents and the loss of of conjugation between the aromatic system of the benzene ring and the double bond of the ethenyl group. Fig. 5 shows the achiral stereoisomers and its diastereomers, the two enantiomers (aS) and (aR).[14]

The model is based on the same assumptions as before, see Sec. 2.2: The molecule is oriented and only the internal rotation of the ethenyl group with respect to the (fixed) phenyl group, determined by the dihedral angle θ, is taken into consideration. The resulting symmetric triple well potential curve of the electronic ground state is shown in Fig. 6. At room temperature the achiral isomer, corresponding to the central minimum ($\theta = 180°$), is almost exclusively found. In addition, the potential energy surfaces along θ of electronic excited singled states were calculated by time-dependent density functional theory (TDDFT), in order to offer reaction paths that may be induced by stereoselective UV-pulses.

The torsional eigenfunctions are either exclusively localized in the central well or in both outer wells ($\theta \approx 50/310°$) characterizing the achiral isomer or the pair of enantiomers, respectively. In case of the outer wells the central minimum acts just like a barrier and doublets of near degenerate eigenenergies are formed due to symmetry. This allows for the construction of localized wavefunctions according

[14]Stated nomenclature is in accordance with Cahn-Ingold-Prelog conventions [73], and will be used throughout the following sections. Differences with respect to references given in Appendix A are due to the opposite direction of rotation of the ethenyl group around the z-axis of the right-handed Cartesian coordinate system, cf. e.g. Fig. 8 in Sec. 2.4 with Ref. [76, A.2].

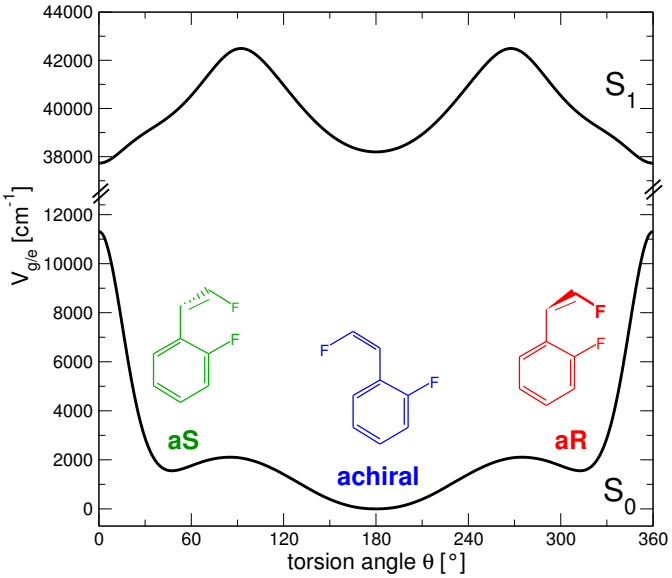

Figure 6: Potential energy surface of 1-(2-*cis*-fluoroethenyl)-2-fluorobenzene along θ for the electronic ground state V_g and the next singlet excited state V_e (TD-B3LYP/6-311G(d)). Adapted from Ref. [76, A.2].

to Eqs. (1) and (2) which are entirely localized in either the left or right outer minimum corresponding to the (aS)- or (aR)-enantiomer. Altogether ten doublets of eigenstates were considered to be practical to represent stable enantiomers, as due to their splitting their lifetimes are, according to Eq. (3), at least three orders of magnitude longer than the simulation time. For eigenenergies close to or above the top of the low barriers ($\theta \approx 85/275°$) eigenfunctions are getting delocalized over all three potential wells making a distinction of the stereoisomers virtually impossible.

The main goal of the developed laser pulse control is to enantioselectively turn on the chirality of the molecule or to switch between its enantiomers. Thus, the molecule is initially achiral, i.e. the initial state of the quantum dynamics is the (fully populated) torsional ground state ($T \to 0$ K). The separation of mixtures of stereoisomers, e.g. a racemate, are not considered here anymore. Any mixture would for this model eventually convert to the most stable achiral conformer due to energy relaxation (if accounted for). The achiral stereoisomer may be seen as the true "off"-state of the chiroptical switch, eliminating all optical activity.[15]

The pulse sequence consists of a non-stereoselective pump pulse, which induces internal rotation, and a enantioselective dump pulse, which prepares the desired chiral form of the molecule. Both pulses are linearly polarized. The dump pulse is, however, polarized according to condition (9) to ensure that only the correct enantiomer is obtained. Here the (aR)-enantiomer is to be prepared, i.e. the sign of the angle α in equation (9) has to be changed (or the Ψ_{vR}'s have to be exchanged by Ψ_{vS}'s). In addition, the frequency of the electric field in Eq. (8) is

[15]Note that a racemate is not achiral although it is optically inactive.

now allowed to vary linearly with time:

$$\omega(t) = \omega_0 + \lambda\ (t - t_c) \tag{10}$$

where λ is the chirp rate, i.e. $\frac{d}{dt}\omega$. The pulse has an up-chirp for $\lambda > 0$ and down-chirp for $\lambda < 0$; for $\lambda = 0$ it is unchirped. The chirp is needed to better adjust to the change in the energy spacing of the eigenstates when going towards the top of the lower barriers. The optimized pulse sequences selectively induces the transformation from the achiral to the (aR)-conformation, see snapshots of the density $|\Psi|^2$ of the wavepacket in Fig. 7. After the laser is turned off, the wavepacket stays well localized in the right potential minimum, corresponding to the (aR)-enantiomer, as observed by the expectation value of the torsional angle $\langle\theta\rangle\,(t)$ (not shown, see Ref. [76, A.2]). This is further confirmed by small oscillations around zero of the expectation value of the angular momentum $\langle l\rangle\,(t)$ (not shown, see Ref. [76, A.2]). A population analysis yields about 95% of the population in the "chiral" states 0R to 10R with more than 75% being found in the two lowest states with the longest lifetimes. Less than 1% was transferred to any of the S-states.

The enantioselectivity of the dump pulse may be proven by changing the phase η of the pump pulse by π alternating the direction the wavepacket initially moves. If the control was only based on the correct timing of the pulses the opposite enantiomer should be prepared. However, the R-selective dump pulse will still be selective, preventing the (aS)-enantiomer to be prepared, although the wavepacket resides "above" the left potential well when the dump pulse sets in [76, A.2]. Thus, the population gets spread over eigenstates above the lower barriers making a distinction between the stereoisomers impossible. To successfully prepare the (aS)-enantiomer the sign of the polarization angle α of the dump pulse had to be changed.

In an alternative laser control approach, the first singlet electronic excited energy surface V_e (Fig. 6) may be used as intermediate state to make the molecule chiral. Here the timing of the IR and UV pulses ensures that the desired handedness is obtained [76, A.2]. Transitions via the electronic excited states may also be utilized to switch the chirality of the system after the chirality had been turned on, or to initiate an unidirectional intramolecular rotation after an initial IR pump pulse. In the latter case a nearly constant angular moment is maintained by a sequence of chirped UV pulses which is timed such that the momentum gained by the form of the potential is transferred during electronic excitation. The resulting unidirectional continuous torsion turns the system into a laser-driven molecular rotor [68,77]. However, energy relaxation and dephasing need to be defeated to maintain a long lasting rotation.

Also in case of a laser-controlled chiral molecular switch, the achieved handedness will be lost with time due to energy relaxation, for instance via intramolecular vibrational energy redistribution (IVR). However, the system will merely return

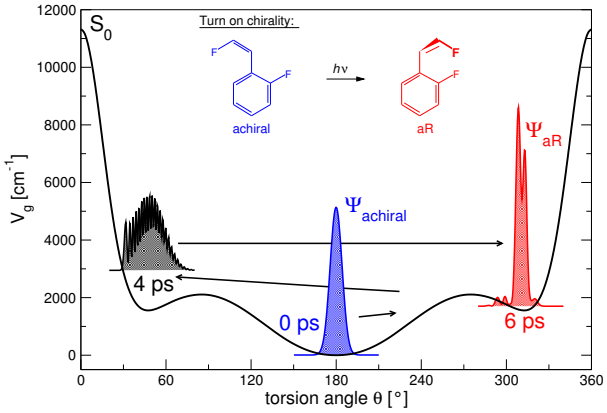

Figure 7: Snapshots of the wavepacket dynamics of the laser pulse induced enantioselective turning-on of (*aR*)-chirality for the axially chiral molecular switch 1-(2-*cis*-fluoroethenyl)-2-fluorobenzene. Shown are the potential energy surface V_g along the torsion angle θ and the densities $|\Psi|^2$ of the wavepacket at times $t = 0$ (blue), $t = 4$ ps (black, end of the pump pulse) and $t = 6$ ps (red, 200 fs after the end of the dump pulse). The baseline of $|\Psi|^2$ corresponds to its total energy.

to its achiral "off" position from where it can be switched on again. This stable achiral state is an unique feature of our chiral molecular switch. The chiroptical switch of, for instance, Feringa et al., a methyl substituted biphenanthrylidene connected by a C=C double bond, undergoes essentially a *cis-trans*-isomerisation upon excitation with light, transforming one chiral stereoisomer into its diastereomer (or vice versa) [59]. The helicity of each phenanthrylidene half of the structure is switched simultaneously, however returns thermally activated spontaneous to its stable (P,P)-form (P and M denote plus/right- and minus/left-handed helices).[16] The chirality can, therefore, not be turned on or off like in the case of our model system.

All control scenarios investigated so far required a high degree of molecular orientation for perfect stereoselectivity of the laser pulses. Although there are several ways to orient molecules in the gas phase employing laser pulses [78–81], physisorption or chemisorption on a surface can also result in certain degree of orientation of the adsorbate depending on its linkage to the surface. Experiments even show that enantiomers may align to form domains of unique chirality on metal surfaces [82, 83] which supports the idea of using a substrate-linked chiral switch. In the next section, Sec. 2.4, we will deal with the question how to extend the stereoselective laser control for an ensemble of adsorbed chiral switches with multiple defined orientations. A new genetic kind of pulse optimization algorithm will be introduced to handle the task.

[16] That is why they called it a light-driven unidirectional molecular rotor in the first place.

2.4 Stochastic pulse optimization [A.3]

Conditions (6) and (7) for the polarization of an enantioselective laser pulse are easy to fulfill for a single state-to-state transition in an oriented molecule. Although a differing orientation might simply decrease the efficiency of the desired transition due to larger angle between polarization, $\vec{e}_\alpha$, and transition dipole, e.g. $\langle\Psi_{vS}|\,\hat{\vec{\mu}}\,|\Psi_{v'S}\rangle$, it may also result in an efficient excitation of the wrong enantiomer if the rotated $\langle\Psi_{vR}|\,\hat{\vec{\mu}}\,|\Psi_{v'R}\rangle$ becomes equal to the initially fixed $\langle\Psi_{vS}|\,\hat{\vec{\mu}}\,|\Psi_{v'S}\rangle$. In other words, we can always find an unitary transformation to make the (R)-enantiomer look like the (S)-enantiomer for a fixed linearly polarized laser, as a single vector carries no chiral information in three-dimensional space. Following this logic, three different, linear independent transition dipole vectors of that kind had to interact with three linearly polarized laser pulses of non-parallel propagation direction[17], in order to distinguish enantiomers of random spatial distribution.

If the molecules are, however, linked to a surface effectively reducing their number of orientations with respect to the laser light, the problem may be even reduced to two-dimensional space. In two-dimensional space two different, linear independent transition dipole vectors are enough to distinguish enantiomers. No rotation by the surface normal can make them congruent. Then, two linearly polarized laser pulses propagating along the surface normal are sufficient for an enantioselective excitation. As their polarization angles α and their frequencies ω must differ to interact selectively with two different, non-parallel transition dipole vectors, the resulting polarization becomes non-linear if the pulses overlap.

While it is, in general, easy to apply expressions (6) and (7) to two different enantioselective transitions, the orthogonality condition (6) would still hold only for two specific orientations[18] of the molecule. The goal is, however, to achieve enantioselectivity for as many orientations as possible. Furthermore, it is not obvious which two transitions to choose, in particular, if a torsional wavepacket is to be created as before. The design of optimal laser pulses is, therefore, left to a numerical optimization [84, A.3].

In the following, the chiral switch is supposed to be chemisorbed directly or via an adequate linker group to a well-defined rigid surface, such that its chiral axis aligns with the surface normal (z-axis), see Fig. 8. We further assume that the frameworks of molecule and linker are rigid and do not significantly change during the laser-driven torsion (θ). Then, the number of possible orientations of the molecule on the surface depends only on its rotational symmetry. For periodic structures rotational symmetries C_n with $n = 1, 2, 3, 4$, and 6 are possible. The angle φ_j, see Fig. 8, defines all possible orientations of the molecule on the surface

[17] Two pulses may propagate parallel as two (polarization) vectors may always be chosen coplanar but non-parallel.

[18] A rotation by π around the surface normal has the same effect as $\alpha \pm \pi$ or $\eta \pm \pi$.

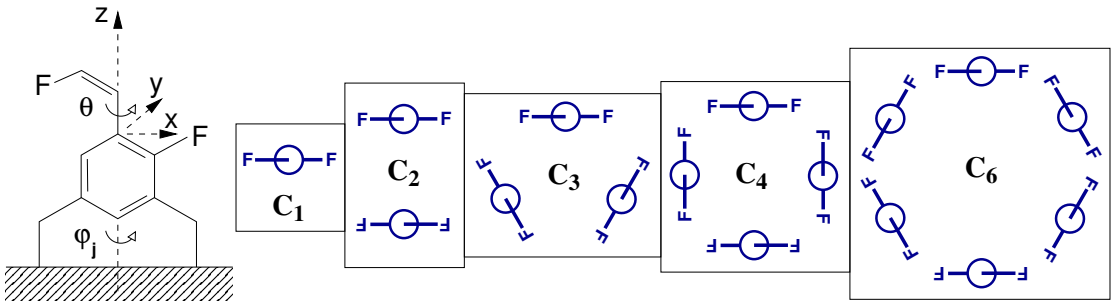

Figure 8: 1-(2-*cis*-fluoroethenyl)-2-fluorobenzene adsorbed on a rigid surface with its chiral axis aligned with the surface normal z. The angles θ and φ_j describe the internal rotation (torsion) and the rotational orientation of the molecule on the surface, respectively. For each rotational symmetry C_n ($n = 1, 2, 3, 4, 6$) all possible orientations of the chiral switch are shown schematically when looking against the direction of the surface normal.

for a given symmetry n:

$$\varphi_j = j \cdot \Delta\varphi, \qquad j = 0, ..., n-1, \tag{11}$$

where $\Delta\varphi = \frac{2\pi}{n}$. Altogether five sets of different numbers of orientations have to be investigated to treat all possible symmetries of the surface, see Fig. 8.

For sufficiently large linker groups or low coverage of isolated molecules, long range intermolecular interactions can safely be neglected. Then, the different molecular orientations are modeled by an incoherent ensemble of wavefunctions $\Psi^{(j)}(t)$, which are completely decoupled, but driven by the same space-fixed laser. Thus, for each orientation j the time-dependent Schrödinger equation is solved separately. The potential energy surface is not influenced by the orientation for the reasons given above, and is, for a start, assumed to be unaffected by the presence of surface or linker group, see Fig. 6. However, different orientations differ in the orientation of their dipole moment with respect to the space-fixed laser. If $j = 0$ denotes the initial orientation of the switch (corresponding to the conditions in Sec. 2.3), then the components of the dipole moment for each orientation j are generated by rotation:

$$\begin{pmatrix} \mu_x^{(j)}(\theta) \\ \mu_y^{(j)}(\theta) \\ \mu_z^{(j)}(\theta) \end{pmatrix} = \begin{pmatrix} \cos(\varphi_j) & -\sin(\varphi_j) & 0 \\ \sin(\varphi_j) & \cos(\varphi_j) & 0 \\ 0 & 0 & 1 \end{pmatrix} \begin{pmatrix} \mu_x^{(0)}(\theta) \\ \mu_y^{(0)}(\theta) \\ \mu_z^{(0)}(\theta) \end{pmatrix}, \tag{12}$$

which makes the interaction Hamiltonian (5) orientation-dependent: $\hat{V}^{(j)} = -\vec{E}(t)\ \hat{\vec{\mu}}^{(j)}(\theta)$.

The aim of the laser control is as before: The chirality of the molecule shall be "switched on" enantioselectively. This is, however, to be best accomplished

for *all* orientations j of symmetry C_n. Let the target states to be those states whose eigenfunctions can be combined to form "chiral" wavefunctions localized, for instance, in the right potential well ($\theta \approx 310°$), i.e. Ψ_{vR}. Then we seek a laser pulse that maximizes the population P of those states for all orientations j of the switch at final time t_f:

$$P^{(j)} = \sum_v \left| \langle \Psi_{vR} | \, \Psi^{(j)}(t_f) \rangle \right|^2 , \tag{13}$$

where the sum includes all localized states with a sufficient lifetime, see Sec. 2.3.

There are well-known approaches to optimize laser pulses for a given target, like *optimal control theory* (OCT) [85,86] employing rapidly convergent iteration algorithms [87,88]. Here we face some challenges in molecular control that would require an extensive modification of the commonly used optimal control algorithms: First of all, the initial wavefunction (torsional ground state, see Sec. 2.3) and the target states have literally no overlap. Therefore, the transition dipole moments between them vanish causing convergence problems, because the laser field is usually generated, inter alia, from the transition dipole moment with the target states. This makes a suitable guess for the initial laser field or an elaborated population seeding of possible intermediate states necessary to steer the quantum system towards the target. Secondly, a laser pulse optimal, that is stereoselective, for one orientation needs not be so for the others. In analogy to the example given in Sec. 2.3, the direction the wavepacket initially moves could be flipped if the molecule was rotated around the surface normal by $\varphi_j = \pi$ steering the system eventually towards the unwanted outer minimum. In order to prevent the algorithm to converge to a pulse which is stereoselective for one orientation but unselective[19] for the others, the population of the target states in Eq. (13) should be maximized for all possible orientations *simultaneously*. This is best approached by requiring the *product* (as opposed to the sum) of the target populations of all orientations to become maximal [84, A.3]:

$$F = \left(\prod_{j=0}^{n-1} P^{(j)} \right)^{\frac{1}{n}} . \tag{14}$$

Here F is called the fitness and measures the success of the applied laser pulse. The flexibility required for the functional form F that specifies the optimal target, plus the control challenges mentioned above, made us develop a new stochastic pulse optimization (SPO) [84, A.3]. This method is inspired by theoretically proposed [89] and experimentally applied evolutionary algorithms [90, 91]. For it, the electric field is assumed to be completely decomposable in a truncated

[19] States above the small barriers will stay populated.

Fourier series of f frequency components:

$$\vec{E}(t) = \frac{\tilde{\omega}}{\sqrt{\pi}} \sum_{l=0}^{f} \left[\vec{A}_{(l)} \ \cos(l \cdot \tilde{\omega}\ t) + \vec{A}_{(l+f+1)} \ \sin(l \cdot \tilde{\omega}\ t) \right] \cdot s(t), \tag{15}$$

in the time interval $[0, t_p]$. Here the lowest frequency is limited by the pulse duration t_p:[20]

$$\tilde{\omega} = \frac{\pi}{t_p}, \tag{16}$$

i.e. the electric field is composed of integer multiples of the minimum frequency $\tilde{\omega}$. In other words, we introduced an overcomplete – because partially linear dependent due to definition (16) – set of $f+1$ basis functions for a signal bandlimited up to the cutoff frequency $f_{max} = f \cdot \tilde{\omega}$. We chose t_p and f to cover the time and frequency range of the stereoselective pulse for the fully oriented switch presented in Sec. 2.3. Then the stochastic algorithm initially determines the $2(f+1)$ amplitude vectors $\vec{A}_{(l)}$ randomly for a certain number of trial laser pulses. To ensure realistic laser fluences, the amplitude vectors are normalized. Then, the fitness for each trial pulse is determined and a new generation of pulses is generated through random mutation. Thereby the amplitude vectors of each pulse are altered according to $\vec{A}_{(l)} + \mathcal{R} \cdot M \cdot \vec{A}_{(l)}$, where $\mathcal{R}$ is a uniformly distributed random number in $[-1, 1]$ and M an adjustable mutation strength. There is, however, no mixing (or crossover) between the parameters of two different pulses, in contrast to a typical genetic algorithm. After renormalization, the mutated pulses are tested as well and the fitnesses of all pulses (parents and children) are compared. The less fit half of pulses is discarded while the fittest half is used to repeat the described steps until convergence is achieved.

For each symmetry C_n an optimal pulse is obtained. All pulses are nonlinearly polarized, as expected, and are highly stereoselective regardless of the orientation j of the switch. If the target is, for instance, the (aR)-enantiomer, less than one percent of the total population (summed up over all orientations j) is found in S-states. The efficiency of the control is, however, decreasing with increasing number of orientations n. While for $n = 1, 2, 3$ and 4 the predominant part of the population ($> 75\%$) is found in the desired target states, more population is lost to higher excited torsional states (above the low barriers) for some orientations j in case of $n = 6$. For C_6-symmetry the electric field components of the optimized pulse and the resulting time evolution of the expectation values of the torsion angle for each individual orientation of the molecule, $\langle\theta\rangle^{(j)}$, are shown in Fig. 9. Although no clear mechanism can be extracted from all $\langle\theta\rangle^{(j)}(t)$, for most orientations ($j = 0, 2, 3, 4$) we observe a period of torsional excitation of the achiral form (up to $\approx 3.5 - 4.0$ ps) followed by a rather quick enantioselective dump into the right potential well ($\theta \approx 310°$). Only orientations $j = 1$ and 5

[20] Except for the constant field component ($l = 0$, i.e. $\tilde{\omega} \to 0$).

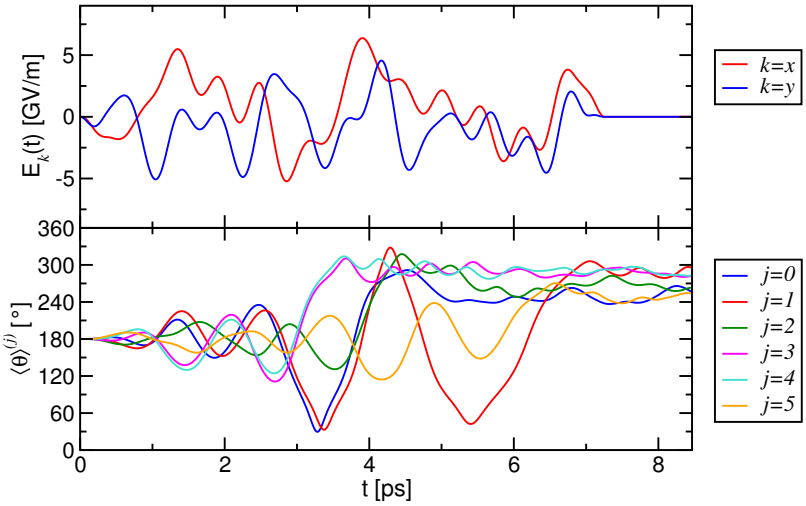

Figure 9: Components of the electric field $\vec{E}(t)$ obtained from stochastic pulse optimization and time evolution of the expectation value of the torsion angle, $\langle\theta\rangle$, for each orientation j of $n = 6$ orientations of the molecular switch on the surface. The target was the (aR)-stereoisomer. Adapted from Ref. [84, A.3].

seem to be trapped in their (aR)-form at a later time ($t > 6.5$ ps). As one can observe in Fig. 9, the efficiency for orientations $j = 0$ and 5 is lower than for the others, because higher excited states are populated, too, causing the expectation value to deviate more from the value of the right minimum.

In order to switch the achiral isomer selectively to the stereoisomer of opposite chirality – in this case the (aS)-enantiomer – the field $\vec{E}(t)$ has to be reflected at the xz-plane, that is changing the sign of its y-component. The former R-selective pulse becomes thus S-selective [84, A.3].

At this point we have a rather sketchy perception of how the molecular switch might be linked to a surface and how the resulting different orientations of the molecule may become a challenge for stereoselective laser pulse control. In the following section we want to extend our model by introducing a real linking group, accounting for its influence on the switch, and by analysing stochastic optimized stereoselective pulses to understand what are the requirements for making them stereoselective regardless of the molecular orientations.

2.5 Surface-mounted chiroptical switch [A.4]

The surface linking schematically depicted in Fig. 8 of the previous section is experimentally rather difficult to achieve for the here investigated chiroptical switch. In addition, it may even cause the molecule to "fall over" such that the benzene ring lies flat on the surface making switching difficult if not impossible. Therefore, the switch will be attached to a rigid molecular frame, in the following,

which may act as a linker. We chose to bind the molecule in *para*-position of the phenyl ring to adamantane, see Fig. 10. The adamantyl can be turned into a rigid molecular tripod if, for instance, provided with thiol "legs" resulting in the formation of self-assembled monolayers on Au(111) [92]. It may also act as a model of a (non-metal) surface of C_3-symmetry with respect to the surface normal, which would immobilize the switch even more.

In any case, the molecular switch cannot easily bend its chiral axis – which runs along the atoms C2, C3 and C4 – far away from the surface normal, the z-axis in Fig. 10. However, a rotation of the molecular switch around the surface normal, or more precisely around the C1-C2-single bond, is now possible. Then again, this rotation is sterically hindered by the *meta*-substituents of the phenyl ring, i.e. H-atoms at C7 and C7' for the currently investigated switch. These *meta*-substituents may also be exchanged by sterically more demanding groups, resulting in three stable conformations, as we will see later. For now we will pretend that our chiroptical switch has only three different, but energetically degenerate, orientations due to the C_3-symmetry of adamantyl linker/surface. Therefore, the angle φ_j – that is the dihedral between C7, C2, C1 and C6 – is now defined for $j = 0, 1, 2$ with $\Delta\varphi = \frac{2\pi}{3}$, cf. Eq. (11).

Because the adamantyl frame is in *para*-position to the fluoroethenyl group, the potential energy surface along the torsional angle θ qualitatively resembles that of the free 1-(2-*cis*-fluoroethenyl)-2-fluorobenzene, cf. Fig. 6 of Sec. 2.3. There are some quantitative differences mainly due to restrictions of the model applied to enforce three energetically degenerate orientations. Most significantly is the lowering of the minima characterizing the two enantiomers, causing the number of long living localized wavefunctions, Ψ_{vS} and Ψ_{vR}, to increase to fifteen. This increase in the stability of the enantiomeric isomers is, however, rather caused by the model setup than by the interactions with the adamantane, see Ref. [93, A.4] for more details.

Before investigating how to control the surface-mounted switch, let us go back to the stereoselective control of the free and optimally oriented system, i.e. $j = 0$ in the present case. The requirement for the polarization of the electric field was expressed in Eq. (9) of Sec. 2.2 for the exclusive impact on the (aS)-enantiomer. According to Eq. (12) we may include the orientation angle φ_j into Eq. (9) to get:

$$\tan(\alpha^{(0)} + \varphi_j) = -\frac{\langle \Psi_{vR}| \, \mu_x^{(0)} \cos(\varphi_j) - \mu_y^{(0)} \sin(\varphi_j) \, |\Psi_{v'R}\rangle}{\langle \Psi_{vR}| \, \mu_x^{(0)} \sin(\varphi_j) + \mu_y^{(0)} \cos(\varphi_j) \, |\Psi_{v'R}\rangle} \tag{17}$$

where $\alpha^{(0)}$ is now the optimal polarization angle for a S-selective excitation for the orientation $j = 0$ ($\varphi_0 = 0°$). In other words, the $\alpha^{(j)}$ optimal for orientation j is given by

$$\alpha^{(j)} = \alpha^{(0)} + \varphi_j \tag{18}$$

which is self-evident, because both $\vec{\mu}$ and $\vec{E}$ are rotated about the z-axis by the same angle to make the induced transition stereoselective. This means, however,

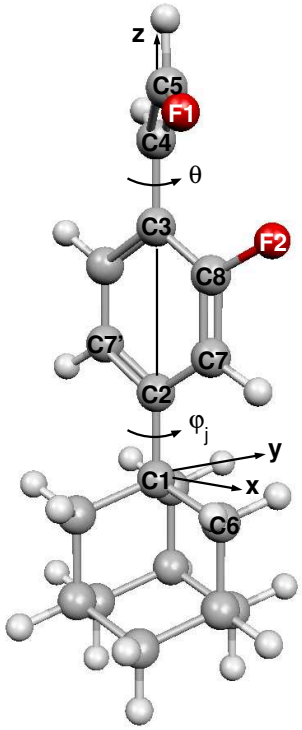

Figure 10: Minimum energy geometry of the (*aR*)-stereoisomer ($\theta = 320.6°$) of 1-(2-*cis*-fluoroethenyl)-2-fluorobenzene mounted on adamantane for $\varphi_0 = 0°$, B3LYP/6-311G(d). The molecule is oriented in the shown space-fixed coordinate system with specific geometrical parameters being fixed to ensure perfect alignment of the chiral axis with the z-axis. Adapted with permission from Ref. [93, A.4]. Copyright 2008 American Chemical Society.

that we cannot apply *simultaneously* three linearly polarized stereoselective laser pulses of that kind[21], each optimal for one orientation, because the result would be a zero field, i.e. $\sum_{j=0}^{2} \vec{e}_\alpha^{\,(j)} = \vec{0}$, due to

$$\sum_{j=0}^{n-1} \cos(\alpha^{(0)} + j\Delta\varphi) = \sum_{j=0}^{n-1} \sin(\alpha^{(0)} + j\Delta\varphi) = 0 \tag{19}$$

for any rotational symmetry $n > 1$ ($n \in \mathbb{N}$) and $\Delta\varphi = \frac{2\pi}{n}$. Then again, if those linearly polarized pulses are shifted in time or differ in their duration (fwhm), their phase η or frequency ω, as defined in Eq. (8), the resulting laser field will not be zero any more. It will also not be entirely linearly polarized, unless the subpulses do not overlap in time at all. This observation is consistent with the findings in Sec. 2.4 where chirality in two dimensions was discussed.

In spite of these considerations, the design of a laser pulse stereoselective for all orientations is still not straightforward. Therefore, the optimal stereoselective laser pulse was initially obtained from stochastic pulse optimization [93, A.4], as described in Sec. 2.4. Afterwards, a detailed analysis of the calculated pulse in terms of the time-frequencies distribution (quasiprobability distribution after Husimi [94]), specific expectations values and the populations dynamics enabled us to design a sequence of four subpulses consisting of eight (pairwise overlapping)

[21] Identical accept for α.

linearly polarized laser pulses of the analytical form given in Eq. (8) and optimize their parameters by hand. This "analytical" laser pulse sequence and the resulting time evolution of the expectation value of the torsion angle, $\langle\theta\rangle$, are shown in Fig. 11.

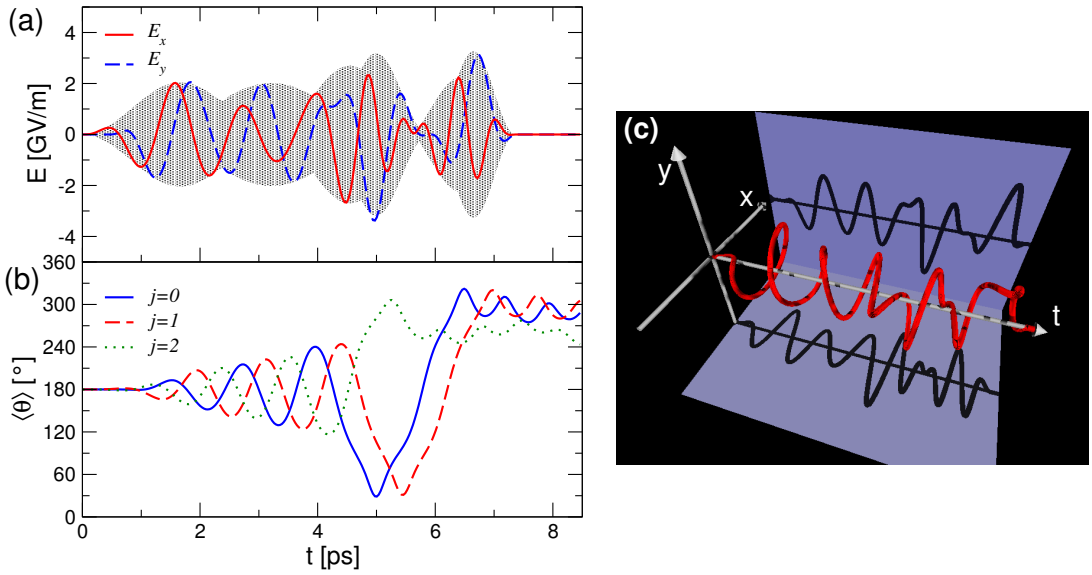

Figure 11: Stereoselective transformation of the achiral conformer of 1-(2-*cis*-fluoroethenyl)-2- fluorobenzene mounted on adamantane to its (aR)-isomer by a laser pulse sequence of optimized subpulses of analytical form (8). Time evolution (a) of the x- and y-component of the electric field (gray shading represent pulse shapes $s(t)$), (b) of the expectation value of the torsion angle θ, (c) of the electric field $\vec{E}(t)$ of the R-selective laser pulse in three-dimensional representation. Adapted with permission from Ref. [93, A.4]. Copyright 2008 American Chemical Society.

Although the overall[22] yield of the (aR)-enantiomer is with about 79% slightly lower than in the case of the initial SPO-pulse (∼85%), the enantioselectivity is very high, because less than 1% of the overall population is found in the S-states. The remaining population is distributed among states whose wavefunctions are either localized within the central "achiral" well (∼6%) or above the lower barriers (∼15%). Even more important is that a very high stereoselectivity is achieved for each single orientation of the switch on adamantane which can be observed, for instance, from the time evolution of the expectation value of the torsion angle, $\langle\theta\rangle^{(j)}$, see Fig. 11 (b). Only for orientation $j = 2$ ($\varphi_2 = \frac{4\pi}{3}$) the yield is slightly lower than for the two other cases, and the wavepacket is not so efficiently dumped into the right well causing the oscillations of $\langle\theta\rangle^{(2)}$ to be further away from the right minimum ($\sim 320°$). Yet the enantioselectivity is very high for this orientation, too: 61% to 1% in favor of the (aR)-enantiomer.

[22] Average over all three orientations.

The stereoselectivity for each orientation is again accomplished by a non-linearly (mainly elliptically) polarized laser pulse of rather complex form, see Fig. 11 (c). Note that no unique helicity is maintained for the full pulse duration. The change of the helicity, or more precisely a reflection of the field at the x-t-plane, will, however, change its enantioselectivity and cause the molecule to switch from achiral to its (aS)-form. Furthermore, a clear distinction in pump and dump pulses is not easy for all subpulses, compare $\langle\theta\rangle(t)$ with pulse shapes (gray shadings) in Fig. 11 (a). While $\langle\theta\rangle(t)$ shows orderly phase-shifted oscillations during initial torsional excitation (pump), the optimal timing (from ∼5 ps onward) for dumping the wavepacket of each orientation j into the target potential well is not systematic. The correct timing is, however, decisive for high efficiency and, indeed, challenging to achieve. Regardless of their efficiency, the dump subpulses are stereoselective and orientation-selective at the same time, i.e. each subpulse is enantioselective for one or two specific orientations of the molecule on adamantane [93, A.4]. This can be proven by comparison with simulations where the phases η of the pump subpulses are changed by π – causing a internal rotation of the ethenyl group in the opposite direction – and still suppressing the preparation of the undesired (aS)-enantiomer for specific orientations.

Although the "analytical" pulse sequence is a significant improvement over the initial SPO-field in terms of (fewer) number of parameters, i.e. less computational effort is needed for the optimization, it still did not give rise to simple rules of how to choose optimal parameters for a laser pulse that is stereoselective and efficient for any number of orientations. This is, however, due to the desire to accomplish perfect stereoselectivity and high efficiency for all orientations at the same time. If we apply the laser pulse sequence in Fig. 11, for instance, to 72 instead of three energetically degenerate orientations, i.e. assuming $\Delta\varphi = 5°$, we still obtain about three times more population in the R-states than in the S-states, but most of the population is found distributed among torsional states above the lower barriers. The efficiency is very low, because the field was optimized for only three orientations. Furthermore, this rough estimation of a free torsion of the C1-C2-bond (φ) gives a foretaste of how challenging control will become, if this second degree of freedom is explicitly included into the model. This will be addressed in the next section.

2.6 Coupled torsions and classical dynamics

The C1-C2 single bond between the chiral switch and the (adamantyl) linker/surface allows an almost free rotation of the switch around the z-axis (or surface normal), see Fig. 10. But so far we always assumed only the ethylene group to rotate leaving the rest of the molecule fixed in space. This is, of course, only a valid approximation if the fixed part of the molecule is (a) much heavier than the moving part (which is the case, although the mass ratio is not very large) and (b) not influenced by the laser field, which is not realistic due to the

F-substituent in *ortho*-position of the benzene ring (F2 in Fig. 10). Therefore, the inclusion of the torsion around the C1-C2 bond is mandatory for an adequate modelling.

From our previous findings we know how challenging control becomes with increasing number of orientations of the switch (Sec. 2.4). The symmetry of adamantane and the molecular switch give rise to six, energetically almost[23] degenerate, stable conformations of the switch with reference to the adamantane, when tracing the C1-C2 torsion. The potential barriers along the corresponding torsion angle φ, measured by the dihedral angle C6-C1-C2-C7 (Fig. 10), are rather low due to the weak steric interactions between the hydrogen substituents in *meta*-position of the benzene ring and those of the adamantane. In order to increase those barriers and, thereby, reduce the number of stable conformers, we replaced the hydrogens in *meta*-position by bromines, see Fig. 12. The result are three energetically degenerate stable conformations (orientations) of the switch (at $\varphi = 60°, 180°$ and $300°$), separated by potential barriers much higher than those we must overcome to control its chirality, see barriers along φ in $V(\varphi, \omega)$ of Fig. 12. The three, in comparison to the previous model, "missing" conformations are less preferred due to the stronger steric demand of the Br-substituent (at C7) next to the F-substituent (at C8) and will not be considered in the following.[24] The Br-substituents were mainly chosen to keep the model simple; any other substituent which hinders the rotation along φ may be used as well.

The second degree of freedom requires a convenient setup of the molecular Hamiltonian as the two rotations are coupled. To avoid coupling terms in the kinetic operator (products of the momenta along θ and φ) we measure both torsion angles with respect to the C6-atom of the adamantane: The angle θ, which described the torsion of the ethylene group with respect to the phenyl group so far, is now exchanged by the angle ω, which describes the torsion of the same group but now with respect to the adamantane. More precisely ω is the dihedral angle C6-C1-C4-C5 (Fig. 10) or $\omega = \theta + \varphi$. In addition, φ does not define the orientation of the complete molecular switch with respect to adamantane any more, but measures only the torsion of the phenyl group with respect to adamantane. Using these definitions the ω-φ-coupling is observed in the potential energy surface $V(\varphi, \omega)$, see Fig. 12. Cuts along ω at $\varphi = 60° + j \cdot 120°$ resemble the known potential energy curve along θ (shifted by the value of φ), see Fig. 6, aside from some small quantitative differences due to the new Br-substituents.

Looking at those valleys of $V(\varphi, \omega)$ along ω and the high barriers between them, one could wonder if the laser pulse sequence of the previous section, optimized for three orientations (Fig. 11), will already stereoselectively switch the molecule. This is, however, not the case, because of the dipole moment $\vec{\mu}$ be-

[23] The switch has no C_2 symmetry.

[24] The large height of the barriers are also partly due to the calculation of an unrelaxed potential energy surface based on the minimum energy geometry as reference.

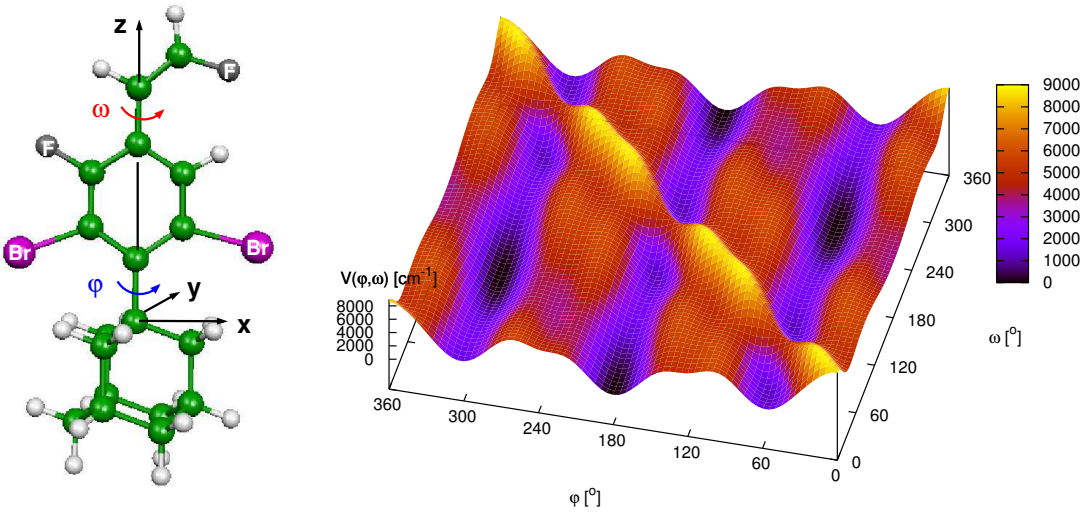

Figure 12: Two-dimensional model of the chiral molecular switch 1-(2-*cis*-fluoroethenyl)-2-fluoro-3,5-dibromobenzene mounted on adamantane. Shown are the minimum energy geometry of the achiral stereoisomer ($\theta = 180°$ or $\omega = 0°$) in one of its three stable conformations ($\varphi = 180°$) on adamantane and the potential energy surface along the angles ω ($= \theta + \varphi$), for the rotation of the ethylene group, and φ, for the rotation of the phenyl group around the space-fixed z-axis, as obtained from B3LYP/6-311G**.

ing now a function of ω and φ (not depicted) and an additional term for the momentum in φ in the kinetic operator. The corresponding moment of inertia of the latter is with more than ten million $m_e a_0^2$ very large due to the two Br-substituents. We must, therefore, expect a high density of torsional eigenstates as well as possibly high momenta during wavepacket propagation. This means, a large number of basis functions, for instance, δ-functions or grid points, is required for the quantum dynamics (QD), which significantly increases computation time. In case of SPO this becomes computationally too expensive, because in the order of a hundred thousand propagations[25] are typically performed before a satisfying high fitness is reached. However, the large momentum of inertia and the high barriers in $V(\varphi, \omega)$ would also justify a classical treatment.

Therefore, the algorithm for SPO was adapted to molecular dynamics (MD). The MD simulations, employing a Velocity Verlet integrator, were found to perform about ten thousand times faster than the corresponding QD simulations, making SPO feasible. However, a single trajectory can never account for all prop-

[25] In general, 500 to 1000 generations are run through for a set of about 100 pulses of different initial conditions.

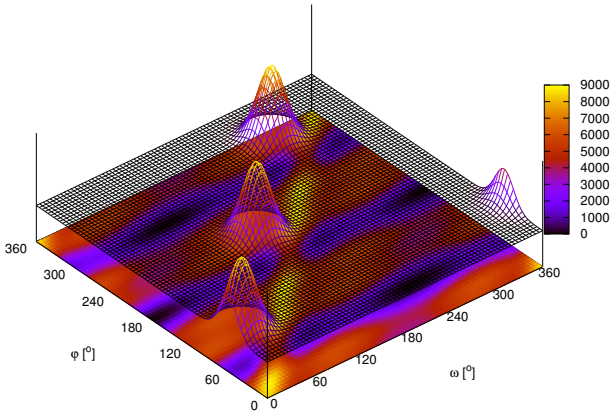

Figure 13: Fitness functions defining the target, i.e. here the (aR)-enantiomer, for the SPO in MD. For the three most stable conformations, $\varphi = 60°, 180°$ and $300°$, 4D-Gaussian functions in phase-space are used. The shown 3D-Gaussian functions are positioned atop of the potential energy surface (depicted as a 2D projection) and display the total momentum as a function of the two torsion angles ω and φ. The coloring denotes energies in cm^{-1}.

erties of a quantum mechanical wavepacket. Therefore, a Wigner distribution of the torsional ground state wavefunction (within in the harmonic approximated potential) was used to determine initial positions and momenta for a small quantity of trajectories (16 in number), intending to keep the computational effort manageable. In doing so, the trajectories are initially positioned in the close vicinity of the three global minima (characterizing the three stable conformations of the achiral isomer), see black regions in Fig. 12. The fitness was redefined using a product of Gaussian functions in four dimensional phase space (positions and momenta of both angles) centered at the three minima characterizing the (aR)-enantiomer for each of the three stable conformations, see Fig. 13.

The SPO in MD converges to a laser pulse of fair fitness (about 0.6). Yet, the SPO-field ensures very high stereoselectivity for all three conformations. We found the second degree of freedom to make control much more demanding, although only three initial conformations on adamantane are to be switched simultaneously. In general, the SPO tends to improve the efficiency of two conformations in favor of the third, despite the product ansatz (14) for the fitness which should prevent this, see also Sec. 2.4. This is an indication that stereoselective laser pulse control may not efficiently be applied to an ensemble of molecules of diverse orientation, at least, if the influenced degree of freedom is coupled to others.

Furthermore, if this optimal pulse is applied in a quantum dynamical simulation, the efficiency decreases further although the stereoselectivity remains very high for all three conformations: About 50% of the total population is found in the target states of the (aR)-enantiomer (33%, 55% and 58% for $\varphi = 60°$, $180°$ and $300°$, respectively), but less than 2% are allotted to its mirror image. Figure 14 shows the wavepacket for each stable conformation ($\varphi = 60°, 180°$ and

300°) at initial and final time. A clear localization of the wavepackets within their (aR)-minima is found after the laser pulse control, cf. Fig. 12. Parts of the wavepackets are, nevertheless, distributed over the full length of the potential valleys and will continue to evolve there with time.

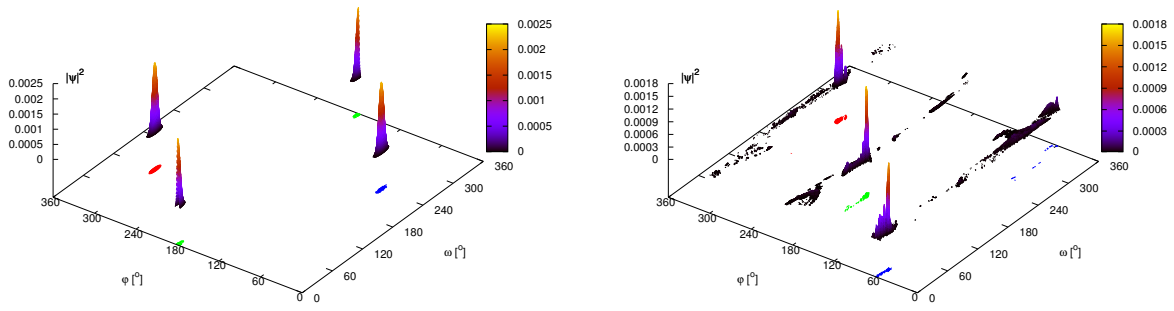

Figure 14: Snapshots of the quantum wavepacket dynamics of the laser pulse induced selective switching of 1-(2-*cis*-fluoroethenyl)-2-fluoro-3,5-dibromobenzene (mounted on adamantane) from its achiral to its (aR)-stereoisomer. Shown are the probability densities of the wavefunctions $\Psi(\omega, \varphi)$ at initial time $t = 0$ (left) and final time $t = 12$ ps (right) for the three stable conformations (blue, green and red contours of $0 + i \cdot 10^{-4}$) of the switch on adamantane. Lowest value printed is 10^{-5}.

The reasons for the differences between MD and QD are manifold: First of all, quantum effects like tunneling are not treated within the MD. Tunneling concerns, however, only torsionally highly excited trajectories trapped in one of the "chiral" potential wells with a rather low fitness. Then, the initial conditions of the QD, namely three incoherent torsional ground state eigenfunctions at T=0K, are not perfectly sampled by the distribution of the few trajectories in the MD. A higher number of trajectories would, however, decrease the performance of the SPO. Moreover, the few and uncorrelated trajectories cannot entirely account for the coherence in the quantum wavepacket dynamics. The control pulse induces, indeed, a coherent wavepacket rather than sequential pure state-to-state transition. And finally, the fitness functions used for the MD, see Fig. 13, are only an approximation of the localized "chiral" wavefunctions needed to determine the percentage of achieved target enantiomer. For the localized wavefunctions a direct diagonalisation of the Hamiltonian in the full grid basis (about 1.7 million grid points) requires too much memory. Therefore, the sought 2D-wavefunctions were expressed as a product of 1D-wavefunctions, obtained from 1D-cuts along ω and φ crossing at the (aR)-minima. After diagonalisation of the Hamiltonian within this product basis of (a several hundred) selected (partly localized) 1D-functions, the energy of the top of the low barriers in $V(\omega)$ – analogous to the

ones of $V(\theta)$ at $\theta \approx 85°$ and $275°$ in Fig. 6 – is used as upper bound for those localized 2D-wavefunctions which are used to determine the enantioselectivity of the laser pulse. Although convergence with the number of 1D-wavefunctions was checked, we cannot completely rule out that more eigenfunctions are found which qualify for localized wavefunctions of sufficient lifetime, see Sec. 2.2, if the full grid basis were used. Therefore, the given populations of the "chiral" states are actually the lower limit and could even be higher.

Leaving all the technical aspects aside, we were able to prove that stereoselective switching is still possible even if a second degree of freedom, which supports the rotation around the chiral axis, is treated explicitly. We note, however, that the overall efficiency decreases due to the desire of orientation independent control. The polarization of the optimized laser pulse is again non-linear.

2.7 Achievements, restrictions and possible applications

The extension and generalization of a laser pulse induced enantioselective excitation in a racemate [46] to a stereoselectively laser pulse-driven chiral molecular switch was accomplished successfully. We showed that the chirality of the investigated axially chiral molecules can enantioselectively be turned on, changed from left-handed to right-handed or vice versa, or may be transformed diastereoselectively in case of the biphenyl switch.

In addition to the investigation of these new models of chiroptical switches and the scientific questions associated with them, we extended laser pulse control by the aspect of orientation-independent stereoselectivity, i.e. being enantio- and diastereoselective for every (allowed) orientation. In doing so, we looked into wavepacket dynamics that described the dynamical change of the molecular chirality and tried to steer it with the time-dependent non-linear polarization of a laser pulse. We found that (sequential) pure state-to-state transitions induced by ultrashort linearly polarized laser pulses – the focus of previous studies on racemate purification based on few levels systems [31, 36, 45, 51] – will neither be sufficient nor realistic for degrees of freedom which show a high density of states. This becomes even more prominent if coupled degrees of freedom are considered. Moreover, with increasing number of orientations of the molecules the task becomes even more challenging if stereoselectivity is to be achieved for each orientation. However, with the help of stochastic pulse optimization, developed for this purpose, an efficient stereocontrol can be accomplished for all investigated models. The stochastic pulse optimization is, furthermore, applicable to many laser control problems, because of the advantage of its virtually unlimited flexibility for setting up the target (fitness).

Despite the success, the restrictions of the models and the control have to be recalled. In addition to the common approximations like, for instance, the dipole approximation, the applied density functionals and finite basis sets, we restricted the molecular switch to a few degrees of freedom and orientations. The former is

wise for being able to efficiently calculate a potential energy surface and to set up a kinetic energy operator easily accessible for the quantum dynamical calculations. And it is reasonable if the mode of interest is sufficiently decoupled from the other modes of the molecule. The examined torsions are, indeed, decoupled from almost all other vibrational modes for the most part. Still, due to the steric interactions of some of the substituents during the internal rotation and the fact that more than just the considered atoms participate in the torsion, a redistribution of energy after laser excitation is very likely. Dissipation could even enhance control though, once the desired configuration of the switch is reached. Still, high relaxation rates and dephasing would make control more challenging at either case.

Note that, although most isomerisations investigated here take place in the electronic ground state and are driven by infrared pulses of (partially very) high intensity, the approach is extendable to UV/vis induced transitions via electronic excited states, see also Ref. [76, A.2]. When going from axial chirality to other forms of molecular chirality (planar, helical), however, new aspects of control have to be take care of, even bond breaking and formation (chiral center). The general concepts remain the same though.

Regarding to the orientation of the chiral switch, we have seen that more flexibility requires a more complex polarization of the laser pulse (aside from the other parameters), in order to maintain high stereoselectivity, and leads to a lower number of successfully switched molecules. Allowing for a completely random orientation of the molecules we, therefore, expect a rather low yield even if stereoselectivity is maintained. Since, for the here presented control, we do not account for position dependence of the electric field[26], switching the enantioselectivity by reflecting the laser pulse at the x-t-plane is equivalent to a reflection of the molecule at the x-z-plane. Therefore, for an ensemble of randomly oriented molecules, the laser control would have to be upgraded by a second, not collinearly propagating, laser pulse. This would, indeed, make control even more challenging and most probably further decrease the efficiency. If in this context, if the laser distillation for randomly oriented chiral molecules based on the coherent control with three perpendicular propagating linearly polarized laser pulses, as proposed by Shapiro and others [31], could be extended to control our chiral switches is arguable: While the coherent control approach is promising, it would eventually struggle with similar efficiency problems if a single cycle is initiated. Although the distillation aspect of employing many cycles could help to increase the yield, it critically depends on the existence of accessible "achiral" (electronic) excited states with short lifetimes and unselective relaxation pathways. These are most certainly some of the reasons why no successful enantioselective laser pulse control of any of these kinds has been reported experimentally so far.

[26]Because the wavelength of the light is at least four orders of magnitude larger than the molecule.

Having said that, we still believe that the selective switching of a chiral molecular switch is feasible if certain conditions are met. For one thing, Feringa et al. have already experimentally proven that the stereoisomerism of a substituted biphenanthrylidene may selectively be controlled by light via a *cis-trans*-isomerisation [59], even when mounted on the surface of gold nanoparticles [95]. And although this approach varies from ours by the fact that only transformations between diastereomers (with different physical and chemical properties) are controlled by light, the underlying concepts are essentially the same. Even applications become conceivable if we think of our chiroptical switch as a dopant in a achiral nematic liquid crystal medium. A suitable dopant can impart its switchable chirality to the mesophase of the medium, changing the optical properties of the liquid crystal in the process [96]. In addition to only influencing the pitch length of the helical superstructure of the cholesteric phase, as experimentally shown for an axially chiral binaphthyl bis-azobenzene derivative [64], our kind of switch could allow for a direct controlled change from achiral nematic to cholesteric phase of either helicity (and back), without relying on tiny enantiomeric excesses in racemic mixtures of chiral dopants achieved by long irradiation with circularly polarized light [57], which is rather ineligible for fast data storage or processing. In contrast, the direct and selective addressing of our switch, accomplished by optimally shaped ultrashort laser pulses based on electric field-electric dipole interactions only, permits a fast change of its chirality, even featuring a true achiral "off" state. However, for any kind of experimental implementation of the stereoselective laser pulse control, proposed in this work, the molecules should be available in as few as possible (defined) orientations. Otherwise high stereoselectivity might only be achieved for few orientations and the overall yield of successfully switched molecules will be low. Although the efficiency could, therefore, be too low for many practical purposes, this should not be so critical where small amounts of the switch suffice, e.g. when employed as dopant in a liquid crystal or as chiroptical catalyst for a asymmetric synthesis. The later was experimentally demonstrated in a similar way for an axially chiral olefin mediator, which light controlled handedness determines the configuration of the stereogenic center of the product of an asymmetric autocatalysis with almost perfect enantiomeric excess and yield [97]. The overall handedness of the chiral olefin is, however, defined by a slight imbalance in its initially prepared racemic photoequilibrium, which is induced by irradiation with circularly polarized light for several days.

At this point it is helpful to recall that so far only electric field-electric dipole interactions have been considered. This makes, indeed, sense as the magnetic field-magnetic dipole interactions (or other higher electric or magnetic multipoles) are usually much smaller and can, therefore, not substantially contribute to an effective change of the molecular geometry. It is, however, the combination of electric and magnetic interactions that allows to distinguish between enantiomers with circularly polarized light exploiting circular dichroism. Although

these interactions might not be sufficient to effectively alter the chirality of a molecule,[27] they are useful for the distinction of enantiomers even in very small quantities, as will be presented in the next chapter.

[27] Exceptions are, for instance, the creation of tiny enantiomeric excesses in racemic photoequilibria, see above and e.g. Refs. [57, 97].

3 Chiral recognition by ultrashort laser pulses

3.1 Circular dichroism in mass spectrometry

In 2003 we proposed an experimental setup to test *enantioselective laser pulses* for their practicability in stereoselective control of real molecules [45], see Fig. 15. The idea is to detect molecular fragments with a mass spectrometer of only those stereoisomers that have before been excited by a linear polarized laser pulse. However, since enantiomers are purely mirror images of each other, a distinction in terms of their mass-to-charge ratio is impossible within a single measurement. Therefore, we proposed three different scenarios, starting off with either a racemate or one of the two pure enantiomers and employing always the same enantioselective – S-selective in our example – laser pulse, see Fig. 15. If the laser pulse is effectively enantioselective, it should only excite one enantiomer – here the (S)-enantiomer – whenever it is present, while not affecting its mirror image at all. Only the excited molecules are assumed to dissociate subsequently. Their fragments should, thus, significantly contribute to the mass spectrum in comparison to the parent ion. By comparing the mass spectra of at least two of the scenarios the degree of enantioselectivity of the laser pulse excitation – and, therefore, the success of the proposed control – may be quantified.

Although the experiments were, to the best of our knowledge, never conducted in the proposed way, they raise two interesting questions: First, is an enantioselective excitation necessary to detect a difference in the spectra or is it sufficient to excite each enantiomer merely to a different extent? And second, how to distinguish enantiomers in mass spectrometry in the first place? The answers to both questions are known and have important consequences:

First, while for stereoselective laser pulse control of, for instance, the chiral molecular switches proposed in Chapter 2, a maximal selectivity is aspired, this is not necessary for a qualitative or even quantitative distinction of enantiomers in a sample. For chiral recognition an enantio*specific* – in contrast to enantio*selective* – excitation or response is sufficient, i.e. both enantiomers interact with the light but by a measurable different degree. This is the essence of circular dichroism (CD), i.e. the wavelength dependent differential absorption of left and right circularly polarized (LCP and RCP) light[28], which is routinely used as analytical method in spectroscopy to identify chiral molecules, e.g. in traditional polarimetry. However, the effect is usually rather weak, because on top of the electric field interactions the magnetic field interactions play a role and are usually small for most molecules. As a consequence, the method could often only be applied to concentrated solutions or undiluted liquid samples, a limitation of its applica-

[28]CD is commonly defined as the difference in the absorption coefficients for LCP (ε_L) and RCP (ε_R) light: $\Delta\varepsilon = \varepsilon_L - \varepsilon_R$.

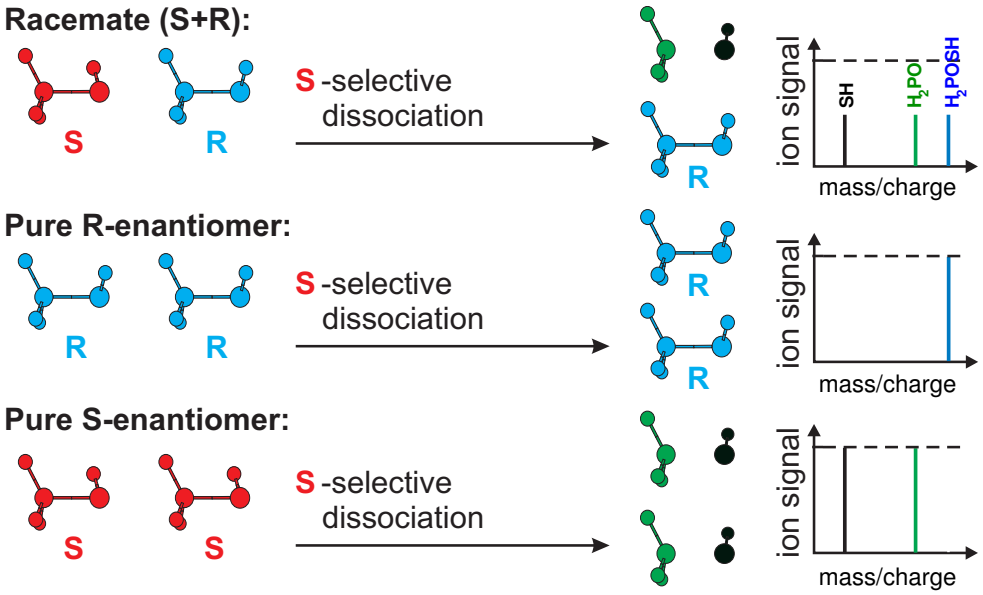

Figure 15: Proposed experimental detection by mass spectrometry of the effect of enantioselective laser pulse excitation. In each of the three experiments a S-selective laser pulse exclusively excites the (*S*)-enantiomer (of axially chiral H_2POSH) such that it dissociates (into H_2PO and SH) subsequently. By comparison of at least two experiments, the success of the enantioselective photodissociation may be evaluated. Adapted from Ref. [45], with permission from Elsevier.

bility in the past. In more recent times CD measurements have been extended to techniques such as chiral second harmonic generation (SHG) [98], cavity ring-down polarimetry (CRDP) [99], X-ray natural circular dichroism (XNCD) [100] or angular resolved photo-electron spectroscopy (PES), so-called photoelectron CD (PECD) [101], which achieve much higher sensitivities and are, thus, efficiently applicable for chiral recognition in low particle densities. PECD is not only accessible via (one-photon) ionization by vacuum ultraviolet (VUV) synchrotron radiation, but also via resonance enhanced multiphoton ionization (REMPI) using femtosecond laser pulses, as recently shown by Baumert et al. [102].

Detecting enantiomers in the gas phase using laser ionization brings us back to the second question: Nowadays mass spectrometry is not only one of the most important techniques for the qualitative analysis of the products of a chemical synthesis, but also allows for the identification of traces of chemicals in parts smaller than per billion. A distinction of stereoisomers in a sample is, in fact, highly desirable. In case of mass spectrometry initiated by electron impact ionization, combined techniques, as for instance preceding gas or liquid chromatography (GC/MS or LC/MS), are required to distinguish structural and stereoisomers, because all those isomers result in indistinguishable mass spectra. Furthermore, these preceding techniques offer a quantitative analysis. However, photoioniza-

tion induced by shaped ultrafast laser pulses allows for better control of the ionization and fragmentation of a sample [90] and is such applied for the distinction of structural isomers in femtosecond laser ionization mass spectrometry (fs-LIMS) nowadays [103, 104]. Applying circularly polarized nanosecond laser pulses to initiate REMPI, Boesl et al. as well as Compton et al. were even able to distinguish enantiomers in mass spectrometry in 2006 [105, 106]. Likewise, Weitzel and co-workers recently accomplished the identification of the (R)- and (S)-enantiomers of 3-methylcyclopentanon by their difference in the ion yields of the mass spectrum, but now employing femtosecond circularly polarized laser pulses [107]. Fs-LIMS offers, hence, the possibility to fast and sensitively identify all kind of stereoisomers in mass spectrometry. Moreover, it allows the determination of the enantiomeric excess, i.e. the weighted difference of the yield of two enantiomers in the products, which is of importance for asymmetric synthesis.

Recently, Weitzel and coworkers carried out further experiments to investigate the effect of the pulse duration on the CD in fs-LIMS and observed a clear interdependency [108, B.1]. In the past Salam et al. had already reported a strong dependence of the difference in excited state population of enantiomers on the duration of circularly polarized laser pulses, however, in quantum mechanical simulations of a two-level system [28, 109]. In addition to electric interactions, they also accounted for magnetic interactions between laser and molecules in their simulations [110]. Using circularly polarized laser pulses they even predicted the stepwise purification of a racemate of randomly oriented molecules in their two-level approach [29]. Based on these investigations and in order to understand the experimental observations of Weitzel and coworkers, we extended our concept of stereoselective laser pulses by magnetic field-magnetic dipole interactions and focussed on electron dynamics rather than nuclear dynamics, as these are the phenomena which seem to be fundamental for the CD in fs-LIMS.

The chapter will continue with a more detailed description of the experiment by the Weitzel group as well as of the observed dependency of the pulse duration on the CD in the ion yield, Sec. 3.2. Time-dependent many electron dynamics will be applied to simulate the essential processes that lead to the chiral distinction and unravel the role of the pulse duration. Afterwards we will take a closer look at the relevance of the magnetic interactions for chiral distinction by laser pulses and study how to improve chiral recognition tuning the various laser parameters, Sec. 3.3. Concluding, we will address additional issues of future investigations, as e.g. ionization by non-resonant excitation and the potential role of the electric quadrupole, Sec. 3.4.

3.2 The role of laser pulse duration [B.1]

As aforementioned, the introduction of CD in mass spectrometry was accomplished by employing circularly polarized laser pulses for the ionization and measuring the normalized difference in the ion yields for left-, Y_{LCP}, and right-

circularly polarized light, Y_{RCP} [105, 107]:

$$\text{CD in ion yield} = \frac{Y_{LCP} - Y_{RCP}}{\frac{1}{2}(Y_{LCP} + Y_{RCP})}. \tag{20}$$

The CD in ion yield can be determined from parent ions and fragments alike, while the latter do not necessarily lead to smaller absolute CD values [107]. In order to monitor the CD in ion yield as a function of the pulse duration, the fs-pulses were linearly chirped using an appropriate pulse shaper [111]. Then, the resulting pulse duration τ may be expressed by the linear chirp parameter γ, which depends on the displacement of the grating of the pulse shaper from the focal plane, and the duration of the unaltered pulse τ_0, 50 fs full width at half maximum (FWHM) in this case:

$$\tau^2(\gamma) = \tau_0^2 + \left(\frac{8\ln(2)\cdot\gamma}{\tau_0}\right)^2. \tag{21}$$

The detected CD in ion yield of the sample (*R*)-3-methylcyclopentanone is plotted as a function of the pulse duration in Fig. 16 (top). For the (*S*)-enantiomer a similar curve is obtained, however, with an opposite sign in the CD value (not shown) [108, B.1]. We observe a fast rise of the CD in ion yield within the first 100-150 fs. For pulse durations from about 150 fs onward the CD levels off at 0.12-0.13 and maintains this value up to the longest investigated pulses. The reason for this behaviour is not immediately evident, because the spectrum and the laser energy remain constant for all pulse durations. In order to understand the observations and get insight into the underlying processes, we developed an approach to simulate the basic steps of the experiment.

In the REMPI process the wavelength of the laser is set in resonance with the transition frequency of the first (singlet) electronic excited state S_1. This excitation is mainly characterized by a $n \to \pi^*$ transition at the carbonyl group. These kind of transitions are known to show a relatively strong CD, although they are typically little intense, because they become electric dipole forbidden (but magnetic dipole allowed) in the limit of formaldehyde in the C_{2v} point group. A measure for the size of the CD is the rotatory strength R_{nm}, derived after Rosenfeld and Condon [112, 113]: For a transition from the electronic state n to the state m, it is given by

$$R_{nm} = \Im\left(\left\langle \psi_n \left| \hat{\vec{\mu}} \right| \psi_m \right\rangle \left\langle \psi_m \left| \hat{\vec{m}} \right| \psi_n \right\rangle\right). \tag{22}$$

R_{nm} depends not only on the size of the electric, $\left\langle \psi_n \left| \hat{\vec{\mu}} \right| \psi_m \right\rangle$, and the magnetic transition dipole moment, $\left\langle \psi_m \left| \hat{\vec{m}} \right| \psi_n \right\rangle$, between states n and m, but also on the relative orientation of the respective vectors. Here ψ_n and ψ_m are the corresponding wavefunctions, while $\hat{\vec{\mu}} = \sum_i q_i \hat{\vec{r}}_i$ is the electric and $\hat{\vec{m}} = \sum_i \frac{q_i}{2m_i} \hat{\vec{r}}_i \times \hat{\vec{p}}_i$ the

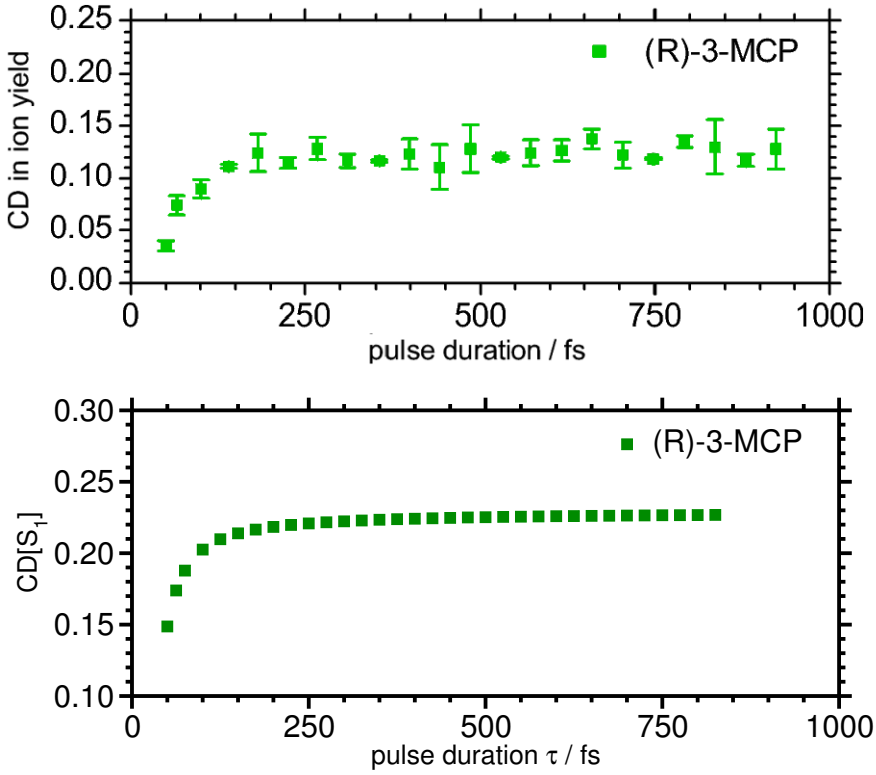

Figure 16: Top: Experimental CD in ion yield of (*R*)-3-methylcyclopentanone as a function of the laser pulse duration. Bottom: Theoretical CD[S_1] of 85% (ax)- and 15% (eq)-conformers of randomly oriented (*R*)-3-methylcyclopentanone as a function of the laser pulse duration. Adapted from Ref. [108, B.1].

magnetic dipole operator with summations over the positions $\hat{\vec{r}}_i$ and momenta $\hat{\vec{p}}_i$ of all particles of charge q_i and mass m_i.[29]

For the $S_0 \rightarrow S_1$ transition in 3-methylcyclopentanone (3-MCP) the absolute magnetic transition dipole moment is with 0.010 c Debye [30] indeed in the same order of magnitude as the value of the electric one of 0.073 Debye (and the respective vectors are not orthogonal) [108, B.1]. The resulting rotatory strength for the $S_0 \rightarrow S_1$ transition of (*R*)-3-(eq)-MCP is $R_{01}^{\mathrm{eq}} = 7.26 \cdot 10^{-40}$ erg esu cm/Gs [31] (CIS/6-311++G(2d,2p)) or of opposite sign for the (*S*)-enantiomer. The cyclopentanone ring of 3-MCP gives, however, rise to two distinct stable conformers, where the methyl group at the stereogenic carbon atom may either be equatorial (eq) or axial (ax). The (eq)-conformer is, as one would expect, more stable and dominant at room temperature. This is of importance, because the (*R*)-3-(ax)-MCP has a rotatory strength ($R_{01}^{\mathrm{ax}} = -6.40 \cdot 10^{-40}$ erg esu cm/Gs)

[29] The nuclei are considered to be fixed.
[30] c is the speed of light.
[31] 1 Gs (Gauss) equals to 10^{-4} kg/(A s^2).

of similar size (and same sign) as the (*S*)-(eq)-3-MCP, i.e. it behaves almost as the (*S*)-enantiomer of the dominant (eq)-conformer. Moreover, the $S_0 \rightarrow S_1$ excitation energies of equatorial and axial conformer are with 4.24 eV and 4.21 eV (CIS(D)/6-311++G(2d,2p)) so close that a laser pulse of 50 fs will excite both even if tuned to the transition of the dominant (eq)-conformer. To ensure that the axial conformer has no significant effect on the experimental observations, it will be considered in the simulations. A ratio of 85% to 15% in favor of the (eq)-form was assumed based on experimental and theoretical reaction enthalpies of the isomerization [114, 115].

We have seen that the first step of the multiphoton ionization, namely the resonant $S_0 \rightarrow S_1$ excitation, may be key to the observed CD in the ion yield. Therefore, we defined a CD in the S_1 populations for the simulation according to

$$\mathrm{CD}[S_1] = \frac{P_{LCP}[S_1] - P_{RCP}[S_1]}{P_{LCP}[S_1] + P_{RCP}[S_1]}. \tag{23}$$

$\mathrm{CD}[S_1]$ ($\in [-1, 1]$) is the normalized difference in S_1-populations, $P[S_1]$, employing either a LCP or RCP pulse. Note that, we do not detect ion yields like in the experiment but excited state populations. The assumption that the non-resonant (multiphoton) transitions, following the resonant $S_0 \rightarrow S_1$ excitation, merely remove the electron and have, hence, rather little influence on the differentiation of the enantiomers, is reasonable since no angular resolved detection of the ions or electrons is performed in the mass spectrometer.[32] In addition, nuclear motion will not be accounted for in our model, because it is not considered to play an essential role during the ultrafast photoexcitation. Yet, the electronic CD (ECD) spectrum of 3-MCP in the vapor phase shows a vivid vibronic structure [116], which could have a small influence on the resonant transition though. Nonetheless pure electron wavepacket dynamics based on ab initio data are performed, namely time-dependent configuration interaction singles with perturbative doubles corrections (TD-CIS(D)) [117–119].[33] For it, the time-dependent electronic Schrödinger equation is expressed in the basis of the time-independent Hartree-Fock (HF) ground state wavefunction, ψ_0, and n CIS excited state wavefunctions, ψ_i:

$$i\hbar \frac{\partial c_i(t)}{\partial t} = \sum_{j=0}^{n} H_{ij}(t)\ c_j(t) = \varepsilon_i\ c_i(t) + \sum_{j=0}^{n} V_{ij}(t)\ c_j(t), \tag{24}$$

using coefficients $c_i(t)$. The ε_i are the electronic energies as obtained from CIS(D). Since a two-level system ($n = 1$, i.e. S_0 and S_1) is not sufficient to simulate the REMPI, for reasons discussed later (Sec. 3.3), we used $n + 1 = 50$ states for the electron dynamics. Actually 18 of the 50 states are energetically (CIS(D)/6-311++G(2d,2p)) above the ionization potential of 9.3 eV [106], but are still bound (however unoccupied virtual) states in our calculations.

[32] In contrast to PECD, for instance.

[33] For another approach on multielectron wavepacket dynamics, see e.g. Ref. [120].

The elements of the time-dependent interaction matrix are given in the basis of the CIS wavefunctions ψ_i by $V_{ij}(t) = \left\langle \psi_i \middle| \hat{V}(t) \middle| \psi_j \right\rangle$. In the semi-classical radiation theory the interaction operator $\hat{V}$ is expressed as [110]:

$$\hat{V}(t) = -\frac{1}{2}\, E_0 s(t) \left[\left(\hat{\vec{D}} \cdot \vec{e}_\delta \right)^\dagger e^{i\omega(t-t_c)} + \left(\hat{\vec{D}} \cdot \vec{e}_\delta \right) e^{-i\omega(t-t_c)} \right] \tag{25}$$

where

$$\hat{\vec{D}} = \hat{\vec{\mu}} - \frac{1}{c}\, \vec{e}_z \times \hat{\vec{m}}. \tag{26}$$

Thus, $\hat{V}$ accounts for the interaction of the electric field $\vec{E} = \frac{1}{2}\, E_0 s(t) \left(\vec{e}_\delta^{\,\dagger} e^{i\omega(t-t_c)} + \vec{e}_\delta e^{-i\omega(t-t_c)} \right)$ with the electric dipole $\hat{\vec{\mu}}$ and of the magnetic field $\vec{B} = \frac{1}{c}\, \vec{e}_z \times \vec{E}$ with the magnetic dipole $\hat{\vec{m}}$. The corresponding electric and magnetic (transition) dipole moment matrix elements between all electronic states are obtained from CIS calculations. As in the previous chapter, E_0 is the field amplitude, ω the laser frequency and $\vec{e}_\delta$ the polarization vector. The latter one is now defined as

$$\vec{e}_\delta = \frac{1}{\sqrt{2}} \left(\vec{e}_x + e^{i\delta}\, \vec{e}_y \right) \tag{27}$$

where $\delta = \pm\frac{\pi}{2}$ for RCP/LCP light and $\vec{e}_x$, $\vec{e}_y$ and $\vec{e}_z$ are unit vectors along the laboratory fixed x-, y- and z-axis, i.e. the laser propagates in positive z-direction.

The form function $s(t)$ in Eq. (25) was chosen Gaussian shaped in this case, more precisely $s(t) = \exp\left(-2\ln(2) \left(\frac{(t-t_c)}{\tau} \right)^2 \right)$, where t_c $(= 2\tau)$ is the again the pulse center. The pulse duration τ (equals the FWHM for the field intensity) is related to the time-dependent laser frequency via the chirp parameter γ (Eq. (21)) [111]:

$$\omega(t) = \omega_0 + \frac{16\, \gamma \left(\frac{\ln 2}{\tau_0^2} \right)^2}{1 + 64\, \gamma^2 \left(\frac{\ln 2}{\tau_0^2} \right)^2} (t - t_c), \tag{28}$$

where the central laser frequency ω_0 matches the vertical $S_0 \rightarrow S_1$ transition frequency of the (eq)-conformer. While the pulse duration τ is elongated, the chirped frequency ensures that the spectrum of the laser pulse stays constant, just like in the experimental setup. Moreover, as the laser energy remains constant throughout the experiment, the field amplitude E_0 must decrease with increasing pulse duration. This is achieved by keeping the pulse area [121], which is proportional to $E_0 \cdot \tau$, constant.

The excited state populations $P[S_1]$, measured at the final propagation time (4τ) – that is when the laser pulse has (almost) completely died down – depends on the orientation of the molecules with respect to the laser, c.f. Sec. 3.3. Since the molecules in the experiment are randomly oriented, rotational averaging is

performed. The resulting CD in the S_1 population is plotted in Fig. 16 (bottom) as a function of the pulse duration.[34] The characteristics of the experimental curve are well reproduced by our simulations. Quantitative differences are, however, noticed. They are due to the applied approximations and the fact that merely the difference in S_1 population is detected and not ion yields.[35]

Despite these restrictions, the electron dynamics allow for a detailed analysis of the influence of the pulse duration on the CD-value. The plotting of the S_1-populations with respect to τ reveals that for pulses shorter than about 150 fs $P_{LCP}[S_1]$ and $P_{RCP}[S_1]$ rise steeply [108, B.1], where their sum grows much faster than their difference (not shown). This causes the pronounced drop of the CD value for small pulse durations. For durations longer than ~ 200 fs $P_{RCP}[S_1]$ and $P_{LCP}[S_1]$ decrease only slowly until their sum and difference run almost parallel resulting the CD$[S_1]$-curve to converge to a constant value of about 0.23.

Due to the spectral width of the ultrashort laser pulses the (ax)-conformer is excited, too, although to a much smaller extend. Its 15% in the mixture basically shift the whole CD$[S_1](\tau)$-curve to smaller values.[36] In addition, the spectrum of the pulse remains unchanged for all τ. Therefore, the presence of the (ax)-conformer is not the source of the decline of the CD-value for small τ.[37]

We recall, however, that the field amplitude E_0 increases with decreasing τ. This causes, in fact, the substantial growth of the final S_1-population. Due to the higher amplitude we also observe a stronger interim interaction with high electronic excited states: When detecting the interim populations at t_c of excited states energetically higher than S_1, more precisely $1 - P[S_1](t_c) - P[S_0](t_c)$, we find a significant increase for durations shorter than 150 fs, while from $\tau = 200$ fs onward these populations begin to vanish.[38] The interim interactions with excited states other than the target state – which are expressed by the dynamic polarization of the enantiomers – result in the significant decrease of the CD$[S_1]$ and, therefore, a partial loss of the chiral distinction. If we stick to the reasonable assumption that even in the experiment mainly the S_1 population is eventually excited to the ionization continuum, then, the very short laser pulses of relative high intensity cause unspecific electronic interactions which do not contribute to the dichroism.

In the next section we will take a closer look at the field amplitude dependence on the detected CD$[S_1]$ as well as at the importance of a sufficiently large number of electronic excited states in the simulations. Beforehand, a more detailed

[34] The unit of the magnetic transition dipole moments, as obtained from GAUSSIAN 09 [122], was corrected retrospectively, c.f. Ref. [108, B.1].

[35] The definitions of the CD in ion yields and S_1 also differ in their normalization.

[36] This effect is actually less pronounced for very short laser pulses, because the (eq)-conformer is, then, proportionally more excited than the (ax)-conformer.

[37] The (ax)-conformer contributes slightly to the decline if the spectral width of the pulse changes with its duration, see Ref. [123, B.2].

[38] At final propagation time all these populations vanish for any τ.

analysis, in particular, of the influence of the magnetic field-magnetic dipole interactions on the CD and its connection to the orientation of the molecules are discussed.

3.3 The relevance of magnetic interactions for chiral distinction [B.2]

In order to explore the influence of the magnetic field-magnetic dipole interactions on the chiral distinction in our simulations, we detect, at first, the population dynamics of the S_1-state during the propagation time. Fig. 17 shows the curve for a LCP and RCP laser pulse of 100 fs (fwhm)[39] for the pure (eq)-conformer of (*R*)-3-MCP. As expected, a difference in the S_1-populations for LCP and RCP is generated during laser-molecule interactions, where P_{LCP} clearly dominates. This gives rise to an increasing positive CD[S_1]-curve.[40]

If we now set all magnetic transition dipole moment elements to zero, no difference between P_{LCP} and P_{RCP} is found any more, although both still increase with time. As a consequence the CD[S_1]-curve remains zero for all times. This means, that the magnetic interactions are responsible for the chiral distinction, while the electric interactions merely cause most of the population transfer.

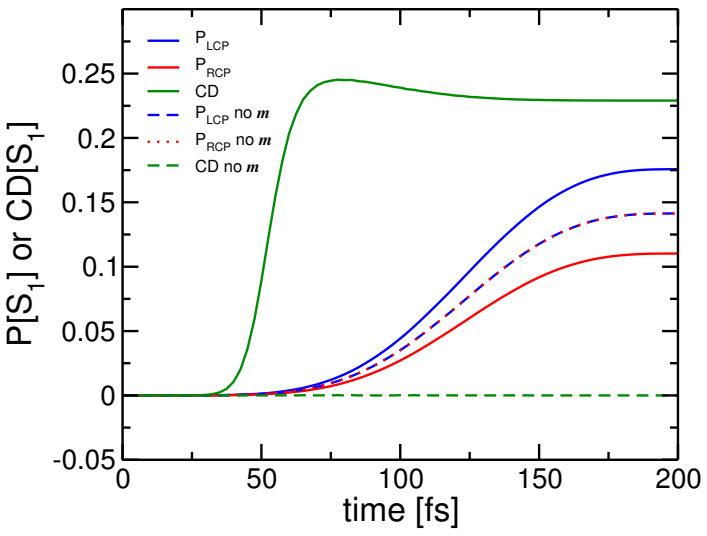

Figure 17: Population dynamics of S_1 for randomly oriented (*R*)-3-(eq)-methylcyclopentanone during the excitation with either a LCP (blue) or RCP (red) laser pulse, and the CD[S_1] (green) calculated from them. Dashed lines are used if the magnetic field-magnetic dipole interactions are disabled (no $\boldsymbol{m}$: $\hat{\vec{m}} = \vec{0}$). Adapted with permission from Ref. [123, B.2]. Copyright 2011 American Chemical Society.

These results are obtained for randomly oriented molecules, i.e. after rotational averaging. The CD[S_1] depends, however, sensitively on the orientation of the molecule with respect to the laser. This dependency is shown in Fig. 18 for

[39] From now on $\cos^2$-shaped pulses are used, as defined in Sec. 2.2 with $t_p = 2\text{fwhm}$.

[40] To prevent artefacts due to populations close to zero, a detection limit is introduces for the CD[S_1] [123, B.2].

a selection of 312 different orientations of the molecule, generated by rotation of all (transition) dipole vectors around the laboratory fixed coordinate axes using an uniform distribution of Euler angles [123, B.2]. Although the CD[S_1]-curve varies around its value for the random ensemble (~ 0.23), the deviations from the averaged value are significant for some orientations. The largest deviations are, however, achieved for very small populations of the S_1-state. They are caused by unfavorable orientations of the electric S_0-S_1-transition vector with respect to the electric field, for instance, for an almost parallel alignment of the transition vector to the propagation direction of the light. If such small S_1-populations, or rather the ions generated from them, are still significant in terms of an experimental detection is arguable. The highest peaks, particularly the ones with the negative CD-value, could, hence, be considered artefacts of the simulations. Nonetheless, the CD is orientation dependent and chiral recognition may be considerably improved if an optimal orientation for all molecules is achieved.

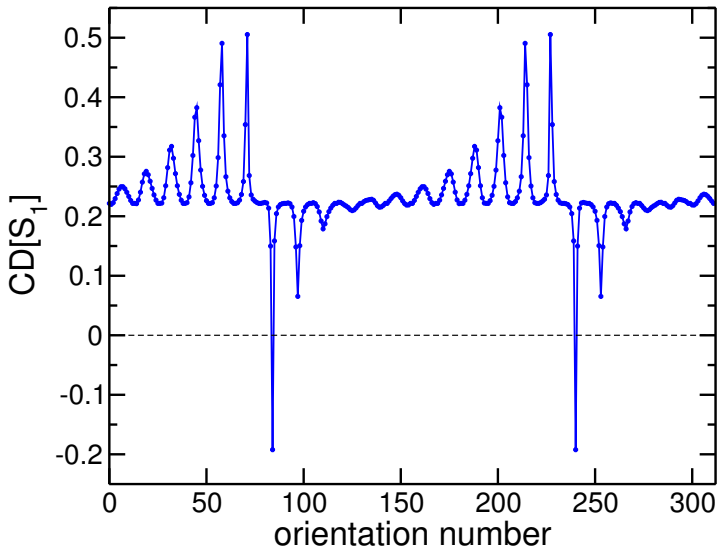

Figure 18: CD[S_1] calculated for 312 different orientations of (*R*)-3-(eq)-cyclopentanone. Adapted with permission from Ref. [123, B.2]. Copyright 2011 American Chemical Society.

For oriented molecules we know that already a linearly polarized laser pulse is sufficient to actually enantioselectively transfer populations from S_0 to S_1, see Chapter 2. Such an excitation can, of course, also be accomplished for oriented enantiomers of 3-MCP, based entirely on electron wavepacket dynamics (in contrast to the mainly nuclear wavepacket dynamics of Chap. 2). While previously enantioselective excitations were mediated only by the electric transition dipole moments, we now allow for magnetic interactions as well. As expected, the magnetic field-magnetic dipole interactions have very little impact on the enantioselectivity though, while the electric field-electric dipole interactions are predominantly responsible for the exclusive population transfer in only one of the two enantiomers.[41] In contrast, for a random ensemble of enantiomers linearly

[41] For an oriented system we could, hence, observe linear dichroism.

polarized laser pulses are incapable of inducing any enantioselective or even only an enantiospecific electronic transition. The reason for these observations can, in simple terms, be attributed to the capability of the laser to distinguish between the pairs of electric and magnetic S_0-S_1-transition dipole vectors of the (R)- and (S)-enantiomer irrespective of their orientation:[42] In randomly oriented molecules there is no way to distinguish the electric dipole vectors of two enantiomers for a single (vertical) electronic transition. The magnetic transition dipole, however, adds quasi an additional vector to the arrangement. Its angle to the corresponding electric transition dipole vector is different for the (R)- and (S)-enantiomer.[43] This difference in the transition vectors is not sufficient for a distinction of randomly oriented enantiomers by a single transition using a linearly polarized laser pulse, but allows for an enantiospecific excitation if circularly polarized light is applied. The best chiral distinction is, hence, achieved for polarization angles δ of $\pm\frac{\pi}{2}$, that is perfect circular polarization. Already elliptical polarization decreases the CD[S_1] [123, B.2].

The considerations just made are based on a single transition between only two electronic states. In the previous section (3.2) we realized, however, that the interactions with more than just two states influence the chiral recognition in mass spectrometry. If in a two-level system the field amplitude of the laser E_0 is increased, more population is transferred from S_0 to S_1 in general. For a certain amplitude, population inversion will eventually be accomplished. At that point higher field amplitudes will cause the S_1-population to be transferred back to the electronic ground state until the initial status is restored. This behaviour is repeated with increasing E_0 (Rabi-oscillations). The phenomenon might not only be considered unrealistic in view of the multiphoton excitation employed in the experiment, but also because of the sign change of the CD[S_1] that is caused by it [109,123, B.2]: $P_{LCP}[S_1]$ passes through its maxima at lower E_0 than $P_{RCP}[S_1]$, such that it falls below $P_{RCP}[S_1]$ for certain E_0 causing CD[S_1] to switch signs. This effect can also be observed if the pulse duration is increased successively, while keeping the field amplitude constant: One obtains a periodic oscillation of the CD[S_1] around zero [109] which should be considered an artefact of the two-level model. Furthermore, the number of electronic states, i.e. the size of the basis applied for the dynamics, determines the quality of the simulation, in particular, with respect to effects such as multiphoton transitions and dynamic polarization [124]. In a two-state model the characteristics of the experimental CD(τ)-curve, see Sec. 3.2, could not have been reproduced for chirped laser pulses. Therefore, a two-level approach, although a common and in general valid approximation, prevents not only the observation of certain effects, but might

[42] Since the local dependence of the light is not accounted for, the projection of these vectors on the polarization plane of the light is in fact essential.

[43] While the electric dipole vectors of two enantiomers can be related by reflection, the corresponding magnetic ones are related by a C_2-rotation orthogonal to the reflection plane (due to the vector product in $\hat{\vec{m}}$).

even bring misleading results about.

Although a manifold of electronic states was used in our model, we only considered resonant transitions so far. In the following section we take a look at non-resonant and multiphoton excitations as well as their influence on chiral recognition in mass spectrometry.

3.4 Non-resonant and multiphoton excitations

In experiments Weitzel and coworkers found a varying wavelength dependence of the CD in ion yield which cannot be attributed to experimental imperfections, as e.g. laser intensity fluctuations or deviations from circular polarization [125]. In our simulations we could not reproduce this dependency and observed a clear decline of the CD[S_1] when tuning the laser frequency off-resonant to the S_0-S_1 transition [123, B.2]. Theoretical vibrationally resolved ECD spectra of 3-MCP show that nuclear vibrations have a significant impact on the shape of the CD-peak for a single electronic state due to vibronic couplings [126]. This is not surprising, since the flip of the cyclopentanone ring of 3-MCP results even in a sign change of the CD-value, see Sec. 3.2. Nuclear degrees of freedom are, therefore, expected to influence the CD in fs-LIMS and could be the reason for the aforementioned discrepancy between theory and experiment, as all nuclei were kept frozen in our electron wavepacket dynamics.

Furthermore, for (*R*)-propylene oxide there is a clear experimental evidence for efficient chiral distinction of enantiomers in fs-LIMS via non-resonant multiphoton ionization, widening the application range of the method [127]. Apparently, the theoretical CD[S_1] is not a meaningful quantity in case of non-resonant excitations any more and the concept of the CD in excited state populations needs to be extended to the manifold of unbound states above the ionization potential, for instance. In addition, two- or higher-photon CD may become important, if resonance with higher excited states is met. Here it is known that higher multipoles, e.g. electric quadrupole moments, play a role [110]. Although calculations of the two-photon CD (TPCD) in the S_1 population of 3-MCP [123, B.2] did not disagree with experimental findings [128] in principle, they differed somewhat from time-independent simulations including contributions from the electric quadrupole [129], which has not been included in our simulations yet.

In spite of the limitations of our approach, by applying electron wavepacket dynamics based on ab initio data we were able to explain the origin of novel experimental observations and to provide guidelines for optimal chiral distinction. The magnetic interactions turned out to be critical in contrast to, for instance PECD, where the asymmetric photoelectron distribution is attributed to electric dipole interactions [130]. On the theory side we showed that a large number of electronic basis functions in combination with all electronic and magnetic transition dipole moments are required to allow for a correct description of, at least, the first and presumably critical step of the REMPI, that results in the observed CD

in ion yields. In case of non-resonant excitations the generation of an electronic wavepacket incorporating a large number of electronic states is even more likely, supporting our approach.

Interestingly, the sign of the CD in ion yield might differ between the parent ion and the fragment ions, as observed for non-resonant multiphoton ionization of (*R*)-propylene oxide, but not fully understood up to now [127]. Explanations based on the character of the molecular orbital from which the electron is ejected, that are reasonable for PECD, seem not to work in this case [125]. A more likely reason for this phenomenon seems to originate from coupled electron-nuclear (wavepacket) dynamics following the ionization which supports the generation of different amounts of fragments. Depending on the distribution of the interim excited state populations, induced by the enantiospecific laser pulse excitation, specific excited states of the ion might be preferred for LCP or RCP.

The theoretical description of electron-nuclear couplings during and after electronic excitation is, however, no trivial task. In the following chapter we will see how vibronic absorption and emission spectra of biologically relevant chromophores can be calculated using time-dependent or time-independent approaches. With explicitly time-dependent methods it is even possible to monitor coupled electron-nuclear dynamics after vertical electronic excitation.

4 Electronic structure and spectroscopy of biochromophores

4.1 Photoinduced processes in biomolecules

Sunlight serves not only as energy source for chemical synthesis in living matter, namely in photosynthesis, where the light absorbing chromophore chlorophyll mediates the transformation of light into chemical energy, but also initiates regulating biochemical processes via highly specialized photoreceptors [131, 132]. For this purpose, organic chromophores are usually embedded in an adapted protein where they selectively and efficiently mediate the light induced reaction. A very common chromophore in plants is, for instance, β-carotene, an orange colored pigment, see Fig. 19. As retinal, a form of vitamin A, obtained by oxidative cleavage of β-carotene, its light-induced *cis-trans*-isomerisation in rhodopsin plays a prominent role in vision.

But the organism does not have to have eyes to adapt to current environmental conditions with the help of photoreceptors: For instance, in phototropism which allows plants to grow towards the source of light, a blue light sensitive flavoprotein mediates the phototropic responses in the plant [133]. Remarkably, the range of processes regulated by those blue light receptors is wide and includes also the migration of the chloroplasts, the organelles that conduct photosynthesis in plant cells, towards illuminated sites or even away from excessively illuminated areas that might be harmful [134]. Furthermore, the opening of the stomatal pores of plants, which are used for exchange of the gases of photosynthesis with the environment, is also be stimulated by blue light receptors [135].

Basically, the number of photoreceptor proteins in nature can be classified into six families based on their light absorbing chromophores and their protein structure [136], namely the rhodopsins, phytochromes, xanthopsins, cryptochromes, the LOV (light, oxygen, voltage) domains of phototropins [137], and BLUF (blue light photoreceptors using flavin adenine dinucleotide) domains containing proteins [138]. The last three photosensors are based on flavins. Prominent derivatives of flavin (7,8-dimethyl substituted isoalloxazine) are vitamin B_2 (riboflavin), see Fig. 19, lumiflavin, flavin mononucleotide (FMN) – the light-sensitive chromophore in phototropins (vide supra) – and flavin adenine dinucleotide (FAD), which serves as redox cofactor in a variety of important metabolisms.

All these light induced processes proceed along a multitude of steps including electronic excitation upon light exposure, excited state dynamics accompanied by nuclear motion (e.g. isomerisation or proton transfer), including radiating, i.e. fluorescence or phosphorescence (after intersystem crossing), and radiationless transitions (by intramolecular vibrational energy redistribution or internal conversion). Eventually signal transductions in terms of energy or charge is con-

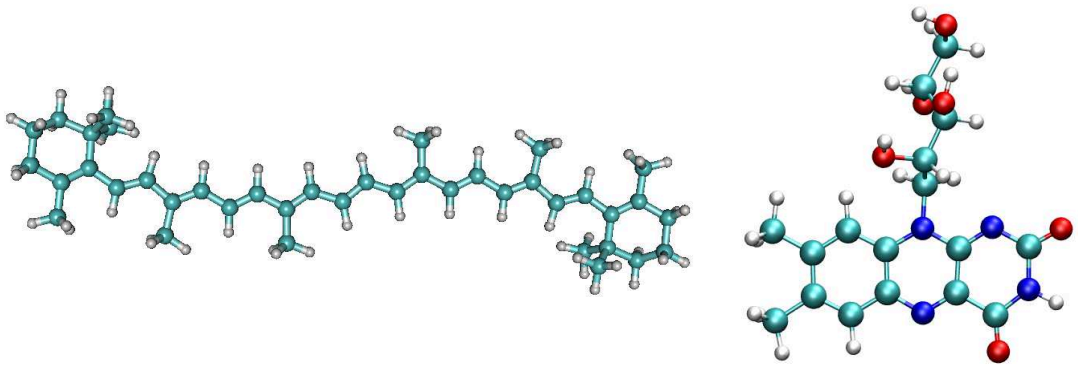

Figure 19: Optimized structures of **left:** *All-trans* β-carotene (CAM-B3LYP/6-31G(d), PCM: DCM); **right:** riboflavin (B3LYP/TZVP, PCM: DMSO). Coloring: cyan: C, white: H, blue: N, red: O atoms. Adapted from Refs. [139, 140, C.2,C.3].

ducted with associated species, while the sensor is often regenerated in the end. The characterization of these processes including the identification of all participating species is a challenge in many cases. Various types of spectroscopy, like X-ray crystallography, nuclear magnetic resonance (NMR), infrared (IR), Raman or ultraviolet/visual (UV/vis) absorbance and emittance, may provide valuable insight. Resonance Raman (RR) spectroscopy is in particular attractive for biosystems, because it permits detection and analysis of a few modes of a chromophore at a time, even within a large (protein) environment [141]. In RR the molecule is excited by a laser tuned to be in (or near) resonance with a transition to an electronic excited state, instead of exciting to a virtual energy state as in traditional Raman spectroscopy. The result is a increased Raman scattering intensity for those vibrational modes which are mainly excited during electronic transition. Moreover, the overall large increase in intensity compared to traditional Raman spectroscopy allows for very low sample concentrations.

Still, some processes are better (or only) understood after an analysis by means of computer simulations. Here theoretical methods based on molecular mechanics or quantum chemistry as well as molecular or quantum dynamics offer excellent approaches to simulate optical steady-state spectra as well as their time-dependent analogues. In the following we will, thus, take a look at the principles of the calculation of vibronic UV/vis and RR spectra of relatively large organic chromophores in general and for the molecules shown in Fig. 19 in particular.

In order to retrieve harmonic vibrational frequencies of the electronic (excited) state(s), the second derivatives of the respective state potential with respect to all (mass-weighted) nuclear Cartesian displacement coordinates (Hessian matrix) have to be determined. Apparently, the size of the molecule puts a restriction to the quantum chemical effort that is achievable without difficulty, bearing in

mind that for UV/vis and RR spectra at least one electronic excited state has to be covered in addition to the ground state. Moreover, many atoms mean many vibrational degrees of freedom, resulting in a multitude of possible transitions between the vibrational states of the ground to those of the electronic excited state. An electronic transition is, in addition, often accompanied by a change of the nuclear structure, if, for instance, a double bond is elongated upon π-π^*-excitation. Hence, the normal modes of electronic ground state might differ from those of the excited state, causing mode mixing after electronic excitation.

All these aspects will be discussed in the next section, Sec. 4.2. Furthermore, methods that are based on time-independent and time-dependent approaches will be applied to simulate UV/vis absorption and fluorescence spectra of riboflavin as well as RR spectra of β-carotene with the objective of explaining experimental findings. Afterwards, that is in Sec. 4.3, the simulation of an explicitly time-dependent UV/vis emission spectrum of riboflavin will be addressed and analysed. The chapter will conclude with a brief outlook, in Sec. 4.4, of the potential influence of the (protein) environment on the electronic structure and spectroscopic response of biochromophores and of a few simple theoretical implementations of the corresponding interactions for systems we investigated.

4.2 Vibronic and Resonance Raman spectra: The role of mode mixing

4.2.1 Absorption and fluorescence spectra of riboflavin [C.1]

The cross section for a vibronic absorption spectrum between two electronic states, say S_0 and S_1, is, within perturbation theory, proportional to $\sum_f \left|\left\langle \Phi_f^1 \left|\vec{\mu}_{01}\right| \Phi_i^0 \right\rangle\right|^2$,[44] where $\vec{\mu}_{01}$ is the electronic transition dipole moment and Φ_i^0 and Φ_f^1 are the vibrational wavefunctions of the initial (i) and final (f) vibrational states of either electronic state. In the Franck-Condon approximation a vertical electronic transition is assumed, such that the Taylor expansion of $\vec{\mu}_{01}$ around the minimum geometry of the electronic ground state is truncated at the zeroth order,[45] resulting in a coordinate independent $\vec{\mu}_{01}$ and the well-known Franck-Condon (FC) factors $\left|\left\langle \Phi_f^1 \right| \Phi_i^0 \right\rangle\right|^2$ [143, 144]. Moreover, each total vibrational wavefunction Φ may be expressed as a direct product of wavefunctions $\varphi_v(\mathrm{Q}_k)$ for each normal coordinate Q_k, which describe harmonic oscillations of quantum number v of a superposition of nuclear displacements belonging to mode k (determined by the eigenvectors of the Hessian matrix), with $k = 1, ..., M$ and $M = 3N_A - 6$ vibrational modes for the N_A atoms of a (non-linear) molecule.

Even if excitations are only allowed from the vibrational ground state of S_0, i.e. $v = 0$ for all modes ($T \to 0$ K), still $(n+1)^M$ vibronic transitions have to

[44] We assume T = 0 K, that is we neglect the sum over initial states i and the thermal averaging.

[45] The first order gives rise to Herzberg-Teller terms [142].

be computed for up to n quanta ($n = 0, 1, 2...$) in each of the M modes of S_1. Thus, the number of FC-integrals to be calculated might become fairly large for biochromophores of dozens of atoms. At least the dimensionality of the otherwise M-dimensional FC-integrals could be reduced to one, due to the product ansatz of Φ, if the normal coordinates of S_0 were parallel to the ones of S_1, which is however generally not true, as discussed in the following.

The minimum geometries of electronic ground and excited states often differ due to e.g. the weakening of a bond upon electronic excitation. This may not only result in a modification of the curvature of the potential energy surface, reflecting a change of the force constants, but also in the displacement of its minimum. In Fig. 20 (left) this situation is shown for the harmonic potential energy surfaces of two electronic states along two normal coordinates, Q_1 and Q_2, of a model system: The minimum of S_1 is displaced (and shifted in energy) with respect to the one of S_0. In addition, the one-to-one correspondence between the normal coordinates of the ground, Q_k, and those of the excited state, Q'_k, is maintained, i.e. the respective axes are parallel. Although this assumption reduces the computational effort immensely, as stated above, and is correct for diatomic molecules, this one-to-one mapping is not necessarily preserved in the case of a polyatomic molecule [145]. As illustrated in Fig. 20 (right) the excited state normal coordinates of the electronic excited state (Q'_k) are rotated with respect to the ones of the electronic ground state (Q_k). This normal mode mixing upon electronic excitation may be expressed, after Duschinsky, in form of a linear transformation [146]:

$$\vec{Q}' = \mathbf{J}\vec{Q} + \vec{K}, \tag{29}$$

where $\vec{Q}$ and $\vec{Q}'$ are M-dimensional column vectors of the respective normal coordinates. $\vec{K}$ is the M-dimensional normal coordinate displacement vector given by

$$\vec{K} = \mathbf{L}'^{\mathrm{T}}\ \mathbf{m}^{\frac{1}{2}}\ \Delta\vec{R} \tag{30}$$

with $\mathbf{m}$ being a diagonal $3N_A \times 3N_A$-matrix containing all atomic masses, and $\Delta\vec{R}$ being the $3N_A$-dimensional Cartesian displacement vector between the equilibrium geometries of the two electronic states. The $M \times M$-dimensional Duschinsky matrix $\mathbf{J}$ is constructed from the $3N_A \times M$-dimensional matrices that transform between (mass weighted) Cartesian displacement coordinates and vibrational normal coordinates in the ground, $\mathbf{L}$, or electronic excited states, $\mathbf{L}'$:

$$\mathbf{J} = \mathbf{L}'^{\mathrm{T}}\ \mathbf{L}. \tag{31}$$

In general, $\mathbf{L}$ and $\mathbf{L}'$ are $3N_A \times 3N_A$-dimensional orthogonal transformation matrices (which diagonalise the Hessian matrix of the respective electronic state). However, the external motions, rotations and translations, are separated from the internal vibrational ones. While for the translations this can be done exactly, for the rotations the rigid rotor approximation has to be applied. In practice,

a molecule-fixed frame is chosen where the $3N_A$ degrees of freedom, represented by the displacement coordinates, are constrained by six (or five, in case of linear molecules) Eckart conditions [147]. Three of these conditions prevent that the nuclear displacements result in the movement of the center of mass, the remaining ones exclude any contribution of the displacements to an overall rotation of the molecule.

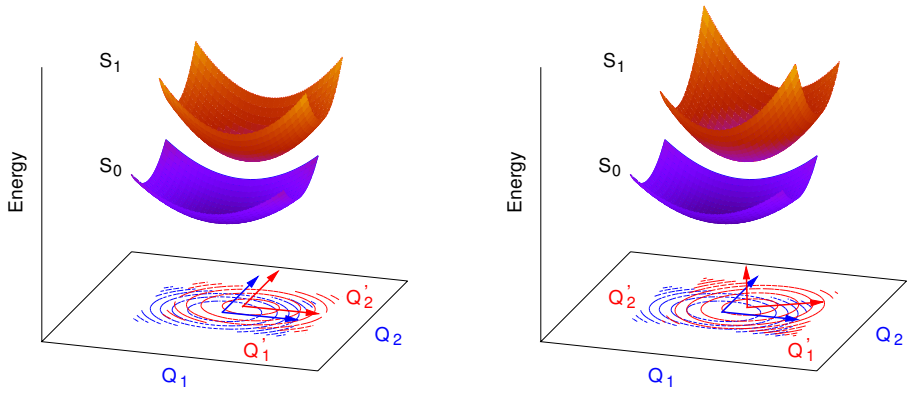

Figure 20: Duschinsky effect: Harmonic potential energy surfaces and corresponding contours of two electronic states of a model system with two normal coordinates, Q_1 and Q_2. **Left:** The potential of the electronic excited state (orange, red contours), S_1, has a different curvature and its minimum is shifted in energy and position with respect to the ground state potential, S_0 (purple, blue contours). **Right:** If in addition the excited state normal coordinates, Q'_1 and Q'_2 (red vectors), are rotated with respect to Q_1 and Q_2 (blue vectors), mode mixing is caused upon electronic excitation.

The chosen molecule-fixed frame depends, however, on the equilibrium geometry of the molecule (and its displacements). Because the equilibrium geometries of ground and excited are, in general, different, each electronic state emerges with its own molecule-fixed coordinate system, fulfilling its three rotational Eckart conditions [148]. The two different coordinate systems are related by a rotation matrix, often referred to as the axis-switching matrix [149]. For all practical purposes, the zero-order axis-switching approximation – also referred to as the static analog of the Eckart conditions [150] – is used,[46] where the matrix does not depend on vibrational displacements, to prevent nonlinear terms in the Duschinsky transformation (29). This may lead to axis-switching effects which occur, because the nuclear displacements described by a normal coordinate in one electronic state cannot be fully expressed as a superposition of only the vibrational normal coordinates of the other state [153].[47] Consequently, **J** becomes non-orthogonal

[46]The rotation matrix which minimizes the root mean square deviation between both geometries, as used by others [151], also satisfies the static Eckart conditions [152].

[47]This concerns particularly displacements along modes with the same symmetry as a rota-

which causes errors in the relative size of the FC-integrals, as the Franck-Condon sum rule is not strictly valid any more. Therefore, the transformation between vibrational coordinates belonging to two different electronic states is, generally speaking, non-linear and non-orthogonal, but may be well approached by the Duschinsky transformation (29) for small amplitude vibrations [148], which is a valid assumption within the harmonic approximation.

The Duschinsky effect can also be observed experimentally, for instance, for single vibronic level fluorescence spectroscopy of styrene or related systems, where in particular out-of-plane bending and single-bond torsional modes of the electronic ground state strongly mix in the excited state – due to bond order changes within the π-system upon electronic transition – preventing a strict distinction of these modes in the excited state [145, 154].

Unless the Duschinsky matrix $\mathbf{J}$ is diagonal, i.e. $\mathbf{L}' = \mathbf{L}$, multidimensional FC-integrals have to be solved for a vibronic spectrum. For a biochromophore like riboflavin, which has 135 normal modes, that could mean 3^{135} 135-dimensional integrals have to be evaluated, if we allow for up to two quanta in the excited state modes and mixing with all modes. Apparently, strategies to select the most important integrals as well as approximations to reduce their dimensionality are in need to keep the computational effort tolerable. For many decades, a number of approaches for the evaluation of multidimensional FC-integrals have been presented by various authors, see e.g. Refs. [151, 155–166], and without intending to be exhaustive, here only two, more recent methods, namely the block diagonalisation of the Duschinsky matrix, as implemented by Dierksen and Grimme [164], and the partition of transitions in classes by Santoro et al. [151, 166], are briefly explained in the following to get the general ideas across.

Since the preparation of a vibronic spectrum often involves the computation of FC-integrals with mainly low vibrational quantum numbers, methods based on recurrence relations [157], that is where the sought FC-integral is expressed in a linear combination of FC-integrals of lower quantum number until the analytically evaluable integral of the vibrational ground state wavefunctions is reached, are usually very efficient. In addition, Dierksen employes a block diagonalisation approximation [164, 167], which relies on the commonly diagonally dominant and otherwise rather sparse structure of the Duschinsky matrix[48]. In his FCFAST algorithm [168], the Duschinsky matrix is efficiently block diagonalised using a threshold – which determines the similarity of approximate final modes (generated by a projection scheme), $\tilde{\mathbf{L}}'$, with respect to the exact ones – effectively reducing the dimension of the integrals. This algorithm adheres, however, the danger that normal modes of different blocks become non-orthogonal due to the procedure of generating approximate modes [164].

tion.

[48] It even has a block-diagonal form for a symmetry group (higher than C_1) which is spanned by the common symmetry elements of both electronic states, because modes belonging to different irreducible representation do not mix.

In the method of Santoro, Barone and coworkers all vibronic transitions are partitioned in classes C_n, corresponding to the total number n of simultaneously excited modes in the electronic target state [151, 166]. In the FCclasses code [169][49], the FC-integrals of C_1 are calculated for increasing number of quanta until they become negligible, thereby limiting the number of integrals to be evaluated also for higher classes, as they are connected to the results of the lower ones by a recursive relation [160]. In addition, the C_1 integrals provide already information on the vibrational progression of the spectrum in terms of position and frequency shifts. The computation of the C_2 integrals, i.e. for all pairs of excited oscillators, give a measure of the Duschinsky mixing, which is applicable to higher classes, too. For classes higher than 2, a threshold controlled scheme selects the most relevant vibronic transitions (integrals) by a priori estimate of their intensity based on the C_1 and C_2 results, efficiently reducing computational costs.

Furthermore, it should be mentioned that Berger and coworkers proposed a prescreening technique, based on analytical sum rules for FC factors, for the prior determination of the maximum quanta in each mode and the maximum number of simultaneously excited modes at a given accuracy [165]. This general applicable extension of their hotFCHT code [162] has, thus, the advantage of knowing the number of relevant FC integrals in advance, which allows for a considerable reduction of the computational effort in many cases.

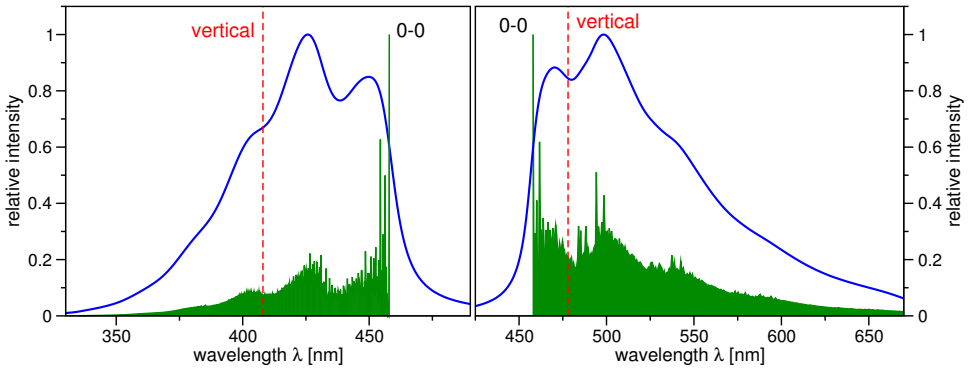

Figure 21: Calculated vibronic absorption (left) and emission spectrum (right) of riboflavin (TD-B3LYP/TZVP @ $T = 0$ K). Stick spectra (green) were broadened by Lorentzian functions with a FWHM of 500 cm^{-1}. Vertical excitation and de-excitation energies are marked by red dashes lines. Adapted with permission from Ref. [170, C.1]. Copyright 2010 American Chemical Society.

Good examples of the capability of these methods are the vibronic absorption and emission spectra between the electronic singlet states S_0 and S_1 of the chromophore riboflavin presented in Fig. 21 [170, C.1], as obtained from FCfast at (TD)-B3LYP/TZVP level of theory. In experiment, riboflavin shows in ethanol

[49] Also available as implementation in Gaussian 09 [122].

at low temperature and in the LOV1 domain of the green alga *Chlamydomonas reinhardtii* well-resolved vibronic fine structures in its absorption and fluorescence spectra [171–173]. The position of the respective main peaks are not particularly well reproduced when comparing merely to the vertical electronic transition energies;[50] the theoretical values are actually blue-shifted with respect to the experimental maxima [174, 175]. If we now look at the 0−0 transition energies in Fig. 21, we realize that they clearly differ from the vertical excitation energies, in particular for absorption. Even if we accept different zero point energies in S_0 and S_1, this is an indication for displaced potential minima, i.e. different minimum geometries, albeit we expect moderate differences, because the 0−0 peak is still the highest in the stick spectrum. The largest changes in the minimum geometries are found within the central pyrazine and the uracil moieties of the isoalloxazine, where especially double bonds are elongated and single bonds are shortened due to the (mainly) $\pi \rightarrow \pi^*$ character of the $S_0 \rightarrow S_1$-transition [170, 176, C.1]. These structural changes are also observed in the calculated IR spectra (not shown), where, in addition to frequency shifts due to the bond strength changes, several stretching modes in the isoalloxazine rings of the ground state are mixed among each other and with bending modes in the electronic excited state.

The overall broadened stick spectra, obtained from the multitudes of (coupled) FC transitions, reproduce eventually the characteristics of the vibronic structure of the corresponding experimental spectra quite well. The positions of their most intense peaks come much closer to the maxima of the experimental spectra compared to the vertical transition energies. The agreement can be even further improved if solvent effects, reflecting better the experimental conditions, are accounted for [170, C.1]. Solvents were here introduced by continuum solvation models such as PCM (polarizable continuum model) [177] or COSMO (conductor-like screening model) [178].

In summary, the best agreement between theoretical and experimental spectra was achieved if vibronic and solvent effects were considered in our simulations. Here, the (computationally demanding) explicit determination of the vibronic transitions is not only essential for the fine structure, but also for the position of the spectral bands. Although the Duschinsky effect is not directly visible in the spectrum, mode mixing plays a role, as stated above, and will result in a shift of the bands if not allowed for. In the following example of the RR spectrum of β-carotene, the consideration of mode mixing will be absolutely necessary to reproduce experimental findings.

4.2.2 Resonance Raman spectrum of β-carotene [C.2]

Before we turn to the simulated spectrum, we recall that the resonance Raman cross section between initial (i) and final (f) vibrational states (of the electronic

[50] The vertical excitation energy is determined from the *minimum potential energy* of the initial electronic state.

ground state) is determined by $\sum_{\rho,\lambda} |\alpha_{\rho\lambda}^{fi}|^2$, where $\alpha_{\rho\lambda}^{fi}$ are the components ($\rho, \lambda \in [x, y, z]$) of the Raman polarizability tensor. These, excitation frequency (ω) dependent, components are given within second order perturbation theory by the Kramers-Heisenberg-Dirac (KHD) sum-over-states formula [179, 180][51]

$$\alpha_{\rho\lambda}^{fi}(\omega) = \sum_k \frac{\left\langle \Phi_f^0 \middle| \mu_{01}^{\rho} \middle| \Phi_k^1 \right\rangle \left\langle \Phi_k^1 \middle| \mu_{01}^{\lambda} \middle| \Phi_i^0 \right\rangle}{\omega - \omega_{ki} + \imath\Gamma} \tag{32}$$

where Φ_i^0 and Φ_f^0 are the initial and final vibrational wavefunctions of the electronic ground state potential (^{0}), and Φ_k^1 the intermediate vibrational wavefunctions in the electronic excited state (^{1}). The Cartesian components of the electronic transition dipole moment, $\vec{\mu}_{01}$, between the two considered states are denoted μ_{01}^{λ}. Furthermore, ω_{ki} is the transition frequency between vibronic states k and i, and Γ determines the homogenous linewidth, i.e. covers the various lifetime effects. For the same reasons discussed above, the sum-over-states approach can become costly, if not even unfeasible, for biomolecules with hundreds of modes.

Alternatively, the RR cross section may be computed by the time-dependent approach popularized by Tannor and Heller [181], which is formally identical to the KHD expression. Within the Condon approximation the RR spectra is basically obtained from the (half) Fourier transformations of the cross-correlation functions $\left\langle \Phi_f^0 \middle| e^{-\imath \hat{H}_1 t} \middle| \Phi_i^0 \right\rangle$ of final wavefunctions Φ_f^0,[52] where $\hat{H}_1$ is the (field-free) excited state Hamiltonian. Although this expression implies a quantum wavepacket propagation on a (beforehand calculated) excited state potential energy surface of hundreds of dimensions, in practice the excited state Hamiltonian is expressed in normal coordinates and (multidimensional) Gaussian wavepackets move on harmonic surfaces, in order to derive applicable analytical expressions.

An advantage of a time-dependent approach is that the propagation time does not increase with the number of modes, the size of minima displacement or the degree of mode mixing, while the number of required intermediate states in the KHD sum-over-states formula will grow fast [181]. Although the calculation of the M-dimensional overlap integrals is still the rate-limiting step (if Duschinsky rotation is allowed for), it is often more efficient to compute cross-correlation integrals for a relative small number of time steps (up to $\sim 10^5$) than a huge number of FC integrals of vibrational eigenstates (from $\sim 10^9$ up).[53] This is due to the fact that the excited state wavepacket, $e^{-\imath \hat{H}_1 t} |\Phi_i^0\rangle$, actually needs to sample only a small fraction of the potential energy surface before it leaves the minimum geometry of the ground state and the cross-correlation integral vanishes [182]. That is why the short-time approximation to the time-dependent

[51] Contributions from the non-resonant term are neglected as resonance is assumed.

[52] For one specific mode, Φ_f^0, a Raman excitation profile is obtained.

[53] Admittedly, the number of time steps depends on the desired spectral resolution and will reach the same order as the number of intermediate states, Φ_k^1, in the limit of resolving every single eigenstate.

Heller formalism [183], where basically the gradients of the excited state potential at the FC region are considered, sometimes suffice for large molecules in solution [184, 185].

Note that, within the Condon approximation the vibronic absorption/emission cross section can also be obtained using this time-dependent approach, namely by a Fourier-transformation of the auto-correlation function $\left\langle \Phi_i^0 \left| e^{-i\hat{H}_1 t} \right| \Phi_i^0 \right\rangle$ [186]. Consequently, there are several additional approaches for the simulation of absorption, fluorescence or Raman spectra based on or derived from the time-dependent formalism, for instance, applying Green's function techniques [187, 188], transform theory [189, 190] or various improvements of Heller's theory [191] as implemented in the electronic structure package ORCA [192]. We will continue with the Heller formalism in what follows, but first a look at experimental findings is necessary.

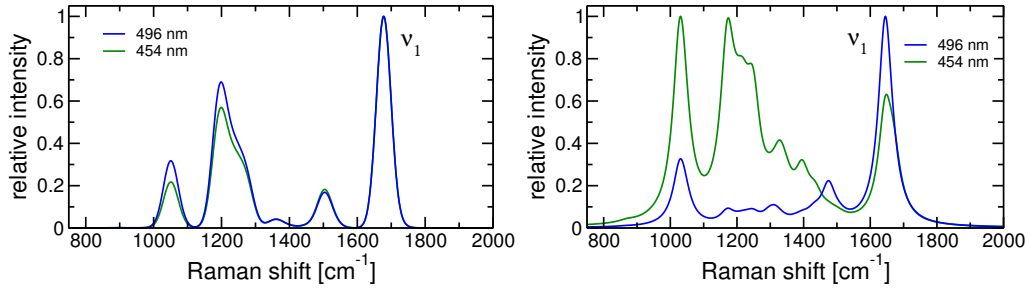

Figure 22: Calculated resonance Raman spectra of β-carotene (CAM-B3LYP/6-31G*, PCM: DCM) at 496 nm (blue lines) and 454 nm (green lines) without Duschinsky rotation (left), or with Duschinsky rotation (right). The calculates stick spectra were broadened by Lorentzian functions with FWHM of 25 cm^{-1}. The peak of interest is marked by ν_1, see text. Adapted from Ref. [139, C.2].

Recently, the RR spectra of β-carotene in solution and in photosystems I and II have been studied experimentally and theoretically in detail by Tschirner et al. [193, 194]. The experimental spectrum shows basically three distinctive vibrational bands, corresponding to stretching modes, of which the first one (at $\sim$1525 cm^{-1}), labelled ν_1, shifts in frequency upon variation of the excitation wavelength. A detailed analysis revealed two different C=C stretching modes, ν_{1a} and ν_{1b}, which are only separated by about six wavenumbers and reach their maximum intensity at different wavelengths in the Raman excitation profile (REP). However, the authors were not able to theoretically reproduce the effect with their applied methodology (DFT and transform theory) neglecting mode mixing.

Therefore, we created our own program code based on the time-dependent formalism explained above [181], that is including displaced potentials, frequency shifts and Duschinsky rotation [139, C.2]. The computed RR spectra of *all-trans*-β-carotene are depicted in Fig. 22 for the two excitation wavelengths for which

the two closely spaced modes become maximal in the theoretical REP. In the broadened RR spectra the two modes merge into a single peak (at ∼1678 cm^{-1}). If Duschinsky rotation is neglected ($\mathbf{J} = \mathbf{1}$) the RR spectra for both excitation wavelengths mostly overlap and the shift of the ν_1-peak cannot be observed. If we allow for mode mixing, however, the ν_1-peak shifts with decreasing excitation wavelengths by about 4 cm^{-1} to the blue, see Fig. 22, which agrees qualitatively and quantitatively quite well with experimental observations [193].[54] The shift can be attributed to the dependency of the intensity ratio of the two contributing modes on the excitation energy [139, C.2]. These C=C stretching modes are directly affected by the π-π^* type of transition between S_0 and S_2,[55] because double bonds are elongated while of single bonds are shortened. Apparently, this decrease in bond length alternation leads to mixing of the C=C stretching modes in the electronic excited states causing the shift of the combined peak in the RR spectra. In addition, significant changes in relative peak intensities (and positions) are also observed in the lower frequency regime of the RR spectrum.

In summary, we have seen that even small changes in the nuclear framework, following an electronic excitation, play an important role in UV/vis spectroscopy and should be included in the simulation. At his point we also realize that, although the minimum geometry of the excited state is the basis for the Duschinsky matrix, the implied harmonic approximation might not result in a good description of the gradient at the FC-point – which in turn is based on the assumption of a vertical excitation – in particular for relatively large geometrical changes. Thus, frequencies determined at the FC-point might, in principle, provide a better description of the vibronic transitions (gradients are actually employed in other, approximative approaches), but lack meaning in terms of a normal mode analysis far away from a minimum.

Either way, there are obviously restrictions for steady-state spectra, although they provide already valuable information on nuclear and electronic structure of the chromophores. However, explicitly time-dependent spectroscopy, which tracks the aftermath of these geometrical changes, can help to unravel details of the nuclear and electronic processes following the illumination. In the following section will take a closer look at the non-adiabatic dynamics, i.e. nuclear motion evolving on multiple potential energy surfaces, of riboflavin after vertical excitation.

[54] The RR spectrum on its own differs from the experimental one, because no scaling of the force constants was done in contrast to Ref. [193].

[55] The ("dark") $S_0 \rightarrow S_1$ transition, formally forbidden by symmetry (in the C_{2h} point group), is dominated by a two electron excitation and, thus, appears wrongly above the "bright" S_2 state in TDDFT [195].

4.3 Past Franck-Condon excitation: Non-adiabatic dynamics of riboflavin [C.3]

As indicated in the introduction to this chapter, Sec. 4.1, riboflavin is the parent chromophore of biological blue-light receptors and, thus, vital to several photo-induced processes. Accordingly, its photophysics has attracted the attention of experimental [196–199] and theoretical researchers [174, 175, 197, 199, 200] alike. In particular time-resolved (transient) spectroscopy, as recently performed by Weigel et al. [196, 199], provide valuable insight into the excited state dynamics after photon absorption which eventually leads to signal transduction. Already stationary spectroscopy, namely the difference in broadening of absorption and stimulated emission bands, indicates ultrafast ($\sim$ 10 fs) relaxation of the Franck-Condon geometry of the initially excited optically active S_1 state towards its potential minimum [196]. Moreover, evidence was found for a subsequent formation of a superposition between the S_1 state of $\pi\pi^*$-character and energetic nearby dark $n\pi^*$ states on an ultrafast timescale due to non-adiabatic couplings. Based on transient fluorescence spectra a time constant of 90 fs was determined by exponential analysis for the observed red-shift of the initial peak frequency of flavin in water [199]. These findings encouraged us to simulate the ultrafast dynamics of riboflavin after vertical electronic excitation.

Because a fully quantum mechanical treatment of nuclear dynamics on several coupled electronic potential energy surfaces of molecules with hundreds of degrees of freedom is in practice impossible, an approximative treatment is required. Thus, we ran non-adiabatic dynamics based on classical trajectories, as implemented in NEWTON-X of Barbatti et al. [201, 202]. In this mixed quantum classical dynamics approach the quantum degrees of freedom are the electronic ones, i.e. quantum chemical calculations provide energy gradients and non-adiabatic coupling vectors between electronic states, while the nuclei follow Newton's equations of motion. Transitions between different electronic states are treated using Tully's surface hopping [203], where by means of non-adiabatic transition probabilities and a stochastic algorithm it is decided on which electronic potential energy surface the classical trajectory is propagated in the following time step. For an ensemble of independently calculated trajectories the fractional number of trajectories in each electronic state should be a good approximation of the quantum population of this state.

In practice the extensive computation of the non-adiabatic coupling vectors is reduced to the computation of the overlaps between wavefunctions at different time steps. This may be understood, first of all, by expanding the total time-dependent wavefunction in the basis of adiabatic electronic wavefunctions of states i, specifically $\psi_i(\vec{r};\vec{R})$, which depend on the electronic coordinates $\vec{r}$ as well as parametrically on the nuclear coordinates $\vec{R}$ of nuclei A of mass M_A. This ansatz is, then, inserted into the time-dependent Schrödinger equation for the total wavefunction using the total Hamiltonian but for the kinetic

term of the nuclei, as they are treated classically. After the typical algebraic transformations, differential equations for the time-dependent expansion coefficients of each electronic state i, describing the time evolution of the system on the Born-Oppenheimer potential energy surfaces, are obtained. In addition, we get terms of the form $-\imath\hbar \left\langle \psi_j \left| \frac{\partial}{\partial t} \psi_i \right. \right\rangle$ according to the product rule for derivatives, because the nuclear coordinates are a function of time, i.e. $\vec{R}(t)$. Applying the chain rule for derivatives we may further re-write $\left\langle \psi_j \left| \frac{\partial}{\partial t} \psi_i \right. \right\rangle$ as $\sum_A \vec{d}_{ji}^{\,A} \, \vec{v}_A$, where we identify $\vec{d}_{ji}^{\,A} = \left\langle \psi_j \left| \vec{\nabla}_A \psi_i \right. \right\rangle$ as non-adiabatic couplings between states j and i, and $\vec{v}_A = \frac{d}{dt}\vec{R}_A(t)$ as velocity of nucleus A. Note that, if the latter is defined as $-\imath\hbar \frac{1}{M_A} \vec{\nabla}_A$, we obtain the well-known terms for the first derivative of the electronic wavefunctions with respect to the nuclear coordinates, namely $-\sum_A \frac{\hbar^2}{M_A} \left\langle \psi_j \left| \vec{\nabla}_A \psi_i \right. \right\rangle \vec{\nabla}_A$.[56] This way the non-adiabatic surface hopping probabilities are actually computed from the time-derivatives of the electronic wavefunctions. In practice they are numerically evaluated using a finite difference approximation [204], and, after linear extrapolation, the calculation of the time-derivative coupling term, $\left\langle \psi_j \left| \frac{\partial}{\partial t} \psi_i \right. \right\rangle$, is finally reduced to the computation of the overlaps between wave functions at different time steps: $-\frac{1}{\Delta t} \left\langle \psi_j(\vec{r}; \vec{R}(t)) \left| \psi_i(\vec{r}; \vec{R}(t - \Delta t)) \right. \right\rangle$ [205]. While this reduces the computational effort, the on-the-fly computation of energy gradients for the Newtonian forces and of the non-adiabatic couplings is still the bottleneck of the method, restricting the number of trajectories or the total number of time steps which can be treated for large molecules with many electrons. Note that we use (linear response) TDDFT for the calculation of non-adiabatic couplings, a method which is based on the electron density and not on wavefunctions. The overlap integrals are, thus, evaluated on the basis of Slater determinants of Kohn-Sham orbitals [206, 207].

Before we turn to the results of the simulations, we note that while the (fast) electronic degrees of freedom are usually covered by quantum chemistry, there is, however, a variety of approaches to treat the slow motion of the nuclei in non-adiabatic dynamics [208], be it fully quantum mechanically, i.e. using nuclear wavepackets as e.g. in the multi-configuration time dependent Hartree (MC-TDH) method [209, 210], or semiclassically, as for instance in Refs. [211, 212], or in the discussed mixed quantum-classical way with surface hopping which may also be implemented by e.g. Carr-Parrinello molecular dynamics (MD) [213].

For our riboflavin chromophore, figure 23 shows a contour plot of the time-dependent stimulated emission cross section, recorded as the average of 158 mixed quantum classical trajectories at TD-B3LYP/TZVP level of theory [140, C.3]. Initial coordinates and momenta of the trajectories were generated along the normal modes of the minimum geometry of the electronic ground state sampling the

[56] The second derivative of the electronic wavefunctions with respect to the nuclear coordinates, as typically obtained before the Born-Oppenheimer approximation, are usually very small and are neglected.

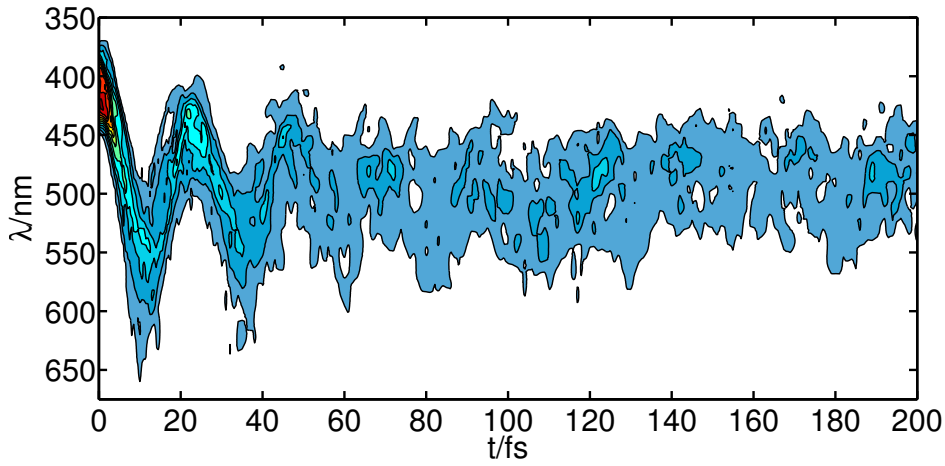

Figure 23: Contour plot of the time-dependent emission spectrum of riboflavin (contours and colors correspond to the relative intensity). The spectrum is obtained as an average of 158 trajectories and was broadened by a Gaussian function with a standard deviation of $\sigma = 300$ cm^{-1}. Adapted from Ref. [140, C.3].

corresponding Wigner distribution in phase space. These initial trajectories are, then, projected onto the excited-state manifold, according to a Franck-Condon transition, and propagated in time if they are within certain energy and oscillator strength thresholds, in order to ensure a transition to the lowest bright $\pi\pi^*$ state. The following non-adiabatic dynamics evolve on the three energetically lowest electronic excited states only, that is allowing surface hopping among the $\pi\pi^*$ state and two energetically close $n\pi^*$ states of very low oscillator strenghts.

After vertical excitation at $t = 0$ the maximum of the stimulated emission spectrum shifts to longer wavelengths within about 10 fs, see Fig. 23, i.e. the Franck-Condon geometry relaxes on a ultrafast time-scale, in accordance with experimental observations [196]. Gradually the oscillation of the emission band is damped and the spectrum is broadened as time evolves. After about 80 to 100 fs oscillations cannot be resolved any more and broadening remains constant, showing the impact of intramolecular vibrational energy redistribution (IVR) in the excited states on the vibrational modes that were dominantly excited by the Franck-Condon transition in the very beginning. Compared to initial time the stimulated emission spectrum is not only clearly broadened, but has considerably lost intensity, and is overall red-shifted, which agrees with experimental findings of fs-resolved fluorescence decay measurements [199]. The oscillation of the peak maximum observed in time-dependent emission spectrum has a period of approximately 22 fs, corresponding to a wavenumber of 1520 cm^{-1}. The C-C and C-N harmonic stretching modes of the isoalloxazine group in the electronic ground and excited state appear at this range of wavenumbers. We recall, that the dom-

inant geometrical differences between ground and excited state potential minima were identified to be bond length changes within the central pyrazine and the uracil moieties of the isoalloxazine due to $\pi \rightarrow \pi^*$ type of transition to S_1, see Sec. 4.2.1 and Ref. [170, C.1]. The corresponding ground state stretching modes were found to mix among each other and with bending modes after electronic excitation. A detailed analysis of the excited state dynamics in terms of dominantly excited normal modes – see Ref. [140, C.3] for more details – confirms that the energy of the C-C and C-N stretching vibrations, which are initially excited by the FC transition, is transferred to low frequency (bending) modes within about 10 fs, and then is gradually spread over all modes of the isoalloxazine ring system due to vibronic couplings. This may be interpreted as validation of experimental evidence for vibronic $\pi\pi^*$-$n\pi^*$ coupling, however, a clear distinction between $\pi\pi^*$ and $n\pi^*$ character of the populated electronic states was not always unambiguous. Non-adiabatic transitions take place though in our simulations, more precisely already within the first 10 fs.

Since experimental (fluorescence) spectra of riboflavin show a solvent dependence [198], and since flavins embedded in proteins form hydrogen bonds at their carbonyl and able amine moieties, it is interesting to repeat the non-adiabatic dynamics, but this time including microsolvation with four water molecules on the polar side of riboflavin, as outlined in Refs. [140, C.3]. Although the simulated fs-resolved stimulated emission spectrum qualitatively resembles the one of the isolated riboflavin, there are still a few noticeable differences due to the hydrogen bonds with the water molecules, as for instance, a red-shift of the emission spectrum and a faster IVR compared to the previous model. Most interesting is, however, an observed tendency for a hydrogen transfer from a water molecule to riboflavin. An analogous (intermediate) hydrogen transfer was postulated based on a combined quantum mechanical-molecular mechanical (QM/MM) model of the BLUF domain, namely between the flavin chromophore and a glutamine in its vicinity due to a light-induced isomerisation of the latter [214]. Furthermore, the nearby tyrosine was also suggested as a proton donor to the flavin in a proposed radical pair mechanism based on ultrafast spectroscopy on BLUF domains [215]. Therefore, the inclusion of the nearest amino acids residues [216] and applying methods suitable to describe hydrogen bonds and proton transfer are advisable for future investigations of photoinduced flavin dynamics. It might be even necessary to extend the timescale, in order to monitor the proposed processes, which can become a formidable task.

We have seen that the simulated non-adiabatic excited state dynamics delivers valuable insight into the ultrafast time evolution of the vibrational dynamics after photoexcitation, and encloses effects like anharmonicity as well as vibronic coupling, allowing to monitor and analyse IVR. The obtained results are not only a reproduction of experimental findings, confirming their interpretations and justifying the applied theoretical methods at the same time, but also helped to gain a deeper understanding of the underlying elementary steps.

In nature these kind of chromophores are embedded within a protein environment, which serves not only as framework to keep the chromophore on-site or as mediator to ensure solubility, but – as already exemplified in this chapter – also influences the electronic structure and, thereby, the photophysics and photochemistry of the chromophore (and its neighbours). To study the impact of the biochemical environment on the chromophore, different approaches are conceivable (if computationally feasible), ranging from continuum solvation models, see Sec. 4.2.1, via the just mentioned microsolvation, and/or an embedding in a point charge field through to hybrid QM/MM models [217]. In the following final section of this chapter we will take a brief look at a chromophore pair in the light harvesting complex II, and give an outlook of some aspects of the interactions between chromophores and their surroundings.

4.4 Influence of the biochemical environment [C.4]

Chromophores in living matter are surrounded by proteins, lipids, water, (solvated) ions and everything else contained in the cell. Therefore, it is reasonable to account for the influence of this biochemical environment on the spectral response of the chromophores. The sheer size of the typical (protein) environment as well as its multiplicity of conformations, however, often exceeds available computational resources by far, in particular, if everything ought to be calculated quantum mechanically. Thus, restrictions have usually to be accepted in terms of the size of the included environment and the methods used to treat it.

Aside of the already discussed continuum solvation and microsolvation models, see Secs. 4.2.1 and 4.3, a treatment of the environment by means of a computationally less demanding, often semi-empirical or molecular mechanical, methodology is a common approach. For the considered flavins, the inclusion of several nearby amino acids of the binding pocket of the BLUF domain was found a convenient model for the chromophore in its natural environment, and has successfully been investigated by means of QM/MM [214], quantum chemical calculations of molecular dynamics snapshots (QM/MD) [200, 218], as well as explicit mixed quantum classical dynamics based on QM/MM calculations [216].

Another example of protein embedded chromophores is the light-harvesting complex II (LHCII). This antenna protein complex, situated within the thylakoid membrane in the chloroplasts of plant cells, contains several chlorophylls and xanthophylls[57], which help to collect the energy of the sunlight and subsequently transfer it by resonance energy transfer[58] to the reaction center of photosystem II for utilization in photosynthesis. While the chlorophylls handle the gradual energy transfer towards the reaction center, xanthophylls, which absorb light in the spectral region of the sunlight not well covered by chlorophylls, are believed to offer their excitation energy to chlorophylls in their proximity [220]. In addition, there is evidence that xanthophylls control the ability of the complex to adapt to low (for light-harvesting) or high light intensities (for protection) [220, 221]. Neither all details of the molecular mechanism of these processes nor the exact influence of the different xanthophylls are, however, fully understood yet [222].

In addition to its huge size, the large number of excitonic coupled chromophores found in LHCII is a challenge for quantum chemistry. Neugebauer and coworkers addressed this problem by means of a subsystem (time-dependent) density functional theory approach [223] based on frozen density embedding [224], where the total electron density is partitioned into a sum of electron densities of subsystems, and the electron density of a subsystem is optimized in the effective embedding potential induced by the others. Despite this, specific chromophores

[57] Xanthophylls are carotenoids and account for the typical yellow pigments of leaves observed in fall, when not concealed by the green chlorophyll.

[58] That is electronic energy transfer (EET) of Förster type [219] through non-radiative dipole-dipole coupling.

of the complex are of interest, too. One of the xanthophylls, violaxanthin, appears close to the border of LHCII and its surrounding thylakoid membrane, and may be converted to zeaxanthin through de-epoxidation as result of the xanthophyll cycle, a process initiated at extensive illumination. The purpose of this transformation is to protect the photosystem from harmful side reactions caused by excessive energy. Here zeaxanthin not only acts as an anti-oxidant but is supposed to facilitate non-photochemical quenching (NPQ)[59] of electronically excited chlorophylls to their ground states, releasing the excessive excitation energy as heat [225].[60] Furthermore, violaxanthin is found in close vicinity of a chlorophyll b molecule in the X-ray structure of the LHCII in peas, see Fig. 24, indicating its excitonic coupling to chlorophyll. Thus, the violaxanthin/zeaxanthin-chlorophyll b pair became subject of theoretical investigations on their relevance in light-harvesting and non-photochemical quenching.

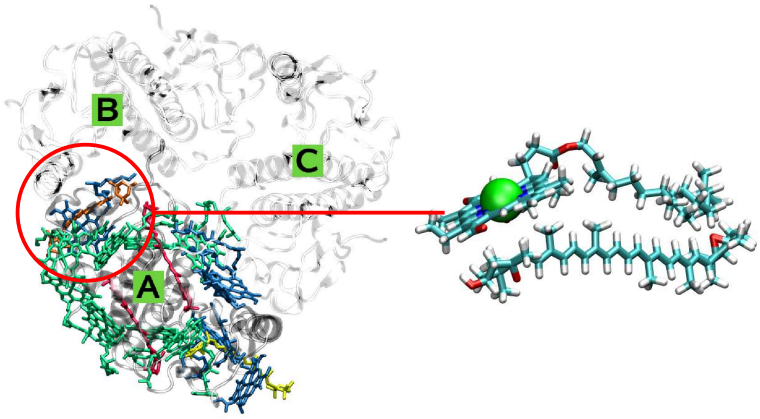

Figure 24: Chromophore pair of chlorophyll b and violaxanthin found in (chain A of) the LHCII trimer of the pea (PDB dataset 2BHW [226]). The complex is viewed from the luminal side of the thylakoid membrane surface. Left: Green - chlorophyll a, blue - chlorophyll b, red - lutein, yellow - 9'-cis-neoxanthin, orange - violaxanthin. Right: Cyan - carbon, white - hydrogen, red - oxygen, blue - nitrogen, green - magnesium. Adapted from Ref. [227].

Dreuw and coworkers extensively studied the electronic excited states of these chromophores, focussing on the their potential for EET and electron transfer by xanthophyll radical cation formation in connection with NPQ [228, 229], as well as on the dependence of the excitation energies on the used xanthophyll geometry [230, 231]. In their studies they addressed the charge-transfer character

[59] In contrast to the photochemical quenching, i.e. the transfer of the energy to the photochemical reaction center.

[60] Otherwise, the singlet excited state of the chlorophyll may decay to a triplet state by inter system crossing (ISC) which in turn supports the formation of highly reactive and damaging singlet oxygen.

of electronic excited states by a combination of the Tamm-Dancoff approximation of TDDFT [232] and CIS. For this system not only the charge-transfer states are a challenge, as they are not adequately described by most density functionals, but also the first excited dark state of the carotenoids which possess a strong double excitation character just like β-carotene, see discussion in Sec. 4.2.2. Marian and coworkers successfully addressed the latter problem by determining the electronic excited states of β-carotene by DFT/multi-reference CI (DFT/MRCI) [195, 233], while Dreuw and coworkers applied ADC(2)-x (extended second-order algebraic diagrammatic construction) [234, 235], an ab initio method related to CIS(D) or CC2 (second order approximate coupled-cluster) [236], which is able to describe doubly excited states.

We chose a different approach for the simulation of the chromophore pair within their natural environment [237, C.4]. As the two methods just mentioned are computationally too expensive for very large systems, we calculated the electronic excited state of the violaxanthin-chlorophyll b pair by linear response TDDFT, however, applying the long-range corrected CAM-B3LYP (Coulomb-attenuated model) functional [238]. This density functional was designed to better account for charge-transfer states by the use of a variable, distance-dependent amount of Hartree-Fock exchange. In addition, improvements in terms of calculated bond length alternation of polyenes are documented [239], which has an impact on their excited state energies. The geometry of the chromophore pair was taken from X-ray structure of LHCII of pea [226] and re-optimized within a shell of surrounding amino acids, lipids and other chlorophylls within about four Ångström radius, applying a hybrid approach, namely a two-layer ONIOM[61] scheme [240], where the high layer of the chromophores was computed by DFT and the low layer environment was treated semi-empirically by PM6[62] [241]. For the computation of the electronic excited states, the optimized structures were embedded in a point charge field (PCF) of all atoms of the LHCII based on the X-ray data. Charges were determined either by the AMBER99[63] force field (for the amino acids) [242] or by a electrostatic potential (ESP) fitting scheme [243, 244] based on B3LYP calculations. Deviations due to appearance of the investigated chromophore pair in each of the three chains of the trimer structure of LHCII, depicted in Fig. 24, were taken into account by averaging the results over subunits A, B and C. Furthermore, an equilibrated thylakoid membrane bilayer, which is in the close vicinity of the chromophores of interest, was included in form of a PCF, based on data provided by Vassiliev and Bruce [245]. For more details on the construction of the PCF see Ref. [237, C.4]. Electronic excited states were computed for different scenarios to determine the impact of the partner chromophore and/or of the environment on the spectral properties of the examined

[61] Our own N-layered Integrated molecular Orbital and molecular Mechanics
[62] Parameterized Model number 6
[63] Assisted Model Building and Energy Refinement

chromophore.

The changes of the energies of the electronic states we observed, when the individual chromophores adjust their geometries to the binding pocket of the LHCII, are rather small. Similar observations are made for the influence of the partner chromophore. However, the oscillator strength of the bright S_2 state of violaxanthin decreases observably when paired with the chlorophyll. This is accompanied by a decrease of the energy of the chlorophyll S_3 state and a small growth of the corresponding oscillator strength. The calculations of the chromophores within the environment clearly confirm this trend, while, apart from that, all excitation energies merely decrease slightly upon insertion into the PCF. We interpret the observed changes, in particular for the S_2 state of violaxanthin and S_3 state of chlorophyll b, as an indication that the protein structure supports a specific distance and orientation of the two chromophores, which allows for an optimal excitonic coupling. In order to further study this effect, we determined the relative orientation (angle) between the transition dipole vectors for those excitation in the individual chromophores. The most favorable relative orientation is, indeed, found between the transition dipoles of the $S_0 \rightarrow S_2$ excitation in violaxanthin and $S_0 \rightarrow S_3$ transition in chlorophyll b [237, C.4]. Moreover, the found decrease in S_3 energy of chlorophyll upon coupling with violaxanthin is the largest of all investigated electronic states, and it is within the same order as the energy shift obtained within the point-dipole point-dipole interaction model [246] based on the calculated transition dipole moments and the distance between the chromophores.

Although the two electronic states of interest are still energetically separated by a few tenth of electronvolts in our simulations, we believe to have given evidence for a potential coupling between the stated electronic excitations within the two chromophores. A relatively large excitonic coupling between the here investigated violaxanthin/chlorophyll b pair was also reported by others based on CIS calculations and the transition density cube (TDC) model [247], however, for the Q_y band (S_2) of chlorophyll b, as higher excited states were not considered. Furthermore, excitation energy transfer from carotenoids to chlorophylls in the LHCII trimer of spinach, in particular from the bright S_2 of xanthophylls to the Soret band (S_3) of chlorophyll b, has also been proposed recently, based on a combined experimental-theoretical study [248]. The effect was, however, most pronounced for the remaining xanthophylls of the LHCII, at least for the used excitation wavelengths. Older experiments on the V1 xanthophyll binding site of the LHCII, which is mostly occupied by violaxanthin, imply that it is not directly involved in light-harvesting [249]. The authors believe that the site mainly acts as a reservoir for the xanthophyll cycle at excess light conditions. The real purpose of the presumably excitonic coupled chromophore pair remains, hence, an interesting research topic.

Concluding we note that the influence of the environment on the investigated chromophores in the LHCII was found to be rather small in our simulations, yet

resulting in a probably essential arrangement of the protein embedded pair. Despite the deficiencies of our model with respect to the determination of doubly excited states, the pure electrostatic interactions of the chromophores with the environment and the omission of nuclear motion (conformations, vibronic progression), we could confirm that violaxanthin widens the spectrum of the nearby chlorophyll b, and found strong indications for an excitonic coupling between these two chromophores.

The understanding of the photophysics and photochemistry of biochromophores, which are essential for light-induced biological processes, is the driving force of a vivid research field. Despite a large variety of detailed experimental studies, few of the many observed mechanisms are fully understood on a electronic molecular level. Here theory may deliver insight into electronic structure and processes for relatively large biochromophores, as exemplified in this chapter, even accounting for the influence of (part of) their natural environment.

5 Achievements and other light-induced processes

5.1 Summary

The analysis and control of light-induced molecular processes is a wide research field and covers a variety of reactions found in nature or used in modern technology. The work at hand focussed on theoretical investigations of a few selected aspects of photoinduced electronic and nuclear changes studied predominantly on a quantum molecular level, namely (i) stereoisomerism and the possibility to control the conformation, and thereby handedness, of molecules or to detect their configuration using laser pulses, as well as (ii) the simulation of electronic structure and (time-dependent) spectra of biochromophores for a better understanding of their functionality in nature. Despite the restrictions of the applied and developed theoretical approaches, mostly due to necessary approximations, several important results were achieved:

We proposed enantio- and diastereo- or, in general, stereoselective laser pulses to control the chirality of molecular switches (Chapter 2). The handedness of the molecules may not only be selectively changed, but it is also possible to "turn on" the chirality of a specific novel molecular switch, featuring a true achiral "off" state. Moreover, a new highly flexible stochastic pulse optimization scheme, inspired by genetic algorithms, was developed in order to maintain the high selectivity and efficiency of our laser pulse control for chiral molecular switches mounted on a surface, which support coupled torsions and different defined orientations. Although the proposed laser pulse control was designed for axially chiral molecular models, the developed concepts may be applied, at least based on their general principles, to all kinds of real stereoisomers, in particular, if they are suited for a direct change of their handedness.

Another, spectroscopic aspect of stereoisomerism, brought to our attention by recent experimental findings, was the distinction of enantiomers in mass spectrometry through multiphoton ionization by circular polarized ultrashort laser pulses. Here we performed laser-driven many electron dynamics based on ab initio calculations, in order to obtain a better understanding of these observations (Chapter 3). In contrast to stereoselective laser pulse control, where the electric field-electric dipole interactions are the driving force, the usually much weaker magnetic field-magnetic dipole interactions were found to be critical for the enantiospecific ionization of the chiral samples. Accordingly, we extended electron wavepacket dynamics, in this case TD-CIS [119], by introducing explicit magnetic field-magnetic dipole transitions between all electronic states. Not only were we able to explain experimental dependencies of the circular dichroism in the ion yield on the pulse duration with our new approach, but we could also make valuable predictions for optimal pulses. The methodology is currently extended

to study new unexplained experimental findings.

Eventually we focussed even more on the spectroscopic aspects of light-molecule interactions. Based on a selection of biologically relevant chromophores we studied, for the most part, electronic spectra (Chapter 4). Aside from the reproduction and explanation of experimental findings, aspects of geometrical changes upon photoexcitation and their impact on the vibronic fine structure as well as on intramolecular energy redistribution were investigated. The inclusion of the changes in vibrational (normal) modes, via either affine transformation or non-adiabatic dynamics, and the resulting coupling of vibrations after vertical excitation were found to be essential for a proper theoretical description and, thus, for a deeper understanding of experimental findings. In particular, for the simulation of resonant Raman spectra we created our own program code based on a time-dependent approach (after Heller [181]), in order to properly account for differences of the normal modes in the electronic excited state in terms of vibrational frequency shifts as well as mode mixing (after Duschinsky [146]). Aspects of environmental effects were treated as well, in form of mechanical embedding, electrostatic interaction, or in form of a fixed surface as a restriction for molecular mobility and orientation (see Chapter 2), as they were found to have an important influence on the investigated systems.

The possibilities and constraints of the used and developed methods were discussed in the corresponding chapters and publications. Not all of the constraints can easily be overcome mainly due to restricted computer power. Still, efforts are made by us to improve the models, for instance, by including (i) more relevant degrees of freedom, either explicitly (if possible) or phenomenologically (e.g. in form of harmonic bath modes), (ii) more interactions with the environment applying e.g. hybrid methods, or (iii) other representations of space and momentum for a better description of e.g. the continuum. The perspectives for our research are manifold and were already stated in the text where appropriate. While the straight experimental implementation of the proposed chiral molecular switches and/or the associated stereoselective laser pulse control are highly desirable, the most satisfying effect of our research would be to see the concept being successfully applied to light-controlled catalysts for asymmetric synthesis, to light-induced chirality transfer for controlled changes of (optical) molecular properties in e.g. liquid crystals (see Sec. 2.7), or eventually even to chiroptical switches for data storage or information processing. In case of the chiral distinction by multiphoton ionization, we hope, by improving our model (see above), to gain further insight into the essentials of the (experimental) laser pulse mediated quantitative and qualitative analysis of stereoisomers in mass spectrometry. In terms of spectroscopy of biochromophores the sought knowledge is still dedicated to the desire for a deeper understanding of the key principles of biological processes, in order to control or even artificially reproduce them. Here our results as well as the indicated improvements of models and methods are believed to be helpful for future investigations.

5.2 Light-induced processes at surfaces

Obviously, light-induced processes are not limited to molecules in gas or liquid phase, as also pointed out for surface mounted chiroptical switches (Sec. 2.5). Indeed, the study of light-induced processes at solid surfaces is of great importance for the understanding of heterogeneous photocatalysis and for the development of important technical applications, such as e.g. solar cells, self-cleaning coatings, or photolithography in semiconductor device fabrication. In general, the study of chemical and physical phenomena at the interface of surfaces, pioneered by scientists such as Haber[64] or Langmuir[65], has become a vivid research field, for instance, for the clarification of the reaction mechanisms in heterogeneous catalysis. In the last decades, this field has been particularly influenced by Ertl, who was awarded the Nobel prize in Chemistry in 2007 for his seminal contributions to the understanding of *chemical processes on solid surfaces* [250].

Aside from the results on light-induced changes in molecules, presented in the work at hand, we also theoretically investigated processes at solid surfaces initiated by light. A detailed review all these studies is beyond the scope of this report. However, a very brief overview is given in the following to emphasize the diversity of such molecular processes and the potential of present theoretical methods to simulate those:

Experiments on solid surfaces are often performed on well-defined single crystal surfaces under ultrahigh vacuum conditions for reasons of reproducibility and defined experimental conditions. Although these ideal conditions are not always a perfect description of real processes on surfaces, they are good prerequisites for theoretical investigations. Just like in case of free molecules, light absorbed by adsorbate and/or substrate may initiate a variety of processes, like dissociation or chemical reaction (at the surface), but also desorption from the surface. In many cases the (electronic structure of the) surface plays a critical role, because it allows for mechanisms which are not possible in gas or liquid phase. Theory is a excellent tool to study and understand these processes, and may help to improve selectivity and yield for reactions at surfaces or even propose new mechanisms [251].

In order to study the laser-induced desorption of small, often diatomic, molecules from metal or non-metal surfaces it is usually mandatory to know the electronic (band) structure of the system. For metal oxide surfaces, such as NiO(100), a cluster approach allows the calculation of the potential energy surface of a representative electronic excited state on multi-configurational ab initio level, in order to simulate the photoinduced desorption of NO by multi-dimensional quantum wavepacket dynamics [252,253]. In those simulations we found a significant bifurcation of the excited state wavepacket, in which the molecular motion parallel to the surface is essentially responsible for the calculated and experimen-

[64] Nobel prize in Chemistry 1918 for the *synthesis of ammonia from its elements*.
[65] Nobel prize in Chemistry 1932 for his *discoveries and investigations in surface chemistry*.

tally observed bimodal velocity distribution of desorbed NO molecules [254].

In case of a metal surface, cluster models are usually not an appropriate approach, as they are not able to correctly describe the electronic band structure of the period solid.[66] In fact, the calculation of the electronic structure of adsorbate/metal complexes, especially their electronic excited states, may become a real challenge, although periodicity can be treated using plane-wave approaches. Thus, model potentials based on parameters adjusted to experimental and, in parts, on first-principle calculation values are often reverted to.

Model potentials allow the study the desorption induced by electronic transition (DIET), for instance, of Cs from a Cu(111) surface by UV laser pulses [255]. For this system we extended an one-electron model potential for Cu(111) by Chulkov and coworkers [256] to account for the Cs adsorbate and its anti-bonding state energetically resided within the band gap. In combination with semi-empirical nuclear potential energy surfaces of electronic ground and the anti-bonding excited states we performed laser-driven electron and nuclear open-system quantum dynamics, in order to determine desorption probabilities caused by the light induced charge transfer from surface to adsorbate [255]. In addition, we proposed a vibrational pre-excitation mechanism for an enhanced photodesorption of Cs through application of an optimal IR laser pulse [257].

If the electronic excited states of the adsorbate are mixed with the conduction band of the solid, a clear separation of electron and nuclear motion for the photodesorption becomes difficult, if not impossible. Harris et al. constructed a (one-)electron-nuclear model potential energy surface for substrate-mediated photodesorption of NO from a Pt(111) slab [258]. Based on this two-dimensional non-Born-Oppenheimer potential energy surface we presented explicitly laser-driven, coupled electron-nuclear quantum wavepacket dynamics, showing that the NO desorption is mediated by the formation and subsequent decay of a negative ion resonance within the conduction band, which corresponds to the excitation of a hot electron and subsequent non-adiabatic transitions within the manifold of electronic excited states [259]. Furthermore, a highly efficient close coupling scheme was developed to propagate the wavepacket in an advantageously adapted diabatic electronic basis.

Light-involved processes at surfaces or within the bulk are, of course, not restricted to well-defined crystalline solids, but also play a role in, for instance, organic polymers. Electronic structure calculations of polymers suffer from similar issues as noted for the previous examples, due to the enormous size of these systems. In addition, they often do not exhibit strict periodicity, but may feature more localized electronic properties than a metal. Therefore, monomer or small oligomer models are a good approximation in many cases. Using trimer models, we simulated X-ray photoelectron spectra (XPS) of poly(vinyl-trifluoroacetate) to study the impact of distant substituents on the C(1s) core binding energy of

[66] Actually quantum size effects might occur in small clusters.

the backbone [260]. We found evidence for an influence of the degree of substitution, but also of the configuration (and, to a lesser extent, conformation) of the oligomers on the probed core binding energy, indicating that the experimentally commonly considered nearest neighbor effects (determined by an increment system) are not sufficient for a correct determination of the chemical shifts. Moreover, there are indications that long-range interactions between polymer strands play a role as well.

Finally, an investigation of the spectral properties of different hole-transporting polyethene-triphenylamine derivatives used in polymer light-emitting diodes (PLED) is worth mentioning: Employing merely monomer models we were able to explain differences observed in experimental fluorescence and phosphorescence spectra of the corresponding polymers based on electronic structure calculations [261]. These, rather small, differences in their electronic structures, caused by geometrical restrictions of the triphenylamine substituents, have eventually an impact on the luminous efficiencies of the respective PLEDs.

Concluding, we realize that theory has great potential for giving insight into light-induced chemical and physical processes on a molecular level, in particular, for problems which go beyond current experimental techniques. Simulations are, however, always restricted by approximations and the available computer hardware. Still, the ongoing advantages in theoretical approaches and efficient algorithms are apparent, although the work at hand could only provide a brief insight into a selection of presently applied and developed methods. The future offers an increasing field of research activities for computational and theoretical chemistry, as the exploration of chemical and physical processes at the molecular level of nuclei and electrons and at the timescale of their inherent dynamics proceeds.

6 Scientific share in discussed publications

In the following, the author's contributions to the presented results, predominantly published in the references listed in Appendices A, B and C, are given:

The idea, the conceptual implementation and the developed general methodology for the scientific questions on chiral molecular switches, discussed in **Chapter 2** and published in the references given in **Appendix A**, were initiated and advanced by the author, who also carried out the major part of the calculations. These investigations were based on the project proposal by the author entitled "*Quantentheorie zur Laserpulskontrolle chiraler molekularer Schalter und Rotoren auf Oberflächen*" (Quantum theory for laser pulse control of chiral molecular switches and rotors on surfaces), financially supported by a research grant of the DFG (German Research Foundation, KR 2942/1) in form of a *Eigene Stelle* (Temporary position for principal investigator). Assistance in quantum chemical or dynamical computations was provided by the students B. Klaumünzer (see Ref. [72, A.1], [76, A.2] and [93, A.4]), and S. Schimka (see Sec. 2.6), respectively. The stochastic pulse optimization technique was developed in close cooperation with PD Dr. T. Klamroth (Universität Potsdam) who also performed the molecular dynamics simulations (see Refs. [84, A.3], [93, A.4] and Sec. 2.6).

The theoretical investigations on chiral distinction in mass spectrometry, presented in **Chapter 3** and the corresponding publications listed in **Appendix B**, were encouraged by experimental findings in the group of the cooperation partner Prof. Dr. K.-M. Weitzel (Philipps-Universität Marburg). The theoretical approach was chosen and methodologically extended by the author based on his project proposal "*Chirale Erkennung und Reaktionskontrolle durch ultrakurze elliptisch polarisierte Laserpulse*" (Chiral detection and reaction control by ultrashort elliptically polarized laser pulses), financially supported by the DFG (KR 2942/2) as *Eigene Stelle*. All theoretical developments and simulations were performed by the author, while all experimental studies were carried out by the experimentalists in Marburg (see Ref. [108, B.1]).

The results on the spectroscopy of biochromophores, covered by **Chapter 4** with corresponding publications given in **Appendix C**, were obtained in cooperation with Prof. Dr. P. Saalfrank (Universität Potsdam) and Dr. J. Götze (Max-Planck-Institut für Kohlenforschung, Mülheim/Ruhr) within different research projects. In the course of some of these projects the author co-supervised J. Götze[67], B. Klaumünzer[68], and S. Banerjee[69] during their doctoral thesis. For the investigations of flavins by B. Klaumünzer the author contributed to Refs. [170,

[67] Thesis 2010, *Influence of protein and solvent environments on quantum chemical properties of photosynthesis enzymes and photoreceptors*

[68] Thesis 2012, *Quantenchemische und molekulardynamische Untersuchungen zur Photoanregung von Riboflavin* (Quantum chemical and molecular dynamical investigations of the photoexcitation of riboflavin)

[69] Thesis in progress.

C.1] and [140, C.3] by giving technical and scientific support, in particular, dealing with the methodological requirements for the calculation of (time-dependent) vibronic spectra – e.g. for the study of mode mixing (see Sec. 4.2) and its impact on IVR (see Sec. 4.3) – as well as with the analysis of the results. These contributions were also the prerequisite for the development of the program code for the simulation of vibronic and resonance Raman spectra based on a time-dependent formalism, in which the author was significantly involved. This code was used by S. Banerjee to calculate the spectra of β-carotene, see Ref. [139, C.2]. Finally, the theoretical study on the electronic structure of chromophores (carotenoids amongst others) in LHCII was done in close cooperation with Dr. J. Götze (MPI für Kohlenforschung). The author significantly contributed, in particular, to the modelling of the environment as well as of the excitonic coupling, and performed most of the calculations. In all cases the author took actively part in the scientific evaluation of the results and in writing the publications.

7 Publications

- S. Banerjee, D. Kröner, P. Saalfrank, Resonance Raman and vibronic absorption spectra with Duschinsky rotation from a time-dependent perspective: Application to β-carotene, *J. Chem. Phys.* **137**, 22A534 (2012).

- B. Klaumünzer, D. Kröner, H. Lischka, P. Saalfrank, Non-adiabatic excited state dynamics of riboflavin after photoexcitation, *Phys. Chem. Chem. Phys.* **14**, 8693–8702 (2012).

- D. Kröner, J. Götze, Modeling of a Violaxanthin-Chlorophyll b chromophore pair in its LHCII environment using CAM-B3LYP, *J. Photochem. Photobiol. B: Biol.* **109**, 12–19 (2012).

- D. Kröner, Chiral distinction by ultrashort laser pulses: Electron wavepacket dynamics incorporating magnetic interactions, *J. Phys. Chem. A* **115**, 14510-14518 (2011).

- D. Kröner, H. Krüger, M. W. Thesen, Electronic structure calculations for hole-transporting triphenylamine derivatives in polymer light-emitting diodes, *Macromol. Theory Simul.* **20**, 790–805 (2011).

- D. Kröner, C. Ehlert, P. Saalfrank, A. Holländer, Ab initio calculations for XPS chemical shifts of poly(vinyl-trifluoroacetate) using trimer models, *Surf. Sci.* **605**, 1513–1521 (2011).

- P. Horsch, G. Urbasch, K.-M. Weitzel, D. Kröner, Circular dichroism in ion yields employing femtosecond laser ionization - the role of laser pulse duration, *Phys. Chem. Chem. Phys.* **13**, 2378–2386 (2011).

- B. Klaumünzer, D. Kröner, P. Saalfrank, (TD-)DFT Calculation of Vibrational and Vibronic Spectra of Riboflavin in Solution, *J. Phys. Chem. B* **114**, 10826–10834 (2010).

- B. Klaumünzer, D. Kröner, N-Inversion in 2-azabicyclopentane derivatives: Model simulations for a laser controlled molecular switch, *New J. Chem.* **33**, 186–195 (2009).

- D. Kröner, B. Klaumünzer, T. Klamroth, From stochastic pulse optimization to a stereoselective laser pulse sequence: Simulation of a chiroptical molecular switch mounted on adamantane, *J. Phys. Chem. A* **112**, 9924–9935 (2008).

- T. Klamroth, D. Kröner, Stereoselective isomerization of an ensemble of adsorbed molecules with multiple orientations: Stochastic laser pulse optimization for selective switching between achiral and chiral atropisomers, *J. Chem. Phys.* **129**, 234701 (2008).

- D. Kröner, S. Klinkusch, T. Klamroth, Enhanced photodesorption by vibrational pre-excitation: Quantum model simulations for Cs/Cu(111), *Surf. Sci.* **602**, 3148–3152 (2008).

- D. Kröner, B. Klaumünzer, Laser-operated chiral molecular switch: Quantum simulations for the controlled transformation between achiral and chiral atropisomers, *Phys. Chem. Chem. Phys.* **9**, 5009–5017 (2007).

- D. Kröner, B. Klaumünzer, Stereoselective laser pulse control of an axial chiral molecular model system supporting four stereoisomers, *Chem. Phys.* **338**, 268–276 (2007).

- D. Kröner, T. Klamroth, M. Nest, P. Saalfrank, Laser-induced charge transfer and photodesorption of Cs @ Cu(111): Quantum dynamical model simulations, *Appl. Phys. A* **88**, 535–546 (2007).

- P. Saalfrank, M. Nest, I. Andrianov, T. Klamroth, D. Kröner, S. Beyvers, Quantum dynamics of laser-induced desorption from metal and semiconductor surfaces and related phenomena, *J. Phys.: Condens. Matter* **18**, 1425–1459 (2006).

- I. Mehdaoui, D. Kröner, M. Pykavy, H.-J. Freund, T. Klüner, Photoinduced desorption of NO from NiO(100): calculation of the four-dimensional potential energy surfaces and systematic wave packet studies, *Phys. Chem. Chem. Phys.* **8**, 1584–1592 (2006).

- T. Klamroth, D. Kröner, P. Saalfrank, Laser-driven coupled electron-nuclear dynamics: Quantum mechanical simulation of molecular photodesorption from metal films, *Phys. Rev. B* **72**, 205407 (2005).

- D. Kröner, I. Mehdaoui, H.-J. Freund, T. Klüner, Three-dimensional ab initio simulation of laser-induced desorption of NO from NiO(100), *Chem. Phys. Lett.* **415**, 150–154 (2005).

- D. Kröner, L. González, Optical Enantioselection in a random ensemble of unidirectionally oriented chiral olefins, *Chem. Phys.* **298**, 55–63 (2004).

- Y. Fujimura, L. González, D. Kröner, J. Manz, I. Mehdaoui, B. Schmidt, Quantum ignition of a model chiral molecular rotor by means of IR + UV laser pulses, *Chem. Phys. Lett.* **386**, 248–253 (2004).

- D. Kröner, L. González, Enantio-selective separation of axial chiral olefins by laser pulses using coupled torsion and pyramidalization motions, *Phys. Chem. Chem. Phys.* **5**, 3933–3942 (2003).

- D. Kröner, M. F. Shibl, L. González, Asymmetric laser excitation in chiral molecules: Quantum simulations for a proposed experiment, *Chem. Phys. Lett.* **372**, 242–248 (2003).

- K. Hoki, D. Kröner, J. Manz, From an oriented racemate via torsionally or electronically excited states to pure enantiomers: Design of pump-dump laser pulses, in Femtochemistry and Femtobiology: Ultrafast Dynamics in Molecular Sciences, edited by A. Douhal and J. Santamaria, World Scientific, Singapore, pp. 337-353 (2002).

- N. Došlić, Y. Fujimura, L. González, K. Hoki, D. Kröner, O. Kühn, J. Manz, Y. Ohtsuki, Quantum control of ultrafast laser-driven isomerization reactions: Proton transfer and selective preparation of enantiomers, in Femtochemistry, edited by F. C. de Schryver, S. de Feyter, and G. Schweitzer, Wiley-VCH, Weinheim, pp. 189–198 (2001).

- L. González, D. Kröner, I. R. Solá, Separation of enantiomers by UV laser pulses. Simulations for H_2POSH: π pulses versus adiabatic transitions., *J. Chem. Phys.* **115**, 2519–2529 (2001).

- K. Hoki, D. Kröner, J. Manz, Selective preparation of enantiomers from a racemate by laser pulses: model simulation for aligned atropisomers with coupled rotations and torsions, *Chem. Phys.* **267**, 59-79 (2001).

- A. Leal, D. Kröner, L. González, Isotopic effects on the control of molecular handedness of H_2POSH by ultrashort laser pulses, *Eur. J. Phys. D* **14**, 185–190 (2001).

- Y. Fujimura, L. González, K. Hoki, D. Kröner, J. Manz, Y. Ohtsuki, From a Racemate to a Pure Enantiomer by Laser Pulses: Quantum Model Simulation for H_2POSH, *Angew. Chem. Int. Ed.* **39**, 4586–4588 (2000), *Angew. Chem.* **112**, 4785–4787 (2000).

- L. González, K. Hoki, D. Kröner, A. S. Leal, J. Manz, Y. Ohtsuki, Selective preparation of enantiomers by laser pulses: From optimal control to specific pump and dump transitions, *J. Chem. Phys.* **113**, 11134–11142 (2000).

References

[1] R. Robinson, Richard Willstätter. 1872-1942, *Obit. Not. Fell. R. Soc.* **8**, 609 (1953).

[2] S. A. Barker, J. A. Bassham, M. Calvin, and U. C. Quarck, Intermediates in the photosynthetic cycle, *Biochim. Biophys. Acta* **21**, 376 (1956).

[3] D. G. Blackmond, The origin of biological homochirality, *Phil. Trans. R. Soc. B* **366**, 2878 (2011).

[4] B. O'Regan and M. Grätzel, A low-cost, high-efficiency solar cell based on dye-sensitized colloidal TiO_2 films, *Nature* **353**, 737 (1991).

[5] P. Nuernberger, R. Selle, F. Langhojer, F. Dimler, S. Fechner, G. Gerber, and T. Brixner, Polarization-shaped femtosecond laser pulses in the ultraviolet, *J. Opt. A: Pure Appl. Opt.* **11**, 085202 (2009).

[6] A. H. Zewail, Femtochemistry: Atomic-scale dynamics of the chemical bond, *J. Phys. Chem. A* **104**, 5660 (2000).

[7] S. Chelkowski, G. L. Yudin, and A. D. Bandrauk, Observing electron motion in molecules, *J. Phys. B: At. Mol. Opt. Phys.* **39**, S409 (2006).

[8] J. Breidbach and L. S. Cederbaum, Universal attosecond response to the removal of an electron, *Phys. Rev. Lett.* **94**, 033901 (2005).

[9] P. B. Corkum and F. Krausz, Attosecond science, *Nature Physics* **3**, 381 (2007).

[10] D. J. Tannor and S. A. Rice, Control of selectivity of chemical reaction via control of wave packet evolution, *J. Chem. Phys.* **83**, 5013 (1985).

[11] D. J. Tannor, R. Kosloff, and S. A. Rice, Coherent pulse sequence induced control of selectivity of reactions: Exact quantum mechanical calculations, *J. Chem. Phys.* **85**, 5805 (1986).

[12] P. Brumer and M. Shapiro, Control of unimolecular reactions using coherent light, *Chem. Phys. Lett.* **126**, 541 (1986).

[13] M. Shapiro, J. W. Hepburn, and P. Brumer, Simplified laser control of unimolecular reactions: Simultaneous (ω_1, ω_3) excitation, *Chem. Phys. Lett.* **149**, 451 (1988).

[14] T. Brixner and G. Gerber, Quantum control of gas-phase and liquid-phase femtochemistry, *ChemPhysChem* **4**, 418 (2003).

[15] G. Vogt, P. Nuernberger, T. Brixner, and G. Gerber, Femtosecond pump-shaped-dump quantum control of retinal isomerization in bacteriorhodopsin, *Chem. Phys. Lett.* **433**, 211 (2006).

[16] R. Ballardini, V. Balzani, A. Credi, M. T. Gandolfi, and M. Venturi, Artificial molecular-level machines: Which energy to make them work?, *Acc. Chem. Res* **34**, 445 (2001).

[17] W. S. Knowless, Asymmetric hydrogenations (Nobel Lecture), *Angew. Chem. Int. Ed.* **41**, 1998 (2002).

[18] R. Noyori, Asymmetric catalysis: Science and opportunities (Nobel Lecture), *Angew. Chem. Int. Ed.* **41**, 2008 (2002).

[19] K. B. Sharpless, Searching for new reactivity (Nobel Lecture), *Angew. Chem. Int. Ed.* **41**, 2024 (2002).

[20] Y. Inoue, Asymmetric photochemical reactions in solution, *Chem. Rev.* **92**, 741 (1992).

[21] M. Avalos, R. Babiano, P. Cintas, J. L. Liménez, J. C. Palacios, and L. D. Barron, Absolute asymmetric synthesis under physical fields: Facts and fictions, *Chem. Rev.* **98**, 2391 (1998).

[22] B. L. Feringa and R. A. van Delden, Absolute asymmetric synthesis: The origin, control, and amplification of chirality, *Angew. Chem. Int. Ed.* **38**, 3418 (1999).

[23] R. A. Harris and L. Stodolsky, Quantum beats in optical activity and weak interactions, *Phys. Lett. B* **78**, 313 (1978).

[24] J. A. Cina and R. A. Harris, Superpositions of handed wave functions, *Science* **267**, 832 (1995).

[25] R. Marquardt and M. Quack, Radiative excitation of the harmonic oscillator with applications to stereomutation in chiral molecules, *Z. Phys. D* **36**, 229 (1996).

[26] R. Berger, M. Gottselig, M. Quack, and M. Willeke, Parity violation dominates the dynamics of chirality in dichlorodisulfane, *Angew. Chem. Int. Ed.* **40**, 4195 (2001).

[27] J. Shao and P. Hänggi, Control of molecular chirality, *J. Chem. Phys.* **107**, 9935 (1997).

[28] A. Salam and W. J. Meath, On the control of excited state relative populations of enantiomers using circularly polarized pulses of varying durations, *J. Chem. Phys.* **106**, 7865 (1997).

[29] Y. Ma and A. Salam, Controlling state populations of enantiomers of real chiral molecules by using a circularly polarized pulsed laser, *Chem. Phys. Lett.* **431**, 247 (2006).

[30] W. Kuhn, The physical significance of optical rotatory power, *Trans. Faraday Soc.* **26**, 293 (1930).

[31] M. Shapiro, E. Frishman, and P. Brumer, Coherently controlled asymmetric synthesis with achiral light, *Phys. Rev. Lett.* **84**, 1669 (2000), Erratum: *Phys. Rev. Lett.* **91**, 129902-1 (2003).

[32] D. Gerbasi, M. Shapiro, and P. Brumer, Theory of enantiomeric control in dimethylallene using achiral light, *J. Chem. Phys.* **115**, 5349 (2001).

[33] E. Frishman, M. Shapiro, D. Gerbasi, and P. Brumer, Enantiomeric purification of nonpolarized racemic mixtures using coherent light, *J. Chem. Phys.* **119**, 7237 (2003).

[34] E. Frishman, M. Shapiro, and P. Brumer, Optical purification of racemic mixtures by 'laser distillation' in the presence of a dissipative bath, *J. Phys. B* **37**, 2811 (2004).

[35] D. Gerbasi, M. Shapiro, and P. Brumer, Theory of "laser distillation" of enantiomers: Purification of a racemic mixture of randomly oriented dimethylallene in a collisional environment, *J. Chem. Phys.* **124**, 074315 (2006).

[36] Y. Fujimura, L. González, K. Hoki, D. Kröner, J. Manz, and Y. Ohtsuki, From a racemate to a pure enantiomer by laser pulses: Quantum model simulations for H_2POSH, *Angew. Chem. Int. Ed.* **39**, 4586 (2000).

[37] K. Hoki, D. Kröner, and J. Manz, Selective preparation of enantiomers from a racemate by laser pulses: model simulation for aligned atropisomers with coupled rotations and torsions, *Chem. Phys.* **267**, 59 (2001).

[38] K. Hoki, L. González, and Y. Fujimura, Control of molecular handedness using pump-dump laser pulses, *J. Chem. Phys.* **116**, 2433 (2002).

[39] K. Hoki, D. Kröner, and J. Manz, From an oriented racemate via torsionally or electronically excited states to pure enantiomers: Design of pump-dump laser pulses, in A. Douhal and J. Santamaria, eds., *Femtochemistry and Femtobiology: Ultrafast Dynamics in Molecular Sciences*, p. 337, World Scientific, Singapore (2002).

[40] K. Hoki, L. González, M. Shibl, and Y. Fujimura, Sequential pump-dump control of photoisomerization competing with photodissociation of optical isomers, *J. Chem. Phys. A* **108**, 6455 (2004).

[41] L. González, B. Schmidt, J. Manz, and M. F. Shibl, Optical resolution of oriented enantiomers via photodissociation: quantum model simulations for H_2POSD, *Phys. Chem. Chem. Phys.* **7**, 4096 (2005).

[42] M. Shapiro and P. Brumer, Controlled photon induced symmetry breaking: Chiral molecular products from achiral precursors, *J. Chem. Phys.* **95**, 8658 (1991).

[43] Y. Fujimura, L. González, K. Hoki, J. Manz, and Y. Ohtsuki, Selective preparation of enantiomers by laser pulses: quantum model simulation for H_2POSH, *Chem. Phys. Lett.* **306**, 1 (1999), Corrigendum: *Chem. Phys. Lett.* **310**, 578 (1999).

[44] D. Kröner, *Theory of selective preparation of enantiomers by laser pulses*, Ph.D. thesis, Freie Universität Berlin (2003).

[45] D. Kröner, M. F. Shibl, and L. González, Asymmetric laser excitation in chiral molecules: Quantum simulations for a proposed experiment, *Chem. Phys. Lett.* **372**, 242 (2003).

[46] D. Kröner and L. González, Enantio-selective separation of axial chiral olefins by laser pulses using coupled torsion and pyramidalization motions, *Phys. Chem. Chem. Phys.* **5**, 3933 (2003).

[47] D. Kröner and L. González, Optical enantioselection in a random ensemble of unidirectionally oriented chiral olefins, *Chem. Phys.* **298**, 55 (2004).

[48] L. González, D. Kröner, and I. Solá, Separation of enantiomers by ultraviolet laser pulses in H_2POSH: π pulses versus adiabatic transitions, *J. Chem. Phys.* **115**, 2519 (2001).

[49] Y. Ohta, K. Hoki, and Y. Fujimura, Theory of stimulated Raman adiabatic passage in a degenerated reaction system: Application to control of molecular handedness, *J. Chem. Phys.* **116**, 7509 (2002).

[50] P. Král and M. Shapiro, Cyclic population transfer in quantum systems with broken symmetry, *Phys. Rev. Lett.* **87**, 183002 (2001).

[51] P. Král, I. Thanopulos, M. Shapiro, and D. Cohen, Two-step enantioselective optical switch, *Phys. Rev. Lett.* **90**, 033001 (2003).

[52] B. Grishanin, H. Takahashi, Y. Vladimirova, D. Zhdanov, and V. N. Zadkov, Laser coherent control of an ensemble of randomly oriented chiral molecules, *Laser Phys.* **15**, 1247 (2005).

[53] D. V. Zhdanov and V. N. Zadkov, Absolute asymmetric synthesis from an isotropic racemic mixture of chiral molecules with the help of their laser orientation-dependent selection, *J. Chem. Phys.* **127**, 244312 (2007).

[54] J.-P. Sauvage, *Molecular Machines and Motors*, Springer, Berlin (2001).

[55] S. A. Bissel, E. Cordova, A. E. Kaifer, and J. F. Stoddart, A chemically and electrochemically switchable molecular shuttle, *Nature* **369**, 133 (1994).

[56] T. C. Bedard and J. S. Moore, Design and synthesis of a "Molecular Turnstile", *J. Am. Chem. Soc.* **117**, 10662 (1995).

[57] N. P. M. Huck, W. F. Jager, B. de Lange, and B. L. Feringa, Dynamic control and amplification of molecular chirality by circular polarized light, *Science* **273**, 1686 (1996).

[58] T. R. Kelly, H. D. Silva, and R. A. Silva, Unidirectional rotary motion in a molecular system, *Nature* **401**, 150 (1999).

[59] N. Koumura, R. W. J. Zijlstra, R. A. van Delden, N. Harada, and B. L. Feringa, Light-driven monodirectional molecular rotor, *Nature* **401**, 152 (1999).

[60] R. A. van Delden, M. K. J. ter Wiel, and B. L. Feringa, A chiroptical molecular switch with perfect stereocontrol, *Chem. Commun.* p. 200 (2004).

[61] B. L. Feringa, R. A. van Delden, and M. K. J. ter Wiel, In control of switching, motion, and organization, *Pure Appl. Chem.* **75**, 563 (2003).

[62] Y. Yu, M. Nakano, and T. Ikeda, Directed bending of a polymer film by light, *Nature* **425**, 145 (2003).

[63] R. Eelkema, M. M. Pollard, N. Katsonis, J. Vicario, D. J. Broer, and B. L. Feringa, Rotational reorganization of doped cholestric liquid crystalline films, *J. Am. Chem. Soc.* **128**, 14397 (2006).

[64] J. Ma, Y. Li, T. White, A. Urbas, and Q. Li, Light-driven nanoscale chiral molecular switch: reversible dynamic full range color phototuning, *Chem. Commun.* **46**, 3463 (2010).

[65] N. Tamai and H. Miyasaka, Ultrafast dynamics of photochromic systems, *Chem. Rev.* **100**, 1875 (2000).

[66] M. Irie, Diarylethenes for memories and switches, *Chem. Rev.* **100**, 1685 (2000).

[67] D. Geppert, L. Seyfarth, and R. de Vivie-Riedle, Laser control schemes for molecular switches, *Appl. Phys. B* **79**, 987 (2004).

[68] Y. Fujimura, L. González, D. Kröner, J. Manz, I. Mehdaoui, and B. Schmidt, Quantum ignition of intramolecular rotation by means of IR + UV laser pulses, *Chem. Phys. Lett.* **386**, 248 (2004).

[69] H. Umeda, M. Takagi, S. Yamada, S. Koseki, and Y. Fujimura, Quantum control of molecular chirality: Optical isomerization of difluorobenzo[c]phenanthrene, *J. Am. Chem. Soc.* **124**, 9265 (2002).

[70] K. Hoki, S. Koseki, T. Matsushita, R. Sahnoun, and Y. Fujimura, Quantum control of molecular chirality: Ab initio molecular orbital study and wave packet analysis of 1,1'-binaphthyl, *J. Photochem. and Photobiol. A: Chem.* **178**, 258 (2006).

[71] B. Klaumünzer and D. Kröner, N-inversion in 2-azabicyclopentane derivatives: model simulations for a laser controlled molecular switch, *New J. Chem.* **33**, 186 (2009).

[72] D. Kröner and B. Klaumünzer, Stereoselective laser pulse control of an axial chiral molecular model system supporting four stereoisomers, *Chem. Phys.* **338**, 268 (2007).

[73] R. S. Cahn, C. Ingold, and V. Prelog, Spezifikation der molekularen Chiralität, *Angew. Chem.* **78**, 413 (1966).

[74] F. Hund, Zur Deutung der Molekelspektren. III. Bemerkungen über das Schwingungs- und Rotationsspektrum bei Molekeln mit mehr als zwei Kernen, *Z. Phys.* **43**, 805 (1927).

[75] J. Trost and K. Hornberger, Hund's paradox and the collisional stabilization of chiral molecules, *Phys. Rev. Lett.* **103**, 023202 (2009).

[76] D. Kröner and B. Klaumünzer, Laser-operated chiral molecular switch: Quantum simulations for the controlled transformation between achiral and chiral atropisomers, *Phys. Chem. Chem. Phys.* **9**, 5009 (2007).

[77] M. Yamaki, K. Hoki, Y. Ohtsuki, H. Kono, and Y. Fujimura, Quantum control of a chiral molecular motor driven by laser pulses, *J. Am. Chem. Soc.* **127**, 7300 (2005).

[78] H. Loesch and A. Remscheid, Brute force in molecular reaction dynamics: A novel technique for measuring steric effects, *J. Chem. Phys.* **93**, 4779 (1990).

[79] B. Friedrich and D. Herschbach, Manipulating molecules via combined static and laser fields, *J. Phys. Chem. A* **103**, 10280 (1999).

[80] J. J. Larsen, K. Hald, N. Bjerre, H. Stapelfeldt, and T. Seideman, Three dimensional alignment of molecules using elliptically polarized laser fields, *Phys. Rev. Lett.* **85**, 2470 (2000).

[81] K. Hoki, L. González, and Y. Fujimura, Quantum control of molecular handedness in a randomly oriented racemic mixture using three polarization components of electric fields, *J. Chem. Phys.* **116**, 8799 (2002).

[82] M. O. Lorenzo, C. J. Baddeley, C. Muryn, and R. Raval, Extended surface chirality from supramolecular assemblies of adsorbed chiral molecules, *Nature (London)* **404**, 376 (2000).

[83] K.-H. Ernst, Y. M. Neuber, M. Grunze, and U. Ellerbeck, NEXAFS study on the orientation of chiral p-heptahelicene on Ni(100), *J. Am. Chem. Soc.* **123**, 493 (2001).

[84] T. Klamroth and D. Kröner, Stereoselective isomerization of an ensemble of adsorbed molecules with multiple orientations: Stochastic laser pulse optimization for selective switching between achiral and chiral atropisomers, *J. Chem. Phys.* **129**, 234701 (2008).

[85] S. Shi, A. Woody, and H. Rabitz, Optimal control of selective vibrational excitation in harmonic linear chain molecules, *J. Chem. Phys.* **88**, 6870 (1988).

[86] R. Kosloff, S. A. Rice, P. Gaspard, S. Tersigni, and D. J. Tannor, Wavepacket dancing: Achieving chemical selectivity by shaping light pulses, *Chem. Phys.* **139**, 201 (1989).

[87] W. Zhu, J. Botina, and H. Rabitz, Rapidly convergent iteration methods for quantum optimal control of population, *J. Chem. Phys.* **108**, 1953 (1998).

[88] W. Zhu and H. Rabitz, A rapid monotonically convergent iteration algorithm for quantum optimal control over the expectation value of a positive definite operator, *J. Chem. Phys.* **109**, 385 (1998).

[89] R. Judson and H. Rabitz, Teaching lasers to control molecules, *Phys. Rev. Lett.* **68**, 1500 (1992).

[90] A. Assion, T. Baumert, M. Bergt, T. Brixner, B. Kiefer, V. Seyfried, M. Strehle, and G. Gerber, Control of chemical reactions by feedback-optimized phase-shaped femtosecond laser pulses, *Science* **282**, 919 (1998).

[91] Š. Vajda, A. Bartelt, E. Kaposta, T. Leisner, C. Lupulescu, S. Minemoto, R. Rosendo-Francisco, and L. Wöste, Feedback optimization of shaped femtosecond laser pulses for controlling the wavepacket dynamics and reactivity of mixed alkaline clusters, *Chem. Phys.* **267**, 231 (2001).

[92] T. Kitagawa, Y. Idomoto, H. Matsubara, D. Hobara, T. Kakiuchi, T. Okazaki, and K. Komatsu, Rigid molecular tripod with an adamantane framework and thiol legs. Synthesis and observation of an ordered monolayer on Au(111), *J. Org. Chem.* **71**, 1362 (2006).

[93] D. Kröner, B. Klaumünzer, and T. Klamroth, From stochastic pulse optimization to a stereoselective laser pulse sequence: Simulation of a chiroptical molecular switch mounted on adamantane, *J. Phys. Chem. A* **112**, 9924 (2008).

[94] K. Husimi, Some formal properties of the density matrix, *Proc. Phys.-Math. Soc. Jpn. 3rd Ser.* **22**, 264 (1940).

[95] R. A. van Delden, M. K. J. ter Wiel, M. M. Pollard, J. Vicario, N. Koumura, and B. L. Feringa, Unidirectional molecular motor on a gold surface, *Nature* **437**, 1337 (2005).

[96] R. Eelkema and B. L. Feringa, Amplification of chirality in liquid crystals, *Org. Biomol. Chem.* **4**, 3729 (2006).

[97] I. Sato, R. Sugie, Y. Matsueda, Y. Furumura, and K. Soai, Asymmetric synthesis utilizing circularly polarized light mediated by the photoequilibrium of chiral olefins in conjuction with asymmetric autocatalysis, *Angew. Chem. Int. Ed.* **43**, 4490 (2004).

[98] G. J. Simpson, Structural origins of circular dichroism in surface second harmonic generation, *J. Chem. Phys.* **117**, 3398 (2002).

[99] T. Müller, K. B. Wiberg, P. H. Vaccaro, J. R. Cheeseman, and M. J. Frisch, Cavity ring-down polarimetry (CRDP): theoretical and experimental characterization, *J. Opt. Soc. Am. B* **19**, 125 (2002).

[100] S. Turchini, N. Zema, S. Zennaro, L. Alagna, B. Stewart, R. D. Peacock, and T. Prosperi, Core electron transitions as a probe for molecular chirality: Natural circular dichroism at the carbon K-edge of methyloxirane, *J. Am. Chem. Soc.* **126**, 4532 (2004).

[101] L. Nahon, G. A. Garcia, C. J. Harding, E. Mikajlo, and I. Powis, Determination of chiral asymmetries in the valence photoionization of camphor enantiomers by photoelectron imaging using tunable circularly polarized light, *J. Chem. Phys.* **125**, 114309 (2006).

[102] C. Lux, M. Wollenhaupt, T. Bolze, Q. Liang, J. Köhler, C. Sarpe, and T. Baumert, CD in the photoelectron angular distribution of camphor and fenchone from multiphoton ionization with femtosecond laser pulses, *Angew. Chem. Int. Ed.* **51**, 5001 (2012).

[103] J. M. D. Cruz, V. V. Lozovoy, and M. Dantus, Isomeric identification by laser control mass spectrometry, *J. Mass Spectrom.* **42**, 178 (2007).

[104] G. Urbasch, H. G. Breunig, and K.-M. Weitzel, Distinction of ortho- and para-xylene by femtosecond-laser mass spectrometry, *ChemPhysChem* **8**, 2185 (2007).

[105] U. Boesl von Grafenstein and A. Bornschlegl, Circular dichroism laser mass spectrometry: Differentiation of 3-methylcyclopentanone enantiomers, *ChemPhysChem* **7**, 2085 (2006).

[106] R. Li, R. Sullivan, W. Al-Basheer, R. M. Pagni, and R. N. Compton, Linear and nonlinear circular dichroism of R-(+)-3-methylcyclopentanone, *J. Chem. Phys.* **125**, 144304 (2006).

[107] H. G. Breunig, G. Urbasch, P. Horsch, J. Cordes, U. Koert, and K.-M. Weitzel, Circular dichroism in ion yields of femtosecond-laser mass spectrometry, *ChemPhysChem* **10**, 1199 (2009).

[108] P. Horsch, G. Urbasch, K.-M. Weitzel, and D. Kröner, Circular dichroism in ion yields employing femtosecond laser ionization – the role of laser pulse duration, *Phys. Chem. Chem. Phys.* **13**, 2378 (2011).

[109] Y. Ma and A. Salam, On chiral selectivity of enantiomers using a circularly polarized pulsed laser under resonant and off-resonant conditions, *Chem. Phys.* **324**, 367 (2006).

[110] W. J. Meath and E. A. Power, On the interaction of elliptically polarized light with molecules; the effects of both permanent and transition multipole moments on multiphoton absorption and chiroptical effects, *J. Mod. Opt.* **36**, 977 (1989).

[111] P. Balling, D. J. Maas, and L. D. Noordam, Interference in climbing a quantum ladder system with frequency-chirped laser pulses, *Phys. Rev. A* **50**, 4276 (1994).

[112] L. Rosenfeld, Quantenmechanische Theorie der natürlichen optischen Aktivität von Flüssigkeiten und Gasen, *Z. Phys.* **52**, 161 (1928).

[113] E. U. Condon, Theories of optical rotatory power, *Rev. Mod. Phys.* **9**, 432 (1937).

[114] D. Kim and T. Baer, Gas-phase measurement of ΔH^0 between axial and equatorial conformations of 3-methylcyclopentanone, *Chem. Phys.* **256**, 251 (2000).

[115] J. He, A. G. Petrovic, and P. L. Polavarapu, Determining the conformer populations of (R)-(+)-3-methylcyclopentanone using vibrational absorption, vibrational circular dichroism, and specific rotation, *J. Phys. Chem. B* **108**, 20451 (2004).

[116] S. Feinleib and F. A. Bovey, Vapour-phase vacuum-ultraviolet circular-dichroism spectrum of (+)-3-methylcyclopentanone, *Chem. Commun. (London)* p. 978 (1968).

[117] J. B. Foresman, M. Head-Gordon, J. A. Pople, and M. J. Frisch, Toward a systematic molecular orbital theory for excited states, *J. Phys. Chem.* **96**, 135 (1992).

[118] M. Head-Gordon, R. J. Rico, M. Oumi, and T. J. Lee, A doubles correction to electronic excited states from configuration interaction in the space of single substitutions, *Chem. Phys. Lett* **219**, 21 (1994).

[119] T. Klamroth, Laser-driven electron transfer through metal-insulator-metal contacts: Time-dependent configuration interaction singles calculations for a jellium model, *Phys. Rev. B* **68**, 245421 (2003).

[120] A. I. Kuleff, J. Breidbach, and L. S. Cederbaum, Multielectron wave-packet propagation: General theory and application, *J. Chem. Phys.* **123**, 044111 (2005).

[121] L. Allen and J. H. Eberly, *Optical Resonance and Two-Level Atoms*, Wiley, New York (1975).

[122] M. J. Frisch, G. W. Trucks, H. B. Schlegel, G. E. Scuseria, M. A. Robb, J. R. Cheeseman, G. Scalmani, V. Barone, B. Mennucci, G. A. Petersson, H. Nakatsuji, M. Caricato, X. Li, H. P. Hratchian, A. F. Izmaylov, *et al.*, Gaussian 09, Revision A.02, Gaussian Inc., Wallingford CT, 2009.

[123] D. Kröner, Chiral distinction by ultrashort laser pulses: Electron wavepacket dynamics incorporating magnetic interactions, *J. Phys. Chem. A* **115**, 14510 (2011).

[124] P. Krause and T. Klamroth, Dipole switching in large molecules described by explicitly time-dependent configuration interaction, *J. Chem. Phys.* **128**, 234307 (2008).

[125] P. Horsch, G. Urbasch, and K.-M. Weitzel, Analysis of chirality by femtosecond laser ionization mass spectrometry, *Chirality* **24**, 684 (2012).

[126] N. Lin, Y. Luo, F. Santoro, X. Zhao, and A. Rizzo, Vibronically-induced change in the chiral response of molecules revealed by electronic circular dichroism spectroscopy, *Chem. Phys. Lett.* **464**, 144 (2008).

[127] P. Horsch, G. Urbasch, and K.-M. Weitzel, Circular dichroism in ion yields in multiphoton ionization of (R)-propylene oxide employing femtosecond laser pulses, *Z. Phys. Chem.* **225**, 587 (2011).

[128] A. Bornschlegl, C. Logé, and U. Boesl, Investigation of CD effects in the multi photon ionisation of R-(+)-3-methylcyclopentanone, *Chem. Phys. Lett.* **447**, 187 (2007).

[129] A. Rizzo, N. Lin, and K. Ruud, Ab initio study of the one- and two-photon circular dichroism of R-(+)-3-methyl-cyclopentanone, *J. Chem. Phys.* **128**, 164312 (2008).

[130] I. Powis, Photoelectron circular dichroism in chiral molecules, *Adv. Chem. Phys.* **138**, 267 (2008).

[131] W. R. Briggs and M. A. Olney, Photoreceptors in plant photomorphogenesis to date. Five phytochromes, two cryptochromes, one phototropin, and one superchrome, *Plant Physio.* **125**, 85 (2001).

[132] P. Hegemann, Algal sensory photoreceptors, *Ann. Rev. Plant Biol.* **59**, 167 (2008).

[133] J. M. Christie, P. Reymond, G. K. Powell, P. Bernasconi, A. A. Raibekas, E. Liscum, and W. R. Briggs, Arabidopsis NPH1: A flavoprotein with the properties of a photoreceptor for phototropism, *Science* **282**, 1698 (1998).

[134] J. A. Jarillo, H. Gabrys, J. Capel, J. M. Alonso, J. R. Ecker, and A. R. Cashmore, Phototropin-related NPL1 controls chloroplast relocation induced by blue light, *Nature* **410**, 952 (2001).

[135] T. Kinoshita, M. Doi, N. Suetsugu, T. Kagawa, M. Wada, and K. Shimazaki, phot1 and phot2 mediate blue light regulation of stomatal opening, *Nature* **414**, 656 (2001).

[136] M. A. van der Horst and K. J. Hellingwerf, Photoreceptor proteins, "Star actors of modern times": A review of the functional dynamics in the structure of representative members of six different photoreceptor families, *Acc. Chem. Res.* **37**, 13 (2004).

[137] J. M. Christie, M. Salomon, K. Nozue, M. Wada, and W. R. Briggs, LOV (light, oxygen, or voltage) domains of the blue-light photoreceptor phototropin (NPH1): Binding sites for the chromophore flavin mononucleotide, *Proc. Natl. Acad. Sci.* **96**, 8779 (1999).

[138] M. Gomelsky and G. Klug, BLUF: a novel FAD-binding domain involved in sensory transduction in microorganisms, *Trends Biochem. Sci.* **27**, 497 (2002).

[139] S. Banerjee, D. Kröner, and P. Saalfrank, Resonance Raman and vibronic absorption spectra with Duschinsky rotation from a time-dependent perspective: Application to β-carotene, *J. Chem. Phys.* **137**, 22A534 (2012).

[140] B. Klaumünzer, D. Kröner, H. Lischka, and P. Saalfrank, Non-adiabatic excited state dynamics of riboflavin after photoexcitation, *Phys. Chem. Chem. Phys.* **14**, 8693 (2012).

[141] B. Robert, Resonance Raman spectroscopy, *Photosynth. Res.* **101**, 147 (2009).

[142] G. Herzberg and E. Teller, Schwingungsstruktur der Elektronenübergänge bei mehratomigen Molekülen, *Z. Phy. Chem. (Leipzig)* **B21**, 410 (1933).

[143] J. Franck, Elementary processes of photochemical reactions, *Trans. Faraday Soc.* **21**, 536 (1926).

[144] E. U. Condon, Nuclear motions associated with electron transitions in diatomic molecules, *Phys. Rev.* **32**, 858 (1928).

[145] C. W. Müller, J. J. Newby, C.-P. Liu, C. P. Rodrigo, and T. S. Zwier, Duschinsky mixing between four non-totally symmetric normal coordinates in the S_1-S_0 vibronic structure of (E)-phenylvinylacetylene: a quantitative analysis, *Phys. Chem. Chem. Phys.* **12**, 2331 (2010).

[146] F. Duschinsky, On the interpretation of electronic spectra of polyatomic molecules, *Acta Physicochim. U.R.S.S.* **7**, 551 (1937).

[147] C. Eckart, Some studies concerning rotating axes and polyatomic molecules, *Phys. Rev.* **47**, 552 (1935).

[148] I. Özkan, Franck-Condon principle for polyatomic molecules: Axis-switching effects and transformation of normal coordinates, *J. Mol. Spec.* **139**, 147 (1990).

[149] J. T. Hougen and J. K. G. Watson, Anomalous rotational line intensities in electronic transitions of polyatomic molecules: Axis-switching, *Can. J. Phys.* **43**, 298 (1965).

[150] A. Warshel and M. Karplus, Vibrational structure of electronic transitions in conjugated molecules, *Chem. Phys. Lett.* **17**, 7 (1972).

[151] F. Santoro, R. Improta, A. Lami, J. Bloino, and V. Barone, Effective method to compute Franck-Condon integrals for optical spectra of large molecules in solution, *J. Chem. Phys.* **126**, 084509 (2007).

[152] K. N. Kudin and A. Y. Dymarsky, Eckart axis conditions and the minimization of the root-mean-square deviation: Two closely related problems, *J. Chem. Phys.* **122**, 224105 (2005).

[153] G. M. Sando and K. G. Spears, Ab initio computation of the Duschinsky mixing of vibrations and nonlinear effects, *J. Phys. Chem.* **105**, 5326 (2001).

[154] J. M. Hollas, H. Musa, T. Ridley, P. H. Turner, K. H. Weisenberger, and V. Fawcett, The $\tilde{A}^1A'$-$\tilde{X}^1A'$ single vibronic level fluorescence and Raman spectra of styrene-β-D_2 vapor and their use in determining the C(1)-C(α) torsional potential function in the $\tilde{X}$ state, *J. Mol. Spectrosc.* **94**, 437 (1981).

[155] T. E. Sharp and H. M. Rosenstock, Franck-Condon factors for polyatomic molecules, *J. Phys. Chem.* **41**, 3453 (1964).

[156] L. S. Cederbaum and W. Domcke, A many-body approach to the vibrational structure in molecular electronic spectra. I. Theory, *J. Phys. Chem.* **64**, 603 (1976).

[157] E. V. Doktorov, I. A. Malkin, and V. I. Man'ko, Dynamical symmetry of vibronic transitions in polyatomic molecules and the Franck-Condon principle, *J. Mol. Spec.* **64**, 302 (1977).

[158] K. C. Kulander, Generalization of the Faulkner-Richardson method for calculating polyatomic Franck-Condon factors, *J. Chem. Phys.* **71**, 2736 (1979).

[159] D. Gruner and P. Brumer, Efficient evaluation of harmonic polyatomic Franck-Condon factors, *Chem. Phys. Lett.* **138**, 310 (1987).

[160] P. T. Ruhoff, Recursion relations for multi-dimensional Franck-Condon overlap integrals, *Chem. Phys.* **186**, 355 (1994).

[161] P.-Å. Malmqvist and N. Forsberg, Franck-Condon factors for multidimensional harmonic oscillators, *Chem. Phys.* **228**, 227 (1998).

[162] R. Berger, C. Fischer, and M. Klessinger, Calculation of the vibronic fine structure in electronic spectra at higher temperatures. 1. Benzene and pyrazine, *J. Phys. Chem. A* **102**, 7157 (1998).

[163] R. Islampour, M. Dehestani, and S. H. Lin, A new expression for multidimensional Franck-Condon integrals, *J. Mol. Spectrosc.* **194**, 179 (1999).

[164] M. Dierksen and S. Grimme, An efficient approach for the calculation of Franck-Condon integrals of large molecules, *J. Chem. Phys.* **122**, 244101 (2005).

[165] H.-C. Jankowiak, J. L. Stuber, and R. Berger, Vibronic transitions in large molecular systems: Rigorous prescreening conditions for Franck-Condon factors, *J. Chem. Phys.* **127**, 234101 (2007).

[166] F. Santoro, A. Lami, R. Improta, J. Bloino, and V. Barone, Effective method for the computation of optical spectra of large molecules at finite temperature including the Duschinsky and Herzberg-Teller effect: The Q_x band of porphyrin as a case study, *J. Chem. Phys.* **128**, 224311 (2008).

[167] M. Dierksen, *Calculations of the vibronic structure of electronic spectra for large molecules*, Ph.D. thesis, Wilhelms-Universität Münster, Germany (2006).

[168] M. Dierksen, FCfast, Universität Münster, Germany, 2004-2006.

[169] F. Santoro, FCclasses: A Fortran 77 code, 2008, available via: http://village.pi.iccom.cnr.it.

[170] B. Klaumünzer, D. Kröner, and P. Saalfrank, (TD-)DFT calculation of vibrational and vibronic spectra of riboflavin in solution, *J. Phys. Chem. B* **114**, 10826 (2010).

[171] M. Sun, T. A. Moore, and P.-S. Song, Molecular luminescence studies of flavins. I. The excited states of flavins, *J. Am. Chem. Soc.* **94**, 1730 (1972).

[172] T. Kottke, J. Heberle, D. Hehn, B. Dick, and P. Hegemann, Phot-LOV1: Photocycle of a blue-light receptor domain from the green alga *Chlamydomonas reinhardtii*, *Biophys. J.* **84**, 1192 (2003).

[173] S. D. M. Islam, A. Penzkofer, and P. Hegemann, Quantum yield of triplet formation of riboflavin in aqueous solution and of flavin mononucleotide bound to the LOV1 domain of Phot1 from *Chlamydomonas reinhardtii*, *Chem. Phys.* **291**, 97 (2003).

[174] C. Neiß, P. Saalfrank, M. Parac, and S. Grimme, Quantum chemical calculation of excited states of flavin-related molecules, *J. Phys. Chem. A* **107**, 140 (2003).

[175] S. Salzmann, J. Tatchen, and C. M. Marian, The photophysics of flavins: What makes the difference between gas phase and aqueous solution?, *J. Photochem. Photobiol. A: Chem.* **198**, 221 (2008).

[176] M. M. N. Wolf, C. Schumann, R. Gross, T. Domratcheva, and R. Diller, Ultrafast infrared spectroscopy of riboflavin: Dynamics, electronic structure, and vibrational mode analysis, *J. Phys. Chem. B* **112**, 13424 (2008).

[177] J. Tomasi, B. Mennucci, and R. Cammi, Quantum mechanical continuum solvation models, *Chem. Rev.* **105**, 2999 (2005).

[178] A. Klamt and G. Schüürmann, COSMO: a new approach to dielectric screening in solvents with explicit expressions for the screening energy and its gradient, *J. Chem. Soc., Perkin Trans.* **2**, 799 (1993).

[179] H. A. Kramer and W. Heisenberg, Über die Streuung von Strahlung durch Atome, *Z. Phys.* **31**, 681 (1925).

[180] P. A. M. Dirac, The quantum theory of dispersion, *Proc. Roy. Soc. London A* **114**, 710 (1927).

[181] D. J. Tannor and E. J. Heller, Polyatomic Raman scattering for general harmonic potentials, *J. Chem. Phys.* **77**, 202 (1982).

[182] A. B. Myers, 'Time-dependent' resonance Raman theory, *J. Raman Spectrosc.* **28**, 389 (1997).

[183] E. J. Heller, R. L. Sundberg, and D. Tannor, Simple aspects of Raman scattering, *J. Phys. Chem.* **86**, 1822 (1982).

[184] C. Herrmann, J. Neugebauer, M. Presselt, U. Uhlemann, M. Schmitt, S. Rau, J. Popp, and M. Reiher, The first photoexcitation step of Ruthenium-based models for artificial photosynthesis highlighted by resonance Raman spectroscopy, *J. Phys. Chem. B* **111**, 6078 (2007).

[185] K. A. Kane and L. Jensen, Calculation of absolute resonance Raman intensities: Vibronic theory vs short-time approximation, *J. Phys. Chem. C* **114**, 5540 (2010).

[186] E. J. Heller, Quantum corrections to classical photodissociation models, *J. Chem. Phys.* **68**, 2066 (1978).

[187] Y. J. Yan and S. Mukamel, Eigenstate-free, Green function, calculation of molecular absorption and fluorescence line shapes, *J. Chem. Phys.* **85**, 5908 (1986).

[188] J. Tatchen and E. Pollak, Ab initio spectroscopy and photoinduced cooling of the trans-stilbene molecule, *J. Chem. Phys.* **128**, 164303 (2008).

[189] V. Hizhnyakov and I. Tehver, Resonance Raman scattering of multimode systems: Fourier amplitude approach, *J. Raman Spectrosc.* **24**, 653 (1993).

[190] T. Rush III and W. L. Peticolas, Ab initio transform calculation of resonance Raman spectra of uracil, 1-methyluracil, and 5-methyluracil, *J. Phys. Chem.* **99**, 14647 (1995).

[191] T. Petrenko and F. Neese, Analysis and prediction of absorption band shapes, fluorescence band shapes, resonance Raman intensities, and excitation profiles using the time-dependent theory of electronic spectroscopy, *J. Chem. Phys.* **127**, 164319 (2007).

[192] F. Neese, ORCA, an ab initio, density functional and semiempirical program package, University of Bonn, Bonn, Germany, 2007.

[193] N. Tschirner, M. Schenderlein, K. Brose, E. Schlodder, M. A. Mroginski, C. Thomsen, and P. Hildebrandt, Resonance Raman spectra of β-carotene in solution and in photosystems revisited: an experimental and theoretical study, *Phys. Chem. Chem. Phys.* **11**, 11471 (2009).

[194] N. Tschirner, K. Brose, M. Schenderlein, A. Zouni, E. Schlodder, M. A. Mroginski, P. Hildebrandt, and C. Thomsen, The anomaly of the equation ν_1-resonance Raman band of β-carotene in solution and in photosystem I and II, *Phys. Status Solidi B* **246**, 2790 (2009).

[195] J. P. Cerón-Carrasco, A. Requena, and C. M. Marian, Theoretical study of the low-lying excited states of β-carotene isomers by a multireference configuration interaction method, *Chem. Phys.* **373**, 98 (2010).

[196] A. Weigel, A. L. Dobryakov, M. Veiga, and J. L. P. Lustres, Photoinduced processes in riboflavin: Superposition of $\pi\pi^*$-$n\pi^*$ states by vibronic coupling, transfer of vibrational coherence, and population dynamics under solvent control, *J. Phys. Chem. A* **112**, 12054 (2008).

[197] M. M. N. Wolf, C. Schumann, R. Gross, T. Domratcheva, and R. Diller, Ultrafast infrared spectroscopy of riboflavin: Dynamics, electronic structure, and vibrational mode analysis, *J. Phys. Chem. B* **112**, 13424 (2008).

[198] P. Zirak, A. Penzkofer, T. Mathes, and P. Hegemann, Photo-dynamics of roseoflavin and riboflavin in aqueous and organic solvents, *Chem. Phys.* **358**, 111 (2009).

[199] A. Weigel, A. Dobryakov, B. Klaumünzer, M. Sajadi, P. Saalfrank, and N. P. Ernsting, Femtosecond stimulated Raman spectroscopy of flavin after optical excitation, *J. Phys. Chem. B* **115**, 3656 (2011).

[200] J. Götze and P. Saalfrank, Serine in BLUF domains displays spectral importance in computational models, *J. Photochem. Photobiol. B: Biol.* **94**, 87 (2009).

[201] M. Barbatti, G. Granucci, M. Persico, M. Ruckenbauer, M. Vazdar, M. Eckert-Maksić, and H. Lischka, The on-the-fly surface-hopping program system Newton-X: Application to ab initio simulation of the nonadiabatic

photodynamics of benchmark systems, *J. Photochem. Photobio. A: Chem.* **190**, 228 (2007).

[202] M. Barbatti, G. Granucci, M. Ruckenbauer, F. Plasser, J. Pittner, M. Persico, and H. Lischka, NEWTON-X: a package for Newtonian dynamics close to the crossing seam, www.newtonx.org, 2011.

[203] J. C. Tully, Molecular dynamics with electronic transitions, *J. Chem. Phys.* **93**, 1061 (1990).

[204] S. Hammes-Schiffer and J. C. Tully, Proton transfer in solution: Molecular dynamics with quantum transitions, *J. Chem. Phys.* **101**, 4657 (1994).

[205] J. Pittner, H. Lischka, and M. Barbatti, Optimization of mixed quantum-classical dynamics: Time-derivative coupling terms and selected couplings, *Chem. Phys.* **356**, 147 (2009).

[206] E. Tapavicza, I. Tavernelli, and U. Rothlisberger, Trajectory surface hopping within linear response time-dependent density-functional theory, *Phys. Rev. Lett.* **98**, 023001 (2007).

[207] M. Barbatti, J. Pittner, M. Pederzoli, U. Werner, R. Mitrić, V. Bonačić-Koutecký, and H. Lischka, Non-adiabatic dynamics of pyrrole: Dependence of deactivation mechanisms on the excitation energy, *Chem. Phys.* **375**, 26 (2010).

[208] J. C. Tully, Perspective: Nonadiabatic dynamics theory, *J. Chem. Phys.* **137**, 22A301 (2012).

[209] H.-D. Meyer, U. Manthe, and L. Cederbaum, The multi-configurational time-dependent hartree approach, *Chem. Phys. Lett.* **73**, 165 (1990).

[210] M. Beck, A. Jäckle, G. Worth, and H.-D. Meyer, The multiconfiguration time-dependent hartree (MCTDH) method: a highly efficient algorithm for propagating wavepackets, *Chem. Phys. Lett.* **324**, 1 (2000).

[211] M. Thoss and G. Stock, Mapping approach to the semiclassical description of nonadiabatic quantum dynamics, *Phys. Rev. A* **59**, 6479 (1999).

[212] A. M. Virshup, C. Punwong, T. V. Pogorelov, B. A. Lindquist, C. Ko, and T. J. Martínez, Photodynamics in complex environments: Ab initio multiple spawning quantum mechanical/molecular mechanical dynamics, *J. Chem. Phys. B* **113**, 3280 (2009).

[213] N. L. Doltsinis and D. Marx, Nonadiabatic Car-Parrinello molecular dynamics, *Phys. Rev. Lett.* **88**, 166402 (2002).

[214] T. Domratcheva, B. L. Grigorenko, I. Schlichting, and A. V. Nemukhin, Molecular models predict light-induced glutamine tautomerization in BLUF photoreceptors, *Biophys. J.* **94**, 3872 (2008).

[215] M. Gauden, I. H. M. van Stokkum, J. M. Key, D. C. Lührs, R. van Grondelle, P. Hegemann, and J. T. M. Kennis, Hydrogen-bond switching through a radical pair mechanism in a flavin-binding photoreceptor, *Proc. Natl. Acad. Sci. USA* **103**, 10895 (2006).

[216] B. Klaumünzer, *Quantenchemische und molekulardynamische Untersuchungen zur Photoanregung von Riboflavin*, Ph.D. thesis, Universität Potsdam, Germany (2012).

[217] H. M. Senn and W. Thiel, QM/MM methods for biomolecular systems, *Angew. Chem. Int. Ed.* **48**, 1198 (2009).

[218] J. P. Götze, C. Greco, R. Mitrić, V. Bonačić-Koutecký, and P. Saalfrank, BLUF hydrogen network dynamics and UV/Vis spectra: A combined molecular dynamics and quantum chemical study, *J. Comput. Chem.* **33**, 2233 (2012).

[219] T. Förster, Zwischenmolekulare Energiewanderung und Fluoreszenz, *Annalen der Physik* **437**, 55 (1948).

[220] T. Polívka and H. A. Frank, Molecular factors controlling photosynthetic light harvesting by carotenoids, *Acc. Chem. Res.* **43**, 1125 (2010).

[221] W. I. Gruszecki, R. Luchowski, M. Zubik, W. Grudzinski, E. Janik, M. Gospodarek, J. Goc, Z. Gryczynski, and I. Gryczynski, Blue-light-controlled photoprotection in plants at the level of the photosynthetic antenna complex LHCII, *J. Plant Physiol.* **167**, 69 (2010).

[222] T. Polívka and V. Sundström, Dark excited states of carotenoids: Consensus and controversy, *Chem. Phys. Lett.* **477**, 1 (2009).

[223] C. König and J. Neugebauer, First-principles calculation of electronic spectra of light-harvesting complex II, *Phys. Chem. Chem. Phys.* **13**, 10475 (2011).

[224] T. A. Wesolowski and A. Warshel, Frozen density functional approach for ab initio calculations of solvated molecules, *J. Phys. Chem.* **97**, 8050 (1993).

[225] P. Müller, X.-P. Li, and K. K. Niyogi, Non-photochemical quenching. a response to excess light energy, *Plant Physiol.* **125**, 1558 (2001).

[226] J. Standfuss, A. C. Terwisscha van Scheltinga, M. Lamborghini, and W. Kühlbrandt, Mechanisms of photoprotection and nonphotochemical quenching in pea light-harvesting complex at 2.5 Å resolution, *EMBO J.* **24**, 919 (2005).

[227] J. P. Götze, *Influence of protein and solvent environments on quantum chemical properties of photosynthesis enzymes and photoreceptors*, Ph.D. thesis, Universität Potsdam, Germany (2010).

[228] A. Dreuw and M. Wormit, Simple replacement of violaxanthin by zeaxanthin in LHC-II does not cause chlorophyll fluorescence quenching, *J. Inorg. Biochem.* **102**, 458 (2008).

[229] M. Wormit, P. H. P. Harbach, J. M. Mewes, S. Amarie, J. Wachtweitl, and A. Dreuw, Excitation energy transfer and carotenoid radical cation formation in light harvesting complexes – a theoretical perspective, *Biochim. Biophys. Acta - Bioenerg.* **1787**, 738 (2009).

[230] A. Dreuw, Influence of geometry relaxation on the energies of the S_1 and S_2 states of violaxanthin, zeaxanthin, and lutein, *J. Phys. Chem. A* **110**, 4592 (2006).

[231] M. Wormit, P. H. P. Harbach, J. M. Mewes, and A. Dreuw, Quantum chemical excited state calculations on pigment–protein complexes require thorough geometry re-optimization of experimental crystal structures, *Theo. Chem. Acc.* **125**, 419 (2010).

[232] S. Hirate and M. Head-Gordon, Time-dependent density functional theory within the Tamm-Dancoff approximation, *Chem. Phys. Lett.* **314**, 291 (1999).

[233] S. Grimme and M. Waletzke, A combination of Kohn-Sham density functional theory and multi-reference configuration interaction methods, *J. Chem. Phys.* **111**, 5645 (1999).

[234] J. Schirmer, Beyond the random-phase approximation: A new approximation scheme for the polarization propagator, *Phys. Rev. A* **26**, 2395 (1982).

[235] J. H. Starcke, M. Wormit, J. Schirmer, and A. Dreuw, How much double excitation character do the lowest excited states of linear polyenes have?, *Chem. Phys.* **329**, 39 (2006).

[236] O. Christiansen, H. Koch, and P. Jørgensen, The second-order approximate coupled cluster singles and doubles model CC2, *Chem. Phys. Lett.* **243**, 409 (1995).

[237] D. Kröner and J. P. Götze, Modeling of a violaxanthin-chlorophyll b chromophore pair in its LHCII environment using CAM-B3LYP, *J. Photochem. Photobiol. B: Biol.* **109**, 12 (2012).

[238] T. Yanai, D. P. Tew, and N. C. Handy, A new hybrid exchange-correlation functional using the Coulomb-attenuating method (CAM-B3LYP), *Chem. Phys. Lett.* **393**, 51 (2004).

[239] M. J. G. Peach, E. I. Tellgren, P. Salek, T. Helgaker, and D. J. Tozer, Structural and electronic properties of polyacetylene and polyyne from hybrid and Coulomb-attenuated density functionals, *J. Phys. Chem. A* **111**, 11930 (2007).

[240] S. Dapprich, I. Komáromi, K. S. Byun, K. Morokuma, and M. J. Frisch, A new ONIOM implementation in Gaussian98. Part I. The calculation of energies, gradients, vibrational frequencies and electric field derivatives, *J. Mol. Struct. (Theochem)* **462**, 1 (1999).

[241] J. J. P. Stewart, Optimization of parameters for semiempirical methods V: Modification of NDDO approximations and application to 70 elements, *J. Mol. Model.* **13**, 1173 (2007).

[242] J. M. Wang, P. Cieplak, and P. A. Kollman, How well does a restrained electrostatic potential (RESP) model perform in calculating conformational energies of organic and biological molecules?, *J. Comput. Chem.* **21**, 1049 (2000).

[243] U. C. Singh and P. A. Kollman, An approach to computing electrostatic charges for molecules, *J. Comput. Chem.* **5**, 129 (1984).

[244] B. H. Besler, K. M. Merz Jr., and P. A. Kollman, Atomic charges derived from semiempirical methods, *J. Comput. Chem.* **11**, 431 (1990).

[245] S. Vassiliev and D. Bruce, Toward understanding molecular mechanisms of light harvesting and charge separation in photosystem II, *Photosynth. Res.* **97**, 75 (2008).

[246] M. Kasha, H. R. Rawls, and M. A. El-Bayoumi, The exciton model in molecular spectroscopy, *Pure Appl. Chem.* **11**, 371 (1965).

[247] J. S. Frähmcke and P. J. Walla, Coulombic couplings between pigments in the major light-harvesting complex LHC II calculated by the transition density cube method, *Chem. Phys. Lett.* **430**, 397 (2006).

[248] J. Martiskainen, R. Kananavičius, J. Linnanto, H. Lehtivuori, M. Keränen, V. Aumanen, N. Tkachenko, and J. Korppi-Tommola, Excitation energy

transfer in the LHC-II trimer: from carotenoids to chlorophylls in space and time, *Photosynth. Res.* **107**, 195 (2011).

[249] S. Caffarri, R. Croce, J. Breton, and R. Bassi, The major antenna complex of photosystem II has a xanthophyll binding site not involved in light harvesting, *J. Biol. Chem.* **276**, 35924 (2001).

[250] G. Ertl, Reactions at surfaces: From atoms to complexity (Nobel Lecture), *Angew. Chem. Int. Ed.* **47**, 3524 (2008).

[251] P. Saalfrank, M. Nest, I. Andrianov, T. Klamroth, D. Kröner, and S. Beyvers, Quantum dynamics of laser-induced desorption from metal and semiconductor surfaces, and related phenomena, *J. Phys.: Condens. Matter* **18**, S1425 (2006).

[252] D. Kröner, I. Mehdaoui, H.-J. Freund, and T. Klüner, Three-dimensional ab initio simulation of laser-induced desorption of NO from NiO(100), *Chem. Phys. Lett.* **415**, 150 (2005).

[253] I. Mehdaoui, D. Kröner, M. Pykavy, H.-J. Freund, and T. Klüner, Photo-induced desorption of NO from NiO(100): calculation of the four-dimensional potential energy surfaces and systematic wave packet studies, *Phys. Chem. Chem. Phys.* **8**, 1584 (2006).

[254] T. Mull, B. Baumeister, M. Menges, H.-J. Freund, D. Weide, C. Fischer, and P. Andresen, Bimodal velocity distributions after ultraviolet-laser-induced desorption of NO from oxide surfaces. Experiments and results of model calculations, *J. Chem. Phys.* **96**, 7108 (1992).

[255] D. Kröner, T. Klamroth, M. Nest, and P. Saalfrank, Laser-induced charge transfer and photodesorption of Cs@Cu(111): quantum dynamical model simulations, *Appl. Phys. A* **88**, 535 (2007).

[256] E. V. Chulkov, V. M. Silkin, and P. M. Echenique, Image potential states on metal surfaces: Binding energies and wave functions, *Surf. Sci.* **437**, 330 (1999).

[257] D. Kröner, S. Klinkusch, and T. Klamroth, Enhanced photodesorption by vibrational pre-excitation: Quantum model simulations for Cs/Cu(111), *Surf. Sci.* **602**, 3148 (2008).

[258] S. M. Harris, S. Holloway, and G. R. Darling, Hot electron mediated photodesorption: A time-dependet approach applied to NO/Pt(111), *J. Chem. Phys.* **102**, 8235 (1995).

[259] T. Klamroth, D. Kröner, and P. Saalfrank, Laser-driven coupled electron-nuclear dynamics: Quantum mechanical simulation of molecular photodesorption from metal films, *Phys. Rev. B* **72**, 205407 (2005).

[260] D. Kröner, C. Ehlert, P. Saalfrank, and A. Holländer, Ab initio calculations for XPS chemical shifts of poly(vinyl-trifluoroacetate) using trimer models, *Surf. Sci.* **605**, 1516 (2011).

[261] D. Kröner, H. Krüger, and M. W. Thesen, Electronic structure calculations for hole-transporting triphenylamine derivatives in polymer light-emitting diodes, *Macromol. Theory Simul.* **20**, 790 (2011).

A Control of chiral molecular switches

A.1 Stereoselective laser pulse control

Stereoselective laser pulse control of an axial chiral molecular model system supporting four stereoisomers

Dominik Kröner and Bastian Klaumünzer

Chemical Physics **338**, 268–276 (2007)
DOI:10.1016/j.chemphys.2007.04.010

We present quantum dynamical simulations on the axial chiral model system 2,2'-difluoro-biphenyl which supports four stereoisomers, i.e. two *diastereomeric* pairs of *enantiomers*, along the torsion around its central C-C bond. A pump-dump control mechanism is developed which consists of *stereo*-selective, i.e. *enantio*- and *diastereo*-selective, ultrashort laser pulses that convert a racemic mixture to one of its diastereomers. For that purpose the enantioselective laser pulse control of previous theoretical investigations is extended for systems that support more than one pair of enantiomers. Still, the polarization of the laser field determines the stereoselectivity of the control mechanism.

A.2 Laser-operated axially chiral switch

Laser-operated chiral molecular switch: Quantum simulations for the controlled transformation between achiral and chiral atropisomers

Dominik Kröner and Bastian Klaumünzer

Physical Chemistry Chemical Physics **9**, 5009–5017 (2007)
DOI:10.1039/b705974d

We report quantum dynamical simulations for the laser controlled isomerization of 1-(2-*cis*-fluoroethenyl)-2-fluorobenzene based on one-dimensional electronic ground and excited state potentials obtained from (TD)DFT calculations. 1-(2-*cis*-fluoroethenyl)-2-fluorobenzene supports two chiral and one achiral atropisomers, the latter being the most stable isomer at room temperature. Using a linearly polarized IR laser pulse the molecule is excited to an internal rotation around its chiral axis, i.e. around the C-C single bond between phenyl ring and ethenyl group, changing the molecular chirality. A second linearly polarized laser pulse stops the torsion to prepare the desired enantiomeric form of the molecule. This laser control allows the selective switching between the achiral and either the left- or right-handed form of the molecule. Once the chirality is "switched on" linearly polarized UV laser pulses allow the selective change of the chirality using the electronic excited state as intermediate state.

A.3 Stochastic laser pulse optimization

Stereoselective isomerization of an ensemble of adsorbed molecules with multiple orientations: Stochastic laser pulse optimization for selective switching between achiral and chiral atropisomers

Tillmann Klamroth and Dominik Kröner

Journal of Chemical Physics **129**, 234701-1–10 (2008)
DOI:10.1063/1.3036927

We present quantum dynamical simulations for the laser driven isomerization of an ensemble of surface mounted stereoisomers with multiple orientations. The model system 1-(2-*cis*-fluoroethenyl)-2-fluorobenzene supports two chiral and one achiral atropisomers upon torsion around the C-C single bond connecting phenyl ring and ethylene group. An infrared picosecond pulse is used to excite the internal rotation around the chiral axis, thereby controlling the chirality of the molecule. In order to selectively switch the molecules – independent of their orientation on a surface – from their achiral to either their left- or right-handed form, a stochastic pulse optimization algorithm is applied. The stochastic pulse optimization is performed for different sets of defined orientations of adsorbates corresponding to the rotational symmetry of the surface. The obtained nonlinearly polarized laser pulses are highly enantioselective for each orientation.

A.4 Surface-mounted molecular switch

From stochastic pulse optimization to a stereoselective laser pulse sequence: Simulation of a chiroptical molecular switch mounted on adamantane

Dominik Kröner, Bastian Klaumünzer, and Tillmann Klamroth

Journal of Physical Chemistry A **112**, 9924–9935 (2008)
DOI:10.1021/jp804352q

Quantum dynamical simulations for the laser-controlled isomerization of 1-(2-*cis*-fluoroethenyl)-2-fluorobenzene mounted on adamantane are reported based on a one-dimensional electronic ground-state potential and dipole moment calculated by density functional theory. The model system 1-(2-*cis*-fluoroethenyl)-2-fluorobenzene supports two chiral and one achiral atropisomers upon torsion around the C-C single bond connecting the phenyl ring and ethylene group. The molecule itself is bound to an adamantyl frame which serves as a model for a linker or a surface. Due to the C_3 symmetry of the adamantane molecule, the molecular switch can have three equivalent orientations. An infrared picosecond pulse is used to excite the internal rotation around the chiral axis, thereby controlling the chirality of the molecule. In order to selectively switch the molecules – independent of their orientation – from their achiral to either their left- or right-handed form, a stochastic pulse optimization algorithm is applied. A subsequent detailed analysis of the optimal pulse allows for the design of a stereoselective laser pulse sequence of analytical form. The developed control scheme of elliptically polarized laser pulses is enantioselective and orientation-selective.

B Chiral recognition in mass spectrometry

B.1 Influence of the pulse duration

Circular dichroism in ion yields employing femtosecond laser ionization – the role of laser pulse duration

Philipp Horsch, Gunter Urbasch, Karl-Michael Weitzel, and Dominik Kröner

Physical Chemistry Chemical Physics **13**, 2378–2386 (2011)
DOI:10.1039/c0cp01903h

The circular dichroism (CD) induced by femtosecond laser pulse excitation of 3-methyl-cyclopentanone has been investigated by means of experiment and theory as a function of the laser pulse duration. In the experiment the CD in ion yields is measured by femtosecond laser ionization via a one-photon resonant excited state. In the theoretical part the CD is calculated by solving laser driven quantum electron dynamics for the same resonant excitation based on ab initio electronic structure calculations employing a complete description of the electric field-electric dipole and magnetic field-magnetic dipole interactions. Both the experimentally measured CD in ion yields and the calculated CD in excited state populations exhibit a marked increase of the CD for pulse duration increasing from 50 fs to about 200 fs. Beyond 200 fs pulse duration the CD levels off. The combination of experimental and theoretical evidences indicates that the CD decreases with increasing laser intensity connected to the increased coupling between the excited states.

B.2 Impact of the magnetic interactions

Chiral distinction by ultrashort laser pulses: Electron wavepacket dynamics incorporating magnetic interactions

Dominik Kröner

Journal of Physical Chemistry A **115**, 14510–14518 (2011)
DOI:10.1021/jp207270s

The qualitative and quantitative distinction of enantiomers is one of the key issues in chemical analysis. In the last years, circular dichroism (CD) has been combined with laser ionization mass spectrometry (LIMS), applying resonance enhanced multiphoton ionization (REMPI) with ultrashort laser pulses. We present theoretical investigations on the CD in the populations of the first electronic excited state of the REMPI process, caused by the interaction of 3-methylcyclopentanone with either left or right circular polarized fs-laser pulses. For this we performed multistate laser driven many electron dynamics based on ab initio electronic structure calculations, namely, TD-CIS(D)/6-311++(2d,2p). For a theoretical description of these experiments, a complete description of the field-dipole correlation is mandatory, including both electric field-electric dipole and magnetic field-magnetic dipole interactions. The effect of various pulse parameters on the CD are analyzed and compared with experimental results to gain further understanding of the key elements for an optimal distinction of enantiomers.

C Electronic structure and spectroscopy of biomolecules

C.1 Vibronic spectra of Riboflavin

(TD-)DFT Calculation of Vibrational and Vibronic Spectra of Riboflavin in Solution

Bastian Klaumünzer, Dominik Kröner, and Peter Saalfrank

Journal of Physical Chemistry B **114**, 10826–10834 (2010)
DOI:10.1021/jp100642c

The photophysics and photochemistry of flavin molecules are of great interest due to their role for the biological function of flavoproteins. An important analysis tool toward the understanding of the initial photoexcitation step of flavins is electronic and vibrational spectroscopy, both in frequency and time domains. Here we present quantum chemical [(time-dependent) density functional theory ((TD-)DFT)] calculations for vibrational spectra of riboflavin, the parent molecule of biological blue-light receptor chromophores, in its electronic ground (S_0) and lowest singlet excited states (S_1). Further, vibronic absorption spectra for the $S_0 \rightarrow S_1$ transition and vibronic emission spectra for the reverse process are calculated, both including mode mixing. Solvent effects are partially accounted for by using a polarizable continuum model (PCM) or a conductor-like screening model (COSMO). Calculated vibrational and electronic spectra are in good agreement with measured ones and help to assign the experimental signals arising from photoexcitation of flavins. In particular, upon photoexcitation a loss of double bond character in the polar region of the ring system is observed which leads to vibronic fine structure in the electronic spectra. Besides vibronic effects, solvent effects are important for understanding the photophysics of flavins in solution quantitatively.

C.2 Resonance Raman spectra with Duschinsky rotation

Resonance Raman and vibronic absorption spectra with Duschinsky rotation from a time-dependent perspective: Application to β-carotene

Shiladitya Banerjee, Dominik Kröner, and Peter Saalfrank

The Journal of Physical Chemistry **137**, 22A534-1–9 (2012)
DOI:10.1063/1.4748147

The time-dependent approach to electronic spectroscopy, as popularized by Heller and co-workers in the 1980s, is applied here in conjunction with linear-response, time-dependent density functional theory to study vibronic absorption and resonance Raman spectra of β-carotene, with and without a solvent. Two-state models, the harmonic and the Condon approximations are used in order to do so. A new code has been developed which includes excited state displacements, vibrational frequency shifts, and Duschinsky rotation, i.e., mode mixing, for both non-adiabatic spectroscopies. It is shown that Duschinsky rotation has a pronounced effect on the resonance Raman spectra of β-carotene. In particular, it can explain a recently found anomalous behaviour of the so-called ν_1 peak in resonance Raman spectra [N. Tschirner, M. Schenderlein, K. Brose, E. Schlodder, M. A. Mroginski, C. Thomsen, and P. Hildebrandt, Phys. Chem. Chem. Phys. **11**, 11471 (2009)], which shifts with the change in excitation wavelength.

C.3 Non-adiabatic excited state dynamics

Non-adiabatic excited state dynamics of riboflavin after photoexcitation

Bastian Klaumünzer, Dominik Kröner, Hans Lischka, and Peter Saalfrank

Physical Chemistry Chemical Physics **14**, 8693–8702 (2012)
DOI:10.1039/C2CP40978J

Flavins are chromophores in light-gated enzymes and therefore central in many photobiological processes. To unravel the optical excitation process as the initial, elementary step towards signal transduction, detailed ultrafast (femtosecond) experiments probing the photo-activation of flavins have been carried out recently [Weigel et al., *J. Phys. Chem. B*, 2011, **115**, 3656–3680.]. The present paper contributes to a further understanding and interpretation of these experiments by studying the post-excitation vibrational dynamics of riboflavin (RF) and microsolvated riboflavin, RF·$4H_2O$, using first principles non-adiabatic molecular dynamics. By analyzing the characteristic atom motions and calculating time-resolved stimulated emission spectra following $\pi\pi^*$ excitation, it is found that after optical excitation C-N and C-C vibrations in the isoalloxazine rings of riboflavin set in. The Franck-Condon (vertically excited) state decays within about 10 fs, in agreement with experiment. Anharmonic coupling leads to Intramolecular Vibrational energy Redistribution (IVR) on the timescale of about 80-100 fs, first to (other) C-C stretching modes of the isoalloxazine rings,

then by energy spread over the whole molecule, including low-frequency in-plane modes. The IVR is accompanied by a red-shift and broadening of the emission spectrum. When RF is microsolvated with four water molecules, an overall red-shift of optical spectra by about 20 nm is observed but the relaxation dynamics is only slightly affected. For several trajectories, a tendency for hydrogen transfer from water to flavin-nitrogen (N_5) was found.

C.4 Chromophores in LHCII environment

Modeling of a violaxanthin–chlorophyll b chromophore pair in its LHCII environment using CAM-B3LYP

Dominik Kröner and Jan Philipp Götze

Journal of Photochemistry and Photobiology B: Biology **109**, 12–19 (2012)
DOI:10.1016/j.jphotobiol.2011.12.007

Collecting energy for photosystem II is facilitated by several pigments, xanthophylls and chlorophylls, embedded in the light harvesting complex II (LHCII). One xanthophyll, violaxanthin (Vio), is loosely bound at a site close to a chlorophyll b (Chl). No final answer has yet been found for the role of this specific xanthophyll. We study the electronic structure of Vio in the presence of Chl and under the influence of the LHCII environment, represented by a point charge field (PCF).

We compare the capability of the long range corrected density functional theory (DFT) functional CAM-B3LYP to B3LYP for the modeling of the UV/vis spectrum of the Vio + Chl pair. CAM-B3LYP was reported to allow for a very realistic reproduction of bond length alternation of linear polyenes, which has considerable impact on the carotenoid structure and spectrum. To account for the influence of the LHCII environment, the chromophore geometries are optimized using an ONIOM(DFT/6-31G(d):PM6) scheme.

Our calculations show that the energies of the locally excited states are almost unaffected by the presence of the partner chromophore or the PCF. There are,

however, indications for excitonic coupling of the Chl Soret band and Vio. We propose that Vio may accept energy from blue-light excited Chl.

Acknowledgement/Danksagung

Before giving individual acknowledgements in German, I wish to thank all coauthors of the publications reviewed in the work at hand. Their contributions to the investigations were essential and are gratefully appreciated. Their names are listed in the following in alphabetical order, together with their current titles and whereabouts (to the best of my knowledge): *Shiladitya Banerjee* (Potsdam University, Germany), *Dr. Jan Philipp Götze* (Max-Planck-Institut für Kohlenforschung, Germany), *Philipp Horsch* (Philipps-University Marburg, Germany), *PD Dr. Tillmann Klamroth* (Potsdam University, Germany), *Dr. Bastian Klaumünzer* (Potsdam University, Germany), *Prof. Dr. Hans Lischka* (University of Vienna, Austria), *Prof. Dr. Peter Saalfrank* (Potsdam University, Germany), *Dr. Gunter Urbasch* (Philipps-University Marburg, Germany), and *Prof. Dr. Karl-Michael Weitzel* (Philipps-University Marburg, Germany).

The research that yielded the discussed publications was financially supported by different organisations and institutions. For financial support I wish to thank: The DFG (German Research Foundation) for the projects **KR 2942/1** (*Quantum theory for laser pulse control of chiral molecular switches and rotors on surfaces*) and **KR 2942/2** (*Chiral detection and reaction control by ultrashort elliptically polarized laser pulses*), the BMBF (Federal Ministry of Education and Research) for the project **GoFORSYS** (*Potsdam-Golm research unit on system biology*), and the **University of Potsdam**.

Viele Personen haben in unterschiedlicher Weise zum Erfolg dieser Arbeit beigetragen. Ihn allen gilt mein Dank:

Herrn **Prof. Peter Saalfrank** möchte ich besonders dafür danken, dass er mir viele wichtige Rahmenbedingungen für meine eigenständige wissenschaftliche Forschung geschaffen hat und mich stets großzügig mit Ratschlägen unterstützt hat. Seine kritischen Fragen sowie die interessanten Diskussionen mit ihm waren von großem Nutzen. Auch hatte er immer ein offenes Ohr für Fragen jeder Art, was ich sehr schätze.

Für seine sehr große Hilfsbereitschaft danke ich **Dr. Tillmann Klamroth**. Ob es technische, methodische oder wissenschaftliche Probleme zu überwinden galt, Tillmann war immer bereit, Ratschläge zu geben und Hilfe anzubieten. Die direkte wissenschaftliche Zusammenarbeit mit ihm war sehr erfolgreich, wofür ich ihm besonders danke.

Großer Dank gilt auch Herrn **Prof. Karl-Michael Weitzel** (Marburg) für die erfolgreiche Kooperation. Seine Experimente haben viele entscheidende Beiträge zu den wissenschaftlichen Fragestellungen geliefert. Besonders schätze ich sein wissenschaftliches Engagement, seine Unterstützung und die ergiebigen

Gespräche. In diesem Zusammenhang schulde ich auch Herrn **Dr. Mikhail Korolokov** (Minsk) besonderen Dank dafür, dass er geholfen hat, Kontakte herzustellen und mich stets mit kritischen Diskussion zur tieferen Analyse meiner Modelle motiviert hat.

Allen weiteren Kooperationspartner und Kollegen, die zu den hier dokumentierten Arbeiten beigetragen habe, möchte ich ebenfalls recht herzlich danken:

Auf der Seite der Theorie gilt mein besonderer Dank **Dr. Bastian Klaumünzer**, der sich den zahlreichen wissenschaftlichen, aber auch technischen Herausforderungen im Laufe der Projekte stets engagiert und zielstrebig gestellt hat und damit wesentlich zum Gelingen beigetragen hat.

Ebenso möchte ich **Shiladitya Banerjee** danken, dessen große Lernbereitschaft und Fleiß erst die erhofften Ergebnisse brachten.

Dr. Jan Philipp Götze gilt mein Dank für sein Ideenreichtum und die vielen wissenschaftlichen Streitgespräche, die zur Festigung bestehender Ansätze beitrugen und auch zu neuen Ansätzen führten.

Für das sehr freundschaftliche und motivierende Arbeitsumfeld der **Arbeitsgruppe Saalfrank** danke ich allen Kollegen, die ich über die Jahre in Potsdam kennen lernen dürfte.

Auf der experimentellen Seite danke ich des Weiteren **Philipp Harbach** und **Dr. Gunter Urbasch** (Philipps-Universität Marburg) für das gute Gelingen des Kooperationsprojekts.

Nicht unerwähnt bleiben sollen diejenigen, die als studentische Hilfskräfte unterstützende Aufgaben wahrgenommen haben und daher direkt oder indirekt einen Beitrag geleistet haben. Ich danke dafür **Selina Schimka**, **Christian Hensel** und **Susanne Eich**. Erster gilt mein besonderer Dank, da sie essenzielle Berechnungen für Ergebnisse durchgeführt hat, die in dieser Arbeit explizit genannt werden, allerdings zum jetzigen Zeitpunkt noch nicht veröffentlicht sind.

Meinem privaten Umfeld gilt spezieller Dank. Die Geduld meiner Frau für meine endlos langen Geschichten aus dem Forschungs- und Büroalltag habe ich sehr zu schätzen gelernt. Ihr großes Engagement bei der Betreuung und Erziehung unseres Sohnes hat außerdem häufig Freiräume geschaffen, die ich für meine Arbeit nutzen konnte. Dafür danke ich ihr ganz herzlich. Meinen Eltern danke ich für alle Unterstützung, die sie geleistet haben. Meinem engen Freundeskreis danke ich für offene Ohren, motivierende Worte sowie den wichtigen Ausgleich von der theoretischen naturwissenschaftlichen Welt.

Dominik Kröner, im März 2013